DISSERTATION

MINERAL DUST LOFTING AND INTERACTIONS WITH COLD POOLS

Submitted by

Jennifer Bukowski

Department of Atmospheric Science

In partial fulfillment of the requirements

For the Degree of Doctor of Philosophy

Colorado State University

Fort Collins, Colorado

Spring 2021

Doctoral Committee:

Advisor: Susan C. van den Heever

Christine Chiu
Kristen Rasmussen
Shantanu Jathar
Mary Barth
Steven Miller

ABSTRACT

MINERAL DUST LOFTING AND INTERACTIONS WITH COLD POOLS

Convective dust storms, or haboobs, form when strong surface winds loft loose soils in convective storm outflow boundaries. Haboobs are a public safety hazard and can cause a near instantaneous loss of visibility, inimical air quality, and contribute significantly to regional dust and radiation budgets. Nevertheless, reliable predictions of convective dust events are inhibited by a lack of understanding regarding the complex and non-linear interactions between cold pools, dust radiative effects, and land surface processes, and their associated uncertainties in numerical models. In this dissertation, model simulations of real and idealized haboobs are used to address limitations in regional dust modeling, the direct radiative effect of mineral dust on cold pool properties and dynamics, and feedbacks between haboobs and the land surface.

In the first study, we assess the influence of horizontal resolution, specifically parameterized versus convection-allowing resolution, on dust lofting, vertical transport, and aerosol heating rates in the WRF-Chem regional model. On average, convection-permitting simulations exhibit higher surface wind speeds, enhanced convective activity, and drier soil, which leads to more dust emissions to the atmosphere. More frequent and stronger vertical velocities also transport dust further aloft and increase the atmospheric lifetime of these particles. We conclude that tuning dust emissions in coarse-resolution regional simulations can only improve the results to first-order and cannot fully rectify discrepancies in the representation of convective dust transport in terms of aerosol distributions or the net aerosol radiative effect.

The second study, WRF-Chem is utilized to simulate the effect dust radiation interactions have on a long-lived haboob case study that spans three distinct radiative regimes: day (high shortwave), evening (low shortwave), and night (longwave only). A sophisticated algorithm, known as TOBAC, is used to track and identify the numerous cold pool boundaries and assemble statistics that represent the impact of including dust radiative effects. To first order, dust scattering of shortwave radiation in the day leads to a colder, dustier, and faster moving cold pool. In the transition period of early evening, the shortwave effects diminish while longwave absorption by dust leads to warmer and slower cold pools that loft less dust as they propagate onward. At night, the haboob is again warmer due to dust absorption, but gustier in the more stable nocturnal surface layer.

Lastly, the third study focuses on feedbacks between parameters that affect both dust mobilization and cold pool dynamics. The Elementary Effects statistical method is applied to an ensemble of 120 idealized RAMS simulations of daytime and nighttime haboobs. This sensitivity analysis identifies and ranks the importance of different input factors in predicting haboob properties as: initial cold pool temperature, surface type, soil type, and finally soil moisture. Most of these parameters modify the cold pool via their impacts on surface fluxes, although the effect of surface type is dominated by the change in roughness length. A semi-linear connection between haboob dust and cold pool temperature is detected in the statistics, and a relationship between dust flux and cold pool temperature is proposed which relates haboob strength to the thermodynamic environment.

ACKNOWLEDGEMENTS

This work would not have been possible without the support and contributions of many people over the years that deserve recognition here. First and foremost, I thank my advisor, Prof. Susan van den Heever. Sue is capable of pushing students to be the best scientists they can, while simultaneously providing unwavering encouragement. She passionately defends the nobility of scientific pursuit and offered me the opportunity to investigate the scientific curiosities I had. Without her guidance, I would not be the independent and confident scientist I am today.

I want to acknowledge my committee members Prof. Christine Chiu, Prof. Kristen Rasmussen, and Prof. Shantanu Jathar at Colorado State University (CSU), Dr. Mary Barth at the National Center for Atmospheric Research (NCAR), and Dr. Steven Miller at the Cooperative Institute for Research in the Atmosphere (CIRA) and thank them for serving on my doctoral committee. Their feedback throughout the years has been insightful and always ask thought-provoking questions for discussion. A special thanks to Dr. Steven Miller for also being the PI of the grant supporting my dissertation and for his mentorship throughout this project. I also acknowledge the fantastic professors in the Department of Atmospheric Science at CSU for their challenging, yet engaging courses and mentoring, especially Prof. Sonia Kreidenweis, Prof. Russ Schumacher, and Prof. Jeff Pierce. Thank you to Prof. Steve Rutledge for the opportunity to teach an introductory weather course and for his guidance during that semester. And lastly, I acknowledge the CSU Department of Atmospheric Science staff for providing administrative and IT support.

A huge thank you to Dr. Derek Posselt at the National Aeronautics and Space Administration Jet Propulsion Laboratory (NASA-JPL), who was my advisor at the University of

Michigan for my master's degree. Derek gave me my first opportunity in atmospheric science and took a risk hiring a Russian major. I would not be here today without his fervent support of non-traditional students in meteorology. Derek sees the potential in people first, and then works to make that potential a reality, and for that I am grateful.

Thank you also to Dr. Jeff Reid at the Naval Research Lab (NRL) in Monterey for his mentorship throughout my graduate studies. Jeff has the remarkable ability see big-picture research goals alongside minute scientific details and has pushed me to refine my science in a way that considers both. Thank you to Dr. Annette Walker at NRL for sharing her expertise and for the fantastic science conversations we continue to have on mineral dust. And thanks to all the outstanding scientists in the Aerosol / Radiation Section at NRL-Monterey for their mentorship and support of students.

Thank you to the current and past members of the van den Heever research group, including Dr. Leah Grant, Dr. Aryeh Drager, Nick Falk, Sean Freeman, Dr. Ross Heikes, Brianna Lund, Dr. Peter Marinescu, Yasutaka Murakami, Dr. Bowen Pan, Dr. Emily Riley Dellaripa, Steve Saleeby, Steve Herbener, Alex Sokolowsky, Dr. Adele Igel, Gabrielle (Bee) Leung, Dr. Ben Toms, and Kristen Van Valkenburg. The group feels like a family and are some of the most honest and caring people who have offered countless hours of feedback and moral support along the way. Thank you to Dr. Stacey Kawecki for your inexhaustible patience while teaching me to run WRF-Chem. A special and loving thank you to Dr. Jungmin (Minnie) Park for being an amazing and encouraging friend. The best part of my time at CSU was getting to share an office with you. Long live the Minnie-Jennie-Office (MJO).

I want to recognize all the incredible students in the CSU Department of Atmospheric Science for creating an unrivaled sense of community and belonging that is often absent in

STEM. You prove that science can be kind. Thank you to the scientists who participated in the CSU Convective Cloud Outflows and UpDrafts Experiment (C^3LOUD-Ex) for showing me how to do field work and for all the karaoke / dino-ball sessions while waiting for storms. Acknowledgements also to the students and staff who have participated in weather / science outreach activities with me, including the Fort Collins Atmospheric Scientists (FORTCAST) and Noah Newman at the Colorado Climate Center (CCC). Educating the public and getting kids and adults excited about STEM is maybe our most imperative, difficult, and fun job we have as scientists.

The most important acknowledgements go to my partner, my friends, and my family. To my partner, Matt Kronwall, for his encouragement and making me laugh even at the most stressful times. To my oldest friends, Mike Watters, Sammy Bina, and Dan Tremmel, for being there for each other essentially our whole lives. To my Russian orchestra friends, including Victor Gorodinsky, Kathy Mittelstadt, Jonathan Johnston, Jason Schreiber, Anya Shatilova, Anya Gubenkova, Tetiana Khomenko, the Trubetskoy family, and so, so many others for reminding me that music, culture, and connections are what makes life worth living. To my favorite roommate and one of my best friends ever, Dante Passmore, for always reaching out. To my brothers, Mike and Kyle, for never being ashamed of their weird sister. To my extended family, specifically my grandparents, those living and those who have passed, for their unconditional love and beaming pride. To my Aunt Kate, for teaching me the alphabet and kickstarting my educational career. And lastly and above all, thank you to my parents, Don and Jeri, who have worked tirelessly and made immense sacrifices to give their children a better life. To my father, thank you for passing down your quantitative skills, for being sentimental, and for showing us that emotion is strength. And to my mother, thank you for passing down your

creativity, for using your curiosity to illuminate the world, and showing us that everyone deserves empathy. To both, thank you for your love and support, and for encouraging me to pursue my interests, even if they led me far from home.

This work was funded by an Office of Naval Research – Multidisciplinary University Research Initiative (ONR-MURI) grant (# N00014-16-1-2040). My time at CSU was partially supported by the CIRA Program of Research and Scholarly Excellence (PRSE) fellowship. The Naval Research Enterprise Internship Program (NREIP) sponsored me for two summers at NRL-Monterey, which provided mentorship and the opportunity to do research with the amazing scientists there. The Department of Energy's Atmospheric System Research (DOE-ASR) program, the Atmospheric Radiation Measurement (ARM) facilities, and the Environmental Molecular Sciences Laboratory (EMSL) at Pacific Northwest National Laboratory (PNNL) provided funding to attend Aerosol Summer School at PNNL. I would like to acknowledge the scientists and staff at PNNL, and other contributing institutions, who volunteered their time to organize and participate in the Aerosol Summer School workshop. Lastly, I would like to thank the National Science Foundation (NSF) for supporting me at the American Meteorological Society (AMS) Summer Policy Colloquium and providing a chance to learn about science policy, and meet passionate scientists making a difference in this world. I would like to recognize Bill Hooke, Paul Higgins, and Kenza Sidi-Ali-Cherif for their incredible program and hard work organizing the colloquium. All simulations were performed on the Navy Department of Defense Supercomputing Resource Center systems *Conrad, Gordon, and Gaffney*. The vast majority of analyses were performed using MATLAB, the NCAR Command Language (NCL), and the Anaconda Python distribution.

TABLE OF CONTENTS

CHAPTER 1 – INTRODUCTION

1.1) Mineral Dust in the Atmosphere

Airborne mineral dust is a major contributor to the Earth's aerosol budget (Ginoux et al., 2012; Zender et al., 2004) and has dilatant influences on the atmosphere and environment. In arid regions, vigorous synoptic-scale winds, mesoscale circulations, and convective storms can loft enormous amounts of dust particles into the air. Dust outbreaks are considered a public safety hazard (Sprigg, 2016; Middleton and Kang, 2017) mainly due to the sudden loss of visibility (Mahowald et al., 2007; Leys et al., 2011; Baddock et al., 2014; Camino et al., 2015). Additionally, dust particles are detrimental to the human respiratory system (Prospero, 1999; van Donkelaar et al., 2010; Goudie, 2014; Middleton, 2017), dust outbreaks are correlated with increased hospitalization and mortality (Stafoggia et al., 2016), and dust serves as a host to a wide array of dust-borne pathogenic microorganisms, including bacteria, viruses, fungi, and allergens (Griffin, 2007; Behzad et al., 2018).

Once lofted to the atmosphere, mineral dust and its microbiota (Kellogg and Griffin, 2006; Behzad et al., 2018) is transported across regional to global scales where it is capable of fertilizing iron-deficient maritime ecosystems (Martin, 1991; Bishop et al., 2002*;* Mahowald et al., 2005; Jickells and Moore, 2015) and modifying weather, climate patterns, and environments far from its original source (e.g. Yu et al., 2015). On the storm scale, dust particles function as efficient ice nuclei (e.g., DeMott et al., 2003; Field et al., 2006; Knopf and Koop, 2006; Boose et al., 2016) and to a lesser extent as cloud condensation nuclei (e.g., Helmert et al., 2006; van den Heever et al., 2006; Lee et al., 2009; Manktelow et al., 2010; Twohy et al., 2009; Karydis et al., 2011; Nabat et al., 2015; Tsikerdekis et al., 2019), thereby altering cloud and precipitation

processes through aerosol indirect effects. In reality, these aerosol effects operate not independently, but concurrently, modifying storm initiation, development, and lifetime (van den Heever et al., 2006; Seigel et al., 2013; Bangert et al., 2012), all while feeding back on the environment, climate, and each other.

Furthermore, mineral dust is of interest due to its distinctive optical properties that constitute the direct aerosol effect: dust both strongly scatters and absorbs shortwave and longwave radiation (e.g., Tegen and Lacis, 1996; Kinne et al., 2003; Dubovik et al., 2006), modifying atmospheric thermodynamics and the Earth's energy budget in the process (e.g., Slingo et al., 2006; Sokolik and Toon, 1996). Dust particles are the largest contributor to the total global aerosol mass and are responsible for 28 % of the worldwide aerosol shortwave effect and dominate the aerosol longwave effect, comprising 74 % of the global budget (Heald et al., 2014). Dust layers above clouds can also absorb and heat the environment, resulting in a decrease in cloud fraction through the semi-direct effect (Hansen et al., 1997; Ackerman et al., 2000; Johnson et al., 2003; Fan et al., 2008; Koch and Del Genio, 2010). Several studies suggest that including the radiative effects of mineral dust in numerical weather prediction (NWP) models could refine the radiation balance of these models and improve forecasts (Kishcha et al., 2011; Haywood et al., 2005; Pérez et al., 2006). Similarly, advances in climate models have been made by incorporating time-varying dust sources and climate–dust feedbacks in the radiative forcing calculations (Kok et al., 2014, 2018; Woodage and Woodward, 2014).

The influence of atmospheric mineral dust is extensive and many sectors would benefit from accurate dust forecasts. Yet, representing the immense range of scales involved between dust mobilization at the surface (microscale) and global transport (planetary scale) is an outstanding challenge, as is characterizing of all the non-linear connections between dust and the

weather and climate system. Combined with the added computational expense of online aerosols in numerical models, this leaves dust forecasting as an ongoing challenge in atmospheric science (Benedetti et al., 2014, 2018). Substantial discrepancies exist across global models of similar resolution (Huneeus et al., 2011), regional models (Uno et al., 2006; Todd et al., 2008), and dust parameterizations (Darmenova et al., 2009) in the magnitudes of predicted dust flux from the surface to the atmosphere.

In particular, convective dust storms, known as haboobs, have been identified as a major source of error in dust models (Knippertz and Todd, 2012; Largeron et al., 2015; Pope et al., 2016). Convective dust storms originate when dust is lofted in the outflow boundary of a cold pool, also referred to as a density current. Cold pools can form as precipitation evaporates below the cloud base of a convective cell or convective system if the air layer is dry. The air, now cooler and therefore denser than its surroundings, is negatively buoyant and sinks until it hits the ground and spreads out as a distinct cold, rapidly moving air mass, that can loft loose soils into the air (Membery, 1985; Roberts and Knippertz, 2012; Knippertz and Todd, 2012; Cowie et al., 2015; Pantillon et al., 2015; 2016; Huang et al., 2018). Estimates of the contribution of convective dust storms to regional dust budgets vary widely and could be as low as 10% in Australia (Strong et al., 2011), 30% in the Arabian Peninsula (Miller et al., 2008), and somewhere between 20-60% in the Sahel (Emmel et al., 2010; Marsham et al., 2011; Heinhold et al., 2013; Bou Karam et al., 2009).

While modeling convective dust storms and dust transport is difficult due to the resolutions required, we are more limited by a lack of knowledge regarding the interactions between dust and the environment than computational resources. Specifically, the underlying physical relationships between convective dust and radiation, as well as interactions with the

underlying land surface, can be highly non-linear, depend on the surrounding environment, and have yet to be explored in detail. Since our knowledge of these processes forms the basis of our parameterization schemes and representation in forecast models, it is important to fully capture the effect of these interactions. This dissertation aims to narrow this gap in our understanding of mesoscale dust processes by addressing some of the largest unknowns relating to feedbacks between convective dust storms, radiation, and surface processes.

1.2) Specific Topics of Research

Throughout the existing body of research on convective dust processes, we have identified three subject areas where our understanding is incomplete and which therefore warrant the research comprising this dissertation: (1) quantifying the uncertainties related to modeling convective dust events at different scales, (2) assessing the effect of dust radiation interactions on haboobs, and (3) examining the feedbacks between the land surface, cold pools, and dust mobilization.

In the first study, we investigate how model resolution affects the prediction of convective dust events and dust concentrations. It has been shown that inadequate representation of convection in coarse model simulations, specifically the underestimation of high surface wind speeds in mesoscale haboobs, is a major contributor to errors in dust forecasts (Largeron et al., 2015; Pope et al., 2016). Because aerosol models are more computationally expensive to run, there is still a need at the regional, and especially global scale, to employ convective parameterizations (Benedetti et al., 2014, 2018). While a handful of studies have tested the difference in dust forecasts based on resolution, there is little agreement on the sign of the response or the processes responsible for the observed disparities in modeled dust fields

(Marsham et al., 2011; Heinhold et al., 2013; Ridley et al., 2013; Roberts et al., 2018). Diagnosing errors in coarse resolution dust models can assist forecasters, provide perspective for interpreting research at different scales, and aid model development by establishing which variables are most important to represent. Thus, the first goal of this dissertation is to:

(1) *Identify the sign and magnitude in the response of modeled dust fields in a regional numerical model to increasing horizontal resolution and identify which processes are responsible for the change in dust emissions and transport.*

In the second part of this dissertation, we explore interactions between the dust radiative effect and haboob dynamics and properties. Dust scatters and absorbs in both the solar shortwave and terrestrial longwave parts of the electromagnetic spectrum, which extinguishes and redirects incoming and outgoing radiation. Dust radiative effects have been studied in haboob-producing environments and were found to reduce insolation and surface temperatures during the day (Slingo et al., 2006; Banks et al., 2014) and prevent radiative cooling at night (Miller et al., 2004; Mallet et al., 2009; Marsham et al., 2016; Saleeby et al., 2019). However, the higher order effects that dust radiation has on stability, surface heat fluxes, and turbulence are unclear, especially for nocturnal cases (Miller et al., 2004; Liu et al., 2016; Saleeby et al., 2019), and whether these changes will elicit feedbacks to the strength and properties of a haboob is uncertain. To examine these mechanisms further, the focus of part two of this dissertation is to:

(2) *Quantify the dust direct radiative effect inside a haboob and the feedback it has on cold pool properties, strength, dust emissions, and deposition.*

The last study of this dissertation examines another uncertain feedback mechanism that occurs in haboobs between dust emissions and cold pool dynamics due to interactions with the land surface. The properties of the underlying land surface, especially soil moisture (Fast et al.,

2019; Drager et al., 2020) and surface heat fluxes (Bryan and Rotunno, 2014; Grant and van den Heever, 2016; 2018; Gentine et al., 2016; Drager and van den Heever, 2017; Kurowski et al., 2018), are important for cold pool strength, dissipation, and propagation, and the strength and lifetime of the cold pool will alter dust emissions (Huang et al., 2018). Yet, the same surface parameters that affect cold pool dynamics also affect dust mobilization from the surface (Marticorena and Bergametti, 1995; Shao et al., 1996; 2002; Shao and Lu, 2000; Ginoux et al., 2001). The interaction between the surface, the cold pool, and dust emissions is non-linear and it is ambiguous which factors are most important for predicting dust concentrations and other haboob properties. Therefore, the aim of part three of this dissertation is to:

(3) *Isolate which surface parameters, specifically surface type, soil moisture, and soil type, are most significant in predicting haboob dust and propagation, and identify the physical mechanisms responsible for the feedback between cold pool processes and dust mobilization.*

To answer these science questions, numerical model simulations of both real and idealized haboobs are utilized. Multiple modeling platforms are used to expand the opportunity to explore a wide range of environments and feedbacks that can occur in convective dust events. The first two parts will be investigated using two related case studies and are simulated with the Weather Research and Forecasting Model coupled with Chemistry (WRF-Chem) (Skamarock et al., 2008; Grell et al., 2005; Fast et al., 2006). The third study uses an ensemble of idealized haboob simulations using the Regional Atmospheric Modeling System (RAMS) (Pielke et al., 1992; Cotton et al., 2003; Saleeby and van den Heever, 2013). With models it is possible to identify the mechanisms responsible for these dust-environment feedbacks and enhance our understanding of haboob physics. In all, these experiments will address limitations in our

knowledge of regional dust modeling, direct radiative effects of mineral dust on cold pool properties and dynamics, and feedbacks between haboobs and the land surface.

1.3) Dissertation Structure

Chapter 2[1] investigates the impact of horizontal model resolution on convective dust lofting, and the contents of this chapter have been published in Bukowski and van den Heever (2020). This study is part of a larger body of collaborative work published in the Atmospheric Chemistry and Physics special issue "The Holistic Analysis of Aerosol in Littoral Environments - A Multidisciplinary University Research Initiative." Chapter 3[2] examines the effect of dust radiation interactions on haboobs, which has been assembled into a manuscript submitted to the Journal of Geophysical Research: Atmospheres and is currently under review. Chapter 4[3] examines the feedbacks between the land surface, cold pools, and dust mobilization, and the research in this chapter is being finalized for submission to the Journal of the Atmospheric Sciences. Chapter 5 summarized the main findings of this dissertation and provides recommendations for future work.

[1] This study, titled "Convective distribution of dust over the Arabian Peninsula: the impact of model resolution" has been published in the journal Atmospheric Chemistry and Physics (© Bukowski and van den Heever 2020) and a pre-typeset and copyedited version appears in this dissertation. Bukowski, J. and van den Heever, S. C. (2020). Convective distribution of dust over the Arabian Peninsula: the impact of model resolution. *Atmos. Chem. Phys*., 20, 2967–2986. https://doi.org/10.5194/acp-20-2967-2020

[2] This study, titled "Direct radiative effects in haboobs**"** has been submitted to the Journal of Geophysical Research: Atmospheres and is currently under review (Bukowski and van den Heever 2021a - submitted).

[3] This study, titled "The impact of land surface properties on haboobs**"** is in preparation for submission to the Journal of the Atmospheric Science (Bukowski and van den Heever 2021b – in preparation).

CHAPTER 2 - THE CONVECTIVE DISTRIBUTION OF DUST: THE IMPACT OF MODEL RESOLUTION

2.1) Introduction

The influence of atmospheric mineral dust is widespread in the weather and climate system, yet generating skillful forecasts of dust concentrations and their temporal and spatial evolution has been difficult to achieve. However, these potential improvements are contingent upon the quality of the dust model and initialization data, which models are known to be especially sensitive to. As such, substantial discrepancies exist across global models of similar resolution (Huneeus et al., 2011) and across regional models (Uno et al., 2006; Todd et al., 2008) in the magnitude of predicted dust flux from the surface to the atmosphere.

A major challenge in modeling dust processes is the scales of motion involved in its emission and subsequent transport. Dust particles mobilize from the surface due to wind erosion of arid soils, a mechanism that occurs on the micrometer scale, but once airborne mineral dust can deposit locally or be transported on the synoptic to global scales. Dust events initiate from both large-scale and synoptic dynamical flow regimes, as well as mesoscale features. Synoptic-scale uplift phenomena include monsoon troughs (e.g., Marsham et al., 2008), Shamal winds (e.g., Yu et al., 2016) and frontal systems (e.g., Beegum et al., 2018), whereas dynamical effects on smaller (meso) scales can raise dust via the production of convective outflow boundaries, or haboobs, (e.g., Miller et al., 2008), daytime turbulence or dry convective processes (e.g., Klose and Shao, 2012), and the morning mixing of the nocturnal low-level jet (NLLJ) momentum to the surface (e.g., Fiedler et al., 2013). When considering only meteorological dust sources, wind drives dust emissions, meaning that the underlying processes that contribute to the wind fields must be resolved in a model to create an accurate dust forecast.

One potential source of disagreement in models stems from the scaling emissions in dust parameterizations, which relate the surface emissions proportionally to the second or third power of surface wind speed. This means that minor miscalculations in modeled wind speeds go on to produce more substantial errors in the dust concentration calculations (e.g., Menut, 2008). Current aerosol forecast and climate models are run at fine enough grid spacing to simulate synoptic events but still typically employ cumulus parameterizations, which are incapable of resolving dry and moist mesoscale updrafts and downdrafts that can potentially loft and/or scavenge dust. Schepanski et al. (2015) found that online dust models are likely to be most sensitive to the initialization data compared with other model options, which adds additional uncertainty to dust forecasts. Pope et al. (2016) and Largeron et al. (2015) both postulated that an inadequate representation of convection in coarse model simulations, specifically the underestimation of high surface wind speeds in mesoscale haboobs, is a major contributor to errors in dust models.

The misrepresentation of dust concentrations in models with cumulus parameterizations has been investigated across several modeling platforms, mostly from the perspective of dust lofting mechanisms at the surface. Heinold et al. (2013) ran the UK Met Office Unified Model (UM) over West Africa with offline dust emissions and found that, of the factors they tested, the model was most sensitive to explicit versus parameterized convection. Furthermore, in the Heinhold et al. (2013) study, dust emissions were reduced by roughly 50 % as the grid resolution was increased to convection-permitting scales. This was found to be due to the parameterized simulations underestimating moist convective activity but drastically overestimating the NLLJ dust uplift mechanism, which is a similar relationship to that originally identified in Marsham et al. (2011).

Conversely, studies using different numerical dust models have identified other relationships between the horizontal resolution and dust emissions. Roberts et al. (2018) also used the UM to investigate this relationship over the Sahara and Sahel and reported little change in the dust emissions when moving from parameterized to explicit convection; however, they also noted that the NLLJ maximum decreased as the convective maximum increased. Reinfried et al. (2009) simulated a haboob case study from Morocco with the Lokal Modell – MultiScale chemistry aerosol transport (LM-MUSCAT, since renamed COSMO-MUSCAT) regional model and found increased dust emissions in a convection-permitting simulation versus those with cumulus parameterizations. They also established that the model was more sensitive to the choice of cumulus parameterization rather than the change in horizontal resolution. Similarly, Bouet et al. (2012) identified an increase in dust emissions with increasing model resolution using the Regional Atmospheric Modeling System coupled to the Dust Prediction Model (RAMS-DPM) while simulating a Bodélé depression case study. Ridley et al. (2013) showed that global aerosol models with parameterized convection were also sensitive to model resolution and that higher horizontal resolution led to higher dust emissions.

With the added computational expense of running aerosol code, the resolution of dust forecast models lags relative to their weather-only prediction counterparts for both global and regional prediction systems (Benedetti et al., 2014, 2018). Global dust forecasts generated by several aerosol models are available through the Sand and Dust Storm Warning Advisory and Assessment System (SDS-WAS; http://www.wmo.int/sdswas, last access: 20 December 2019), but none of the models in the SDS-WAS are currently run at fine enough grid spacing to be considered convection-permitting (SDS-WAS Model inter-comparison and forecast evaluation technical manual; last updated January 2018). While regional numerical weather prediction

models have moved into convection-permitting scales, the added computational cost of aerosol parameterizations means that convective parameterizations will be a necessity for longer in models that employ online aerosol predictions. It is also clear that horizontal model resolution remains an understudied factor in regional dust modeling. As such, exploring differences across cumulus parameterizations and those relative to convection-permitting resolutions continues to be relevant and vital to better understand aerosol forecasting and aerosol–cloud–environment interactions.

While previous studies have begun to examine the effect of horizontal model resolution on dust emissions and airborne dust concentrations, there are several factors that warrant more investigation. As it stands, there is little agreement on the sign of the response in dust emissions to a change in horizontal model resolution, which seems to vary based on the regional model being utilized. Most studies have concentrated on the change in dust emissions based on moving from parameterized convection to convection-permitting scales, while ignoring the possible sensitivity due to the choice of the cumulus parameterization itself. Furthermore, much of the previous literature focused on how the increase in resolution affects convective outflow boundaries and surface/near-surface processes as dust sources rather than convective transport and the vertical redistribution of dust and its radiative effects at different levels of the atmosphere. In this paper, we seek to address these limitations in the understanding of the effects of horizontal model resolution on dust concentrations. Therefore, the goal of the research presented here is to quantify the sign and magnitude in the response of modeled dust fields in a regional numerical model to increasing horizontal resolution.

In order to achieve our stated goal, we will use numerical simulations of a case study to examine the variability in dust emissions and vertical dust concentrations and fluxes due to

(1) the choice of convective parameterization, (2) convection-permitting versus parameterized convection, and (3) the impact of these variations on radiation, specifically aerosol heating rates. These simulations are performed using the Weather Research and Forecasting Model coupled with Chemistry (WRF-Chem) (Skamarock et al., 2008; Grell et al., 2005; Fast et al., 2006) a platform that has been tested for its sensitivity to vertical resolution for dust extinction coefficient profiles (Teixeira et al., 2016) as well as horizontal model resolution and convective transport for chemical species such as carbon monoxide (e.g., Klich and Fuelberg, 2014) but not for dust. These simulations will represent a case study of a summertime coastal convective dust event over the Arabian Peninsula, a relatively understudied region compared with areas such as the Sahara (Jish Prakash et al., 2015), despite being the world's second largest dust emission region (Tanaka and Chiba, 2006).

2.2) Case Study and Model Description

2.2.1) WRF-Chem Model Description and Physics

To investigate the Arabian Peninsula case study, WRF-Chem version 3.9.1.1 was used to simulate the dust outbreak meteorology and aerosol fields. WRF-Chem is an online numerical chemical transport model that allows for interactive aerosol processes, including feedbacks between the meteorology, aerosol, and radiation. The model was coupled to the Goddard Chemistry Aerosol Radiation and Transport (GOCART) module (Ginoux et al., 2001), which allowed for feedbacks between the meteorology and aerosols and is described in more detail in Sect. 2.2.2. The model was tested with and without dust initial and boundary conditions from the Community Atmosphere Model with Chemistry (CAM-Chem) global model (Emmons et al., 2010). The concentrations of dust advected through the lateral boundary conditions was too

small to have an effect on the results, and the initial conditions introduced a spurious decreasing integrated dust trend over time when modeled aerosol optical depth (AOD) was compared to AERONET observations. While the initial conditions led to a higher integrated dust mass, it did not change the conclusions of the study. To remove this factor and focus more on the meteorological processes that actively loft and transport dust in real-time, no chemistry or aerosol initial/lateral boundary conditions were used. Rather, the aerosol fields were initialized with zero concentrations and were allowed to evolve naturally from the model meteorology, aerosol, surface, and radiation processes.

The meteorological and sea surface temperature initial and lateral boundary conditions were sourced from the 0.25 °, 6-hourly Global Data Assimilation System Final analysis (GDAS-FNL) (National Centers for Environmental Prediction/National Weather Service/NOAA/U.S. Department of Commerce, 2015). The model was run from 00:00:00 UTC on 2 August 2016 to 00:00:00 UTC on 5 August 2016 and produced output at 30 min intervals. The following model parameterizations were employed and kept constant across the simulations, with similar WRF physics options being utilized elsewhere to study dust effects (e.g., Alizadeh Choobari et al., 2013): the Morrison double-moment microphysics scheme (Morrison et al., 2005, 2009), the RRTMG longwave scheme (Iacono et al., 2008), the Goddard shortwave radiation scheme (Chou and Suarez, 1999), the Noah land surface model with multiparameterization options (Niu et al., 2011; Yang et al., 2011), and the MYNN level 3 boundary layer parameterization (Nakanishi and Niino, 2006; 2009). The convective parameterizations and horizontal resolutions tested will be discussed in Sect. 2.2.4. A summary of the physics options utilized can be found in Table 2.1.

2.2.2) GOCART Dust Emissions and Dust Uplift Potential

WRF-Chem is coupled to the GOCART dust module, which parameterizes the emission of dry mineral dust mass from the surface. GOCART is single-moment in mass, meaning there is no number information available to change the number of cloud condensation nuclei or ice nuclei in the microphysics. As such, the indirect effects of dust cannot be simulated with this setup. Using this model, dust is emitted to the atmosphere in five discrete effective radii bins (0.5, 1.4, 2.4, 4.5, and 8.0 μm) based on Eq. 2.1:

$$F_p = CSs_p\, U^2(U - U_t)\ \ if\ U > U_t \qquad [2.1]$$

In Eq. 2.1, F_p is the dust flux from the surface (kg m^{-2} s^{-1}) for each of the radii bins (p), S represents the wind erosion scaling factor (0 to 1) established by the Ginoux et al. (2001) soil erodibility map, s_p is the fraction of each size class within the soil (0 to 1) based on the silt and clay fraction of the soil type, U is the 10 m wind speed (m s^{-1}), and U_t is the threshold velocity of wind erosion (m s^{-1}). C is a tuning constant (set here to a default 1 kg s^2 m^{-5}), which can be set by the user to increase or decrease the total dust flux based on regional observations (e.g., Zhao et al., 2010; Kalenderski et al., 2013; Dipu et al., 2013). If the wind speed is less than the threshold velocity, no dust will loft from the surface. Most of the terms in Eq. 2.1 are time invariant (C,S,sp), except for the wind speed (U) and wind erosion threshold (U_t). U_t is a function of soil wetness, and is calculated using the relationship found in Eq. 2.2:

$$U_t = \begin{cases} 6.5\sqrt{\frac{\rho_p - \rho_a}{\rho_a} g D_p}(1.2 + log_{10} w_{soil}) & if\ w_{soil} < 0.5 \\ \infty & if\ w_{soil} \geq 0.5 \end{cases} \qquad [2.2]$$

For Eq. 2.2, ρ_p is the dust particle density (kg m^{-3}), ρ_a is the density of air (kg m^{-3}), g is gravitational acceleration (m s^{-2}), and w_{soil} is the soil wetness fraction (0 to 1). Similar to Eq. 2.1, Eq. 2.2 includes a threshold, whereby above a soil wetness of 0.5, no dust will be emitted. If the

threshold criteria are met and dust lofts from the surface, it is then transported based on the simulated meteorological fields from WRF, including advection, convection, and turbulent mixing, and is removed from the atmosphere via gravitational settling and wet deposition. Here, wet deposition (Yang et al., 2015) is included as a scavenging mechanism to provide a more realistic picture of the moist convection transport process. Aerosol radiation interactions in the SW and LW (Barnard et al., 2010) are included in the simulations to understand the implications that lofted dust has on the energy budget of the case study and are discussed in Sect. 2.3.3.

Before dust can amass in and influence the atmosphere, it must first be emitted from the surface. Because of the threshold values included in the GOCART dust parameterization equations (Eqs. 2.1-2.2), it is important to understand how often the modeled near-surface wind speeds exceed the wind threshold value. A parameter useful in describing the influence of the wind on dust emissions is dust uplift potential (DUP), proposed by Marsham et al. (2011) and based on Marticorena and Bergametti (1995). The DUP parameter is an offline approximation for the relative amount of dust expected to loft from the surface. DUP is a convenient way to perform first-order sensitivity tests on the meteorology without having to rerun the model and provides a framework for deconvolving the variables in Eqs. 2.1-2.2. Here, we have adapted the DUP parameter from Marsham et al. (2011) into three variations (Eqs. 2.3, 2.4, 2.5); these variations allow researchers to alter the complexity of the analysis by varying the degrees of freedom.

$$DUP(U) = U^3 \left(1 + \frac{A}{U}\right)\left(1 - \frac{A^2}{U^2}\right) \quad [2.3]$$

$$DUP(U, U_t) = U^3 \left(1 + \frac{U_t}{U}\right)\left(1 - \frac{U_t^2}{U^2}\right) \quad [2.4]$$

$$DUP(U, U_t, S) = SU^3 \left(1 + \frac{U_t}{U}\right)\left(1 - \frac{U_t^2}{U^2}\right) \quad [2.5]$$

In Eq. 2.3, U_t is set to a constant wind speed, A, thereby making DUP a function of only the near-surface wind speed; for the purpose of this paper U_t is set to 5 m s^{-1}, but it has been tested elsewhere across the range of 5–10 m s^{-1} (e.g., Marsham et al., 2011; Cowie et al., 2015; Pantillon et al., 2015). This simplified equation for dust uplift has been used in previous dust studies and is useful to include here to place this manuscript in the context of existing literature. Equation 2.4 is slightly more intricate in that it considers the model evolution of U_t due to changing soil wetness from precipitation and land surface processes, calculated by Eq. 2.2. Lastly, Eq. 2.5 builds on Eq. 2.4 by including the soil erodibility scaling factor (S), which recognizes that the U and U_t relationship is valid only if it occurs over potential dust source regions. As U, U_t, and S are entangled in the GOCART dust parametrization found in Eqs. 2.1–1.2, the seemingly minor variations between the DUP parameters in Eqs. 2.3–2.5 are crucial for isolating which processes, or combination of processes, are sensitive to the horizontal resolution of the model and, hence, to the analysis performed here.

2.2.3) Domain, Nesting, and Cumulus Parameterizations

Several horizontal model grid spacings (45, 15, and 3 km) of the Arabian Peninsula domain (Fig. 2.3) were tested to identify the sensitivity of modeled dust concentrations to the model's horizontal resolution. For the two coarsest simulations (45 and 15 km), cumulus parameterizations were employed to represent shallow and deep convection. The 45 km simulation was run with only the Betts–Miller–Janjic (BMJ) cumulus parameterization (Janjic, 1994), while five different cumulus parameterizations were tested for the 15 km simulations to determine the sensitivity of dust lofting to different cumulus parameterizations, including the following: the BMJ; the Kain–Fritsch, KF (Kain, 2004); the Grell 3-D ensemble, GD (Grell,

1993; Grell and Dévényi, 2002); the Tiedtke scheme, TD (Tiedtke, 1989; Zhang and Wang, 2011); and the simplified Arakawa–Schubert scheme, AS (Arakawa and Schubert, 1974; Han and Pan, 2011). A 15 km simulation with no cumulus parameterization was also run, but the results were similar and within the spread of the 15 km simulations that employed cumulus parameterizations and are not included here. The finest-resolution simulation (3 km) was run at convection-permitting scales; hence, no cumulus parameterizations were invoked. The 3 km simulation was initialized as a one-way nest from the 15 km BMJ simulation, which served as its parent lateral boundary conditions. Other combinations of nests were tested, but the results were not sensitive to which 15 km simulation was used as the parent nest, or lateral boundary conditions, for the 3 km simulation. A summary of the model domains is also found in Fig. 2.3.

The cumulus parameterizations tested in this study for the 15 km simulations vary with respect to their methods for triggering and then characterizing convective processes at the sub-grid-scale level. BMJ is a moisture and temperature adjustment scheme that acts to restore the pre-convective unstable thermodynamic profile to a post-convective stable and well-mixed reference profile, whereas the other cumulus parameterizations (KF, GD, TD, and AS) employ a mass-flux approach to determine updraft and downdraft mass transport. Across the mass-flux parameterizations, GD is unique in that it computes an ensemble of varying convective triggers and closure assumptions and then feeds the ensemble mean back to the model. Furthermore, all five schemes represent shallow convection in addition to deep convection, the mass-flux schemes include detrainment of water and ice at cloud top, and AS and TD are formulated to include momentum transport in their calculations. These differences across parameterizations will result in varying updraft and downdraft speeds and precipitation rates, which will have consequences for the vertical transport of airborne dust as well as the strength of convective

outflow boundaries and, therefore, dust emission at the surface. Several cumulus parameterization schemes were tested to introduce spread into the solutions and to represent the 15 km results as a five-member ensemble mean with uncertainty estimates. Because this paper seeks to investigate the effect of horizontal resolution on dust transport, comparing individual cumulus schemes against one another is outside the scope of this study.

2.2.4) Averaging and analysis methods

Because the representation of convective processes varies across the simulations, the results will focus on composite statistics from the 3 d case study. The authors make no attempt to track and match individual convective elements across simulations, as their triggering, timing, and development (or lack of development) will fluctuate depending on the model resolution and cumulus parameterization, thus making a truly consistent analysis problematic. Instead, this paper takes a step backward and aims to quantify, in an average sense, how the choice of horizontal resolution and parameterized convection affects dust concentrations in the WRF-Chem model across the Arabian Peninsula. The analyses and averages are processed within the yellow box shown in Fig. 2.3, disregarding all other grid points outside the Arabian Peninsula study area. Analyses that are temporally averaged are only averaged over the last 2 d of the simulation (00:00:00 UTC on 3 August 2016 to 00:00:00 UTC on 5 August 2016) to account for model spin-up in the first 24 h. All results are summed over the five dust bins in the GOCART model rather than being treated separately. Lastly, the results from the five 15 km simulations are averaged together to produce a mean 15 km resolution response; this mean is presented, along with the maximum and minimum spread across these simulations for reference.

2.2.5) Case Study Overview

The dust event simulated for this study occurred from 2 to 5 August 2016 across the Arabian Peninsula, originating from a combination of synoptic and mesoscale dust sources. A meteorological analysis of this event, including an attribution of specific dust sources to meteorological features can be found in Miller et al. (2019) and will not be reiterated in detail here. Rather, a snapshot of the meteorology and dust fields from the WRF-Chem simulation on 3 August at 15:00:00 UTC can be found in Figs. 2.1–2.2 as a reference to the typical meteorological setup for this case study.

For this event, the high summertime temperatures in the desert of the Arabian Peninsula produce a thermal low couplet at the surface, with one low centered over Iraq and the other over the Rub' al Khali desert in Saudi Arabia (Fig. 2.1c). The local low-pressure couplet leads to cyclonic surface winds between these two areas (Fig. 2.1e), comprised of northerly flow from Iraq into Saudi Arabia, with retuning southerly flow from Oman over the Persian Gulf and into Kuwait, and is a major non-convective contributor to the dust budget for this case study (Fig. 2.1f). In addition to these large-scale flow patterns, a daytime sea breeze brings moist, maritime air from the coast of Yemen and Oman inland into the otherwise arid Saudi Arabian basin (Fig. 2.1e, d). This moisture gradient is also evident in the skew-T diagrams, which represent an inland radiosonde release site at Riyadh (Fig. 2.2a), and a site closer to the coast in Abha (Fig. 2.2b), both located in Saudi Arabia. There is a stark difference in low-level moisture between the two sites, although both display a subsidence inversion aloft between 500 and 600 hPa. Furthermore, nocturnal low-level jets form along the Zagros Mountains (in Iran and Iraq) and the Red Sea, both of which have been studied previously in the literature (Giannakopoulou and Toumi, 2012; Kalenderski and Stenchikov, 2016).

Due to the region's inherent moisture constraints, convection is limited spatially to the coastal regions of the Arabian Peninsula, as is most summertime convective and non-convective precipitation in this region (e.g., Shwehdi, 2005; Almazroui, 2011; Hasanean and Almazroui, 2015; Babu et al., 2016). Moist convective cells develop along a low-level convergence line between the northerly basin flow and sea breeze front (Fig. 2.1g, h) aided by elevated terrain in Yemen and Oman (Fig. 2.1a). This convective setup along the southern portion of the Arabian Peninsula is a feature evident in each day of this case study, initializing diurnally in the local late afternoon and early evening, thereby providing 3 days of data for analysis, with the height of convective activity occurring on 3 August. Individual convective cells form along the convergence line, a typical Middle Eastern characteristic (Dayan et al., 2001), but do not organize further, owing to a lack of upper-level synoptic support and insufficient moisture in the interior of the peninsula. Nevertheless, the convective line does produce outflow boundaries, which loft dust from the surface and are the main convective dust source for this case study. More information on model validation of this study, including comparisons of these simulations with AOD observations can be found in Saleeby et al. (2019), which shows that WRF-Chem systematically underestimates the dust AOD for this event

2.3) Results

2.3.1) Temporal Evolution

2.3.1.a) Dust Uplift Potential

The first process of interest in determining the sensitivity of modeled dust concentrations to horizontal resolution in WRF-Chem is the amount of dust lofted from the surface to the atmosphere. Figure 2.4 depicts the average DUP for the simulations at each 30 minute output,

using Eq. 2.3–2.5 to separate out the importance of the different mechanisms regulating dust emissions.

Regardless of which DUP parameter is used, almost all of the simulations capture the bimodal daily maximum in dust emissions in the local midmorning (06:00 UTC) and late afternoon (13:00 UTC) due to the mixing of the NLLJ with the surface and convective outflow boundaries, respectively. The only resolution where the bimodality is absent is the 45 km simulation, which captures the NLLJ mechanism but misses the second convective activity maximum. The coarsest simulation overestimates the near-surface wind speeds related to the NLLJ mechanism, which subsequently inhibits convection later in the day. Because of this, the 45 km simulation has the highest DUP(U) (Fig. 2.4a) based only on wind speed (Eq. 2.3), which is a result similar to the Heinhold et al. (2013) and Marsham et al. (2011) studies over the Sahara.

However, when taking the calculated threshold wind velocity into account (Eq. 2.4), the convection-permitting simulation (3 km) displays the strongest DUP(U,U_t) at the local late afternoon convective maximum (Fig. 2.4c). For this to be the case compared with the DUP(U) parameter, the 3 km simulation must have a lower threshold wind velocity (Fig. 2.5a) than the simulations with parameterized convection. As the threshold wind velocity is proportional to soil wetness (Eq. 2.2), this implies that the convection-permitting simulation will on average have drier soil, or more grid points below the soil wetness threshold than the parameterized simulations. Rainfall is generated differently in parameterized versus convection-permitting simulations, and it has been well documented that parameterized simulations produce more widespread light rainfall, whereas more intense rainfall tends to develop over smaller areas in convection-permitting simulations (e.g., Sun et al., 2006; Stephens et al., 2010). From a domain

average perspective, rainfall in the 3 km simulation will cover less area, leading to the soil moisture threshold not being exceeded as frequently as in the parameterized cases.

This spatial difference in rainfall leads to the 3 km case having drier soil on average across the domain, which is evident in the surface fluxes represented by the Bowen ratio of sensible to latent heat fluxes in Fig. 2.5c. When the Bowen ratio is above one, more of the surface heat exchange with the atmosphere is in the form of sensible heat flux, rather than latent heat flux. Dry soils are characterized by low values of latent heat flux, and therefore exhibit higher Bowen ratios. The 3 km simulation exhibits a higher Bowen ratio on 3 and 4 August, indicating that the soil is drier in the convection-permitting simulation on average. This result implies that disparities in land surface properties across the varying model grid resolutions are important for modulating dust emissions, both from the perspective of convection-permitting versus parameterized convection and associated precipitation as well as latent and sensible heat fluxes.

Adding on to the complexity of the DUP parameter, when the location of dust sources is considered in the DUP(U,U_t,S) calculations (Eq. 2.5), some of variability between the local NLLJ and convection maxima is lost in the 3 km simulation (Fig. 2.4e) on 3 August. Furthermore, including the scaling factor reduces the magnitude of the DUP parameter to roughly 10 % of the initial values for DUP(U) and DUP(U,U_t). Incorporating the dust source function in DUP works not only as a scaling factor for the magnitude of potential dust emissions but also impacts the relative importance of dust production mechanisms (NLLJ versus convection). This shift is a consequence of the location in which these processes occur. For instance, the reduction in the 3 km convective maximum on 3 August between DUP(U,U_t) and DUP(U,U_t,S) signifies that convection is occurring in locations that are not active dust source

regions. Without information on the dust source regions, this process would be assigned an unrealistic dominance over the NLLJ mechanism in terms of DUP.

All simulations are similar for the first 24 h of spin-up until the processes begin to diverge on 3 August, where the convection-permitting simulation produces the maximum DUP(U,U_t,S) both during the local daytime and nighttime hours. On the final day of the case study (4 August), the convection-permitting simulation has the lowest DUP(U,U_t,S), with the NLLJ maximum dominating over the convective maximum in both the 3 and the 15 km mean, due to reduced convective activity in the fine-resolution simulations. Examining the percent difference in DUP between the coarse and fine simulations (Fig. 2.4b, d, f), the average percent difference between the 3 and 15 km simulations is at a minimum when only wind speed is considered and increases as the degrees of freedom in DUP increases. For the DUP(U,U_t,S) case, the average percent difference is between 10 % and 65 % lower in the 15 km simulations than in the convection-permitting simulation, with a maximum difference of 85 % and a spread across parameterizations of 20 %. This implies that the convection-permitting WRF-Chem simulation has the potential to loft up to 85 % more dust than those with parameterized convection.

2.3.1.b) Vertically Integrated Dust Mass

The differences in DUP(U,U_t,S), or dust flux from the surface to the atmosphere, specifically the enhanced values for the convection-permitting simulation on 3 August, will lead to more dust lofting than in the coarse simulations. To see how differences in the dust emissions translate into differences in airborne concentrations of dust, Fig. 2.6 demonstrates the temporal evolution of the spatially averaged, vertically integrated dust mass throughout the vertical column. Here, the convection-permitting simulation records upwards of 150 % more integrated

dust mass compared with the coarse-resolution simulations. Across the coarse simulations, the 45 and 15 km runs have similar vertically integrated dust magnitudes, despite the temporal differences in DUP(U,U_t,S). This is due to the overestimation of the NLLJ in the 45 km simulations being offset by the enhanced convective dust lofting in the 15 km simulations.

The discrepancy in the diurnal maxima across horizontal resolutions is similar to the results of the UM in Marsham et al. (2011) and Heinhold et al. (2013). However, the results here differ in that both of these previous studies found a stronger NLLJ response in 12 km simulations with convective parameterizations than was found here in the 15 km parameterized ensemble. In contrast to the findings of Marsham et al. (2011) and Heinhold et al. (2013), dust emissions and airborne dust mass increase in the WRF-Chem simulations in the convection-permitting simulation, which is in closer agreement with the studies of Reinfried et al. (2009) and Bouet et al. (2012), who used COSMO-MUSCAT and RAMS-DPM, respectively. Considering each study used a different model and therefore different physics, it is unsurprising that the results vary. However, it is not apparent how much of a role the region or specific case study plays in this difference, and this is an area for future work.

The temporal trends in vertically integrated dust mass lag behind those observed in the DUP plots in Fig. 2.4. Particularly at time steps where DUP decreases, the change in integrated dust mass follows several hours later. The time series of gravitational settling rates at the surface (Fig. 2.5b) also lags behind the DUP trends, which implies that the removal mechanisms for dust take time to act on the airborne particles once they are emitted. The rates of gravitational settling are higher in the convection-permitting simulation compared with the coarse simulations because more dust is available aloft to settle out. Nevertheless, Fig. 2.6a suggests that this increase in gravitational settling rates in the 3 km case is not enough to offset the higher dust emissions, or

that the vertically integrated dust quantities would be similar across all the simulations. The fact that the vertically integrated dust values are higher in the 3 km simulation, despite higher rates of gravitational settling, implies that there must be a mechanism that acts to keep dust suspended longer in the convection-permitting simulations than in those with parameterized convection. There are clearly more processes occurring above the surface to influence the vertically integrated dust quantities than just a simple surface emission to surface deposition ratio. This will be further deconstructed by examining vertical profiles in the following section.

2.3.2) Vertical Characteristics

2.3.2.a) Vertical Dust and Velocity Profiles

Moving away from vertically integrated quantities to a time- and domain-averaged vertical snapshot of dust (Fig. 2.7a), the vertical dust profile follows a generally exponentially decreasing function and tapers off to low dust concentrations in the range of 5–6 km above ground level (a.g.l.). A widespread subsidence inversion is present near 6 km throughout the case study time period over the inner basin of the Arabian Peninsula (Fig. 2.2), acting as a cap on vertical motions and dust transport. Because dust concentrations do not vary much above this height, the plots in Fig. 2.7 have been truncated at 9 km. There is a higher concentration of dust at every level in the convection-permitting simulation compared with that in the coarse simulations. Examining the percent difference plot between the convection-permitting and other simulations in Fig. 2.7b, there is a difference of approximately 80 % at the surface, which increases upwards to ∼180 % at 6 km. Above this level, the percent difference between the convection-permitting and coarse simulations changes sign, but the overall concentration is

extremely low, and, as such, the authors make no attempt to assign meaning to the differences above 6 km.

For dust to reach higher levels in the atmosphere, it must undergo vertical transport to move it aloft from its initial source region at the surface. Several mechanisms could be responsible for vertical dust transport in the Arabian Peninsula, including flow over terrain, daytime mixing (dry convection), and, lastly, moist convective updrafts, whose representation (explicit versus parameterized) is a defining difference between the horizontal resolutions tested in this paper. An investigation of the effect that increasing resolution has on updraft and downdraft strength can be found in Fig. 2.8, which represents the mean of all vertical velocities above or below 0 m s^{-1}, including points that are not vertically continuous. As resolution increases, the average range in vertical velocity also increases. The simulations with parameterized convection have lower mean updraft/downdraft speeds than the convection-permitting simulation, which are of the order of ∼75 % weaker near the surface for the 15 km runs and ∼110 % weaker for the 45 km run. It is known that the updraft radius scales with the grid spacing in numerical models (e.g., Bryan and Morrison, 2012), with a compensating increase in updraft speed as the radius decreases. This relationship skews the frequency of vertical velocities to higher values. Irrespective of resolution, the mean updraft speeds in the WRF-Chem simulations are slightly higher than the downdraft speeds, whereas at the surface mean downdraft speeds are higher than updraft speeds; this is a consideration that will be discussed further in Sect. 2.3.2.b.

2.3.2.b) Vertical Dust Flux

The implication for dust transport based on vertical velocities is convoluted, as updrafts and downdrafts work concurrently to redistribute aerosol. As noted in Jung et al. (2005), convective updrafts will lift aerosol particles upward into the free atmosphere, while downdrafts simultaneously limit the maximum vertical extent of these particles. However, the convective transport simulations in Jung et al. (2005) demonstrate that these opposing processes do not act as equal opposites in time, magnitude, and space. This canon holds true for the Arabian Peninsula simulations as well. Figure 2.9 contains contoured frequency by altitude diagrams (CFADs) of vertical velocity (Yuter and Houze, 1995) normalized by the total number of grid points in each simulation. The normalization is performed to remove an artificial larger frequency in the higher-resolution simulations that arises because there are more grid spaces available to count. Because no vertical velocity threshold is imposed, a majority of points straddle zero. To highlight variability away from the zero line, the CFAD contours are plotted using a log scale.

Similar to the mean plots in Fig. 2.8, as resolution increases so does the variability in updraft and downdraft speeds. There is a striking difference between the spread in vertical velocities at all altitudes across the 45 km, 15 km mean, and 3 km simulations in Fig. 2.9. In the 45 km run, most of the velocities straddle ±1–2 m s^{-1}, whereas the convection-permitting simulation ranges from −10 to 30 m s^{-1}. Not only is the range larger, but the normalized frequency is greater in the fine-resolution simulation as well. The inference here is that stronger updrafts will transport dust higher in the atmosphere, and that stronger updrafts are observed more frequently in the convection-permitting simulation, thereby enhancing the vertical dust transport.

Combining the information on the vertical distribution of dust and updraft/downdraft speeds, it is possible to calculate a domain-averaged dust flux profile (Fig. 2.8). Again, the magnitude of the dust flux upwards and downwards from the surface through 6 km a.g.l. is higher in the convection-permitting simulation compared to the parameterized simulations. Moreover, the mean near-surface upwards dust flux is stronger than that for the downward dust flux, which coincides with the mean updraft speeds being slightly higher than the mean downdraft speeds at these same vertical levels (Fig. 2.8). This relationship also holds in the dust flux CFADs (Fig. 2.9), in which the upward and downward flux of dust has more variability in the 3 km simulation, and stronger vertical dust fluxes are more frequent.

Similarly, there is more dust transport evident at higher vertical levels in the convection-permitting simulation, which has implications for the residence time of the dust particles. As dust is transported higher in the atmosphere, absent any sort of external motion or coagulation outside of gravitational settling, the atmospheric lifetime of the particles will increase. Figure 2.10 shows the theoretical terminal velocity of dust particles in WRF-Chem using the Stokes settling velocity with slip correction for pressure dependence (Fig. 2.10a) and their lifetime based on different starting heights in the atmosphere (Fig. 2.10b), which increases exponentially away from the surface. As such, dust in the convection-permitting simulation will take longer to settle out, leading to the higher observed vertically integrated dust values (Fig. 2.5) compared with the parameterized simulations. Looking at the distribution of downdrafts in the vertical velocity CFADs (Fig. 2.9), there is a clear bimodal signal aloft in both the convection-permitting and 15 km simulations; this is representative of two distinct subsidence layers, which act as a cap on vertical transport. The local minimum occurs around 6 km, which could explain why dust fluxes also taper off at this level.

At the surface, higher dust flux values are found in association with the downdrafts, producing a pronounced skewness towards high, yet infrequent values of strong negative dust flux towards the ground (Fig. 2.9). It is hypothesized that this skewness is a consequence of the dissimilar background dust conditions in the vicinity of near-surface downdrafts and updrafts, similar to the results found by Seigel and van den Heever (2012), who studied the ingestion of dust by a supercell storm. Updrafts originate in relatively clear air, and they consume background dust and transport it upwards. However, downdrafts occur through the cold pool; hence, their source is, at least partially, within the dusty cold pool. As such, downdrafts will have access to more dust and, thus, transport more of it in the downward direction. This skewness warrants further research, preferably from an idealized perspective, to better understand the relationship between storm dynamics, dust emissions, and transport.

In all, the increased vertical dust concentration profile and vertically integrated dust values in the 3 km run are a product of several processes working together. Compared with the simulations with parameterized convection, the 3 km run has enhanced potential for dust uplift due to stronger resolved downdrafts and lower wind velocity thresholds; higher vertical transport due to more frequent, stronger updrafts; and a lengthier theoretical residence time once being lofted to higher levels.

2.3.3) Impacts on Radiation

Beyond the first-order sensitivity of model resolution to dust emissions and concentrations for the Arabian Peninsula case study, there are higher-order effects that disseminate from changing dust concentrations. One example is the modification of atmospheric heating/cooling rates and the radiation budget due to dust absorption and scattering (see

Sect. 2.1). The domain- and time-averaged shortwave (SW), longwave (LW), and net dust heating/cooling rates are found in Fig. 2.11. The average dust heating and cooling rates were calculated over the last 48 h of the simulation as a difference between the radiation tendency with dust aerosols and without. Ostensibly, as dust concentrations increase in the model as resolution increases so does the magnitude of the radiative effects. There is a stronger SW cooling and LW heating effect in the 3 km simulation, and this trend follows the vertical distribution of dust from Fig. 2.7, again tapering off near 5–6 km a.g.l.

Most interestingly, however, is the difference in the net aerosol heating rate. In the lowest layer (<1.5 km), there is a sign change between the fine and coarse simulations. The SW effect in the convection-permitting simulation is strong enough to elicit a net cooling effect in this near-surface layer. Conversely, the LW aerosol heating effect dominates in the coarse simulations, resulting in a net warming effect. The model has a stronger SW effect for dust based on the prescribed index of refraction, but is also related to the timing of dust emissions, considering the SW effect is only active during the daytime. The difference between warming and cooling can have cascading effects on the thermodynamic profile, static stability, and future convective development, which, in turn, impacts the relative importance between convection and the NLLJ discussed earlier. The sensitivity of dust concentrations to horizontal model resolution is important to understand in its own right, but this sensitivity also leads to higher-order changes in model predictions. If NWP models or global climate models (GCMs) are going to incorporate dust radiative effects, concentrations need to be highly constrained, not only to accurately capture the magnitude but also the sign of the response.

2.4) Discussion and Recommendations

For this Arabian Peninsula event, the horizontal resolution in the WRF-Chem model has a considerable effect on the dust budget of the region. Because aerosol prediction models and GCMs still employ cumulus parameterizations, it is important to discuss the uncertainties unearthed in this paper as well as recommendations for past and future forecasts and research that will be generated prior to our ability to consistently run these models at convection-permitting resolutions.

In an average sense, there will be higher dust concentrations produced in convection-permitting simulations compared with those with parameterized convection. The major point here is that the uncertainty in dust concentrations for simulations using different cumulus parameterizations (15 km ensemble) or those using different horizontal resolutions with the same cumulus parameterizations (45 km versus 15 km) is small relative to the differences between the use of parameterized versus convection-permitting scales. *Most of the uncertainty in the model's predicted dust concentrations comes from the choice to either parameterize convection or run at convection-permitting scales*.

The results of this research do not stand alone in the literature focused on the impact of horizontal model resolution on dust emissions, and there are several similarities and differences to note when comparing this paper to previous studies. Firstly, concerning the diurnal variation in dust emissions, we find a similar response in the NLLJ mechanism to that of Heinhold et al. (2013) and Marsham et al. (2011), whereby the coarsest simulations overestimate the early morning wind speeds caused by the mixing of the jet to the surface and fail to capture the late afternoon/early evening convective dust lofting mechanism. In these previous studies, the convection-permitting simulation reduces the importance of the NLLJ and enhances the

convective maximum, but it still retains the NLLJ as the dominant process for dust uplift. Overall, Heinhold et al. (2013) and Marsham et al. (2011) found a net reduction in dust uplift while running at convection-permitting scales. While the NLLJ mechanism is found to be similar here, the analysis reveals an opposite response in WRF-Chem for the Arabian Peninsula, in which the convective maximum dominates, but the NLLJ is still an important mechanism, which thereby leads to more rather than less dust in the convection-permitting simulations. The net increase in dust concentrations in WRF-Chem is similar to the findings of Reinfried et al. (2009), although Reinfried et al. (2009) focused mainly on haboobs, which may point to convection being the source of agreement rather than the balance between the NLLJ and convection. At this point, we cannot determine whether the discrepancies between our results and previous literature comes from regional or case study differences in the importance of these mechanisms to the dust budget, differences in the models' representation of these processes, or a combination of the two. In all, more work needs to be carried out to investigate the relationship between the NLLJ and subsequent late afternoon convection in dust-producing regions as well as the representation of this in numerical models.

For the Arabian Peninsula region, from a vertically integrated viewpoint, it is possible to rudimentarily tune the dust concentrations of the coarse simulations to that of the convection-permitting simulation by multiplying by an average constant derived from the dust difference plots in Figs. 2.6–2.7, which would be of the order of ~2. This is an offline solution, which would aid in enhancing the accuracy of a first-order forecast of vertically integrated or surface dust, and/or AOD. This factor would have to be scaled further, as comparison of the WRF-Chem model to AERONET sites and other AOD observations (Saleeby et al., 2019) shows that WRF-Chem underestimates dust under these conditions. Nevertheless, attempting to use this tuning

parameter online in the model (i.e., adjusting the tuning constant, *C*, in Eq. 2.1) would not reconcile the differences from a dust flux standpoint. Even if more dust were to be emitted from the surface, the parameterized simulations still lack the necessary variability in updrafts and downdrafts, especially updraft strength, to transport the dust upwards and away from the surface, thus misrepresenting the atmospheric lifetime of these particles in the process.

Moreover, tuning the dust concentrations will not change the effect that horizontal resolution has on the soil characteristics, particularly soil moisture, and, hence, on the a priori threshold wind speeds which are important in calculating dust lofting in the first place (Fig. 2.4). If dust concentrations are inaccurately predicted in the coarse simulations, or erroneously tuned, the higher-order online feedbacks will also be incorrect, such as modifications to the radiative budget and feedbacks to the thermodynamic profile, static stability and mesoscale features, particularly those driven by differences in thermodynamic gradients, such as sea breezes and cold pool propagation.

2.5) Conclusions

In this study, we have quantified the response sign and magnitude in modeled dust fields in the WRF-Chem regional model to increasing horizontal resolution and the manner in which convection is represented for a summertime Arabian Peninsula event. We have investigated the variability in dust concentrations and fluxes due to the choice of convective parameterization, the representation of convection in the model (explicit versus parameterized), and the effect that these differences in dust concentrations have on aerosol heating rates. The case study was simulated at three different horizontal resolutions (45, 15, and 3 km), with the two coarsest simulations run with cumulus parameterizations, and the 3 km simulation run at convection-

permitting resolution. To understand the uncertainty across different parameterizations, five separate cumulus parameterizations were tested in an ensemble (BMJ, AS, GD, TD, and KF) at 15 km grid spacing.

The convection-permitting simulation exhibited a stronger potential for dust uplift as a function of modeled wind speed, wind threshold, and the location of dust sources. The wind threshold for dust lofting in the 3 km simulation was lower on average than that for the 15 km or 45 km. This is due to differences in grid resolution leading to changes in the soil moisture, whereby the 3 km simulation displays lower soil wetness across the domain. Furthermore, a distinct difference across simulations was identified in the representation of the bimodal daily maximum in dust emissions in the local midmorning (mixing of the NLLJ to the surface) and late afternoon (convective outflow boundaries). Compared with the 3 km case, the 45 km simulation overestimates the contribution from the NLLJ and underestimates the role of convection in dust emissions.

The 3 km simulation also produced higher vertically integrated dust values at every time step as well as higher dust concentrations at every vertical level in the lower troposphere (below 6 km a.g.l.). The uncertainty in dust concentrations for simulations using different cumulus parameterizations (15 km ensemble spread) is much smaller than the difference between the parameterized and convection-permitting convection cases. For the WRF-Chem Arabian Peninsula simulations, the modeled dust fields were most sensitive to the choice of parametrizing or explicitly resolving convective processes. The enhanced dust concentrations in the convection-permitting case are the result of stronger downdrafts lofting more dust from the surface and stronger updrafts carrying dust to higher levels of the atmosphere, thereby increasing the airborne lifetime of the dust particles. The difference in dust mass across the simulations

leads to a significant modification of the radiation budget, specifically the aerosol heating rate. The convection-permitting simulation revealed a greater SW and LW effect; moreover, for aerosol heating rates in the lowest levels, the SW cooling is stronger than LW heating, leading to a net cooling effect. Conversely, the opposite radiative response is present in the parameterized cases, resulting in a net warming effect, causing a change in sign in the lowest levels compared with the convection-permitting case.

There are a number of implications these results may have on forecasting and future studies. The dust concentrations in the coarse simulations could be tuned offline to match those in the convection-permitting simulation using the percentage difference plots included in Figs. 2.5–2.6. This tuning would be of the order of ~2. However, because vertical transport is essential to the vertical concentrations and lifetime of the particles, this tuning factor cannot be applied online. Even if such a tuning were applied, this change will not accurately capture higher-order feedbacks to the meteorology, thermodynamic environment, and radiation budget of the Arabian Peninsula, or to the soil moisture wind threshold velocities. Finally, this work also points to the need to better constrain dust concentrations in numerical models and further develop our understanding of the relationship between storm dynamics and dust processes.

2.6) Addendum

Since the publication of Bukowski and van den Heever (2020), it has been recommended that modifications be made to the size distribution and partitioning of dust particles into mass bins in the WRF-Chem coupled GOCART model (Ukhov et al., 2021) to address the model underpredicting dust AOD. For the GOCART version used in Bukowski and van den Heever (2020), the size partitioning fractions are set to (0.1, 0.25, 0.25, 0.25, 0.25) for the 5 effective

radii bins (0.5, 1.4, 2.4, 4.5, and 8.0 μm), respectively. Based on observations of AOD, Ukhov et al. (2021) suggests the size fractions be changed to (0.15, 0.1, 0.25, 0.4, 0.1) so that fine-mode submicron particles contribute more to AOD. Because small particles are more efficient per unit mass in contributing to AOD compared to large particles, less dust mass would be necessary to match AOD values than in the current configuration where large particles dominate the contribution to AOD.

Nevertheless, the modeled volumetric size distribution from Bukowski and van den Heever (2020) was compared to AERONET size distribution measurements in Figure 10 of Miller et al. (2019) and the two were found to be similar. Complicating matters, when AOD from Bukowski and van den Heever (2020) was compared to MODIS and AERONET AOD in Figures 6-7 in Saleeby et al. (2019), AOD was underpredicted. The underestimation of AOD is consistent with Ukhov et al. (2021), but the size distribution seems to match with the previous size partitioning values in GOCART. From a radiation perspective (Sec. 2.3.3), because small particles scatter and absorb more strongly per unit mass, we hypothesize that shifting the size distribution toward smaller values may enhance scattering and absorption. However, it is uncertain if the ratio between shortwave scattering and longwave absorption, represented by the single scattering albedo (SSA), would be affected and whether that would change the results in Chapter 2 and in Chapter 3. The simulations in Bukowski and van den Heever (2020) and those from Chapter 3 will have to be rerun with the GOCART improvements and be compared to AERONET and MODIS AOD a second time to identify the effect on the results.

2.7) Figures and Tables

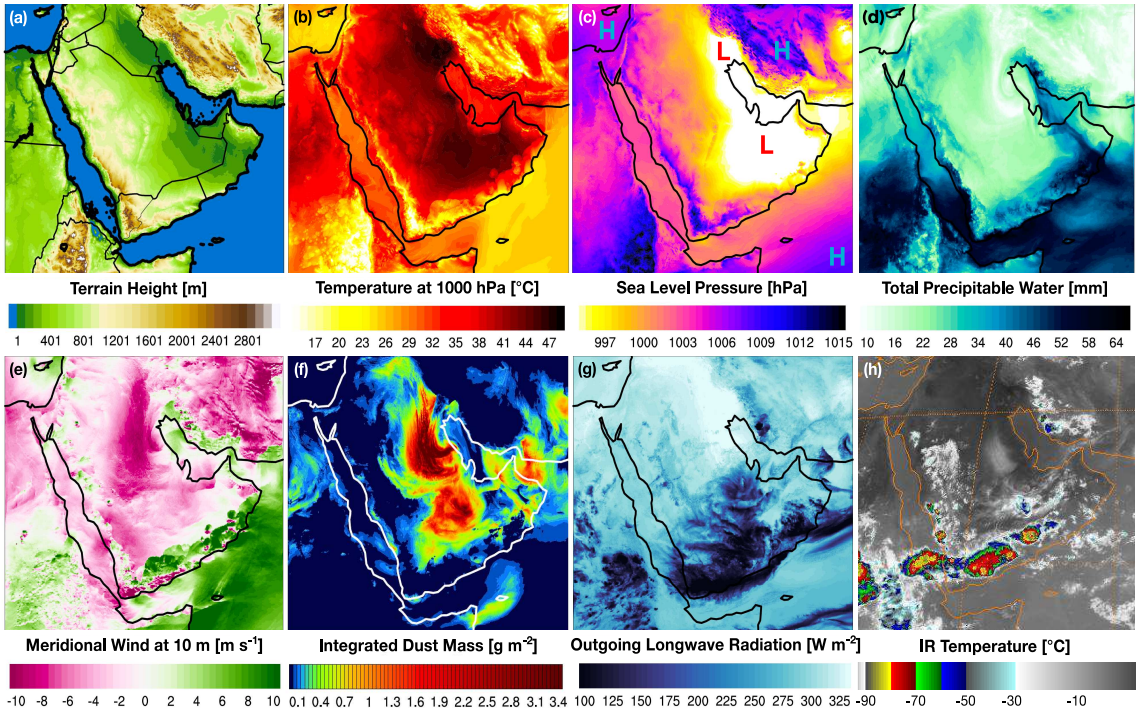

Figure 2.1) Case study topography and meteorology for 3 August 2016 at 15:00 UTC: (a) terrain height and national boundaries, (b) 1000 hPa temperature, (c) sea level pressure, (d) total precipitable water**,** (e) meridional winds at 10 m a.g.l**.,** (f) vertically integrated dust mass, (g) outgoing longwave radiation, and (h) IR temperature. Panel (h) is observed from Meteosat-7, whereas panels (a)–(g) are snapshots from the 3 km WRF-Chem simulation.

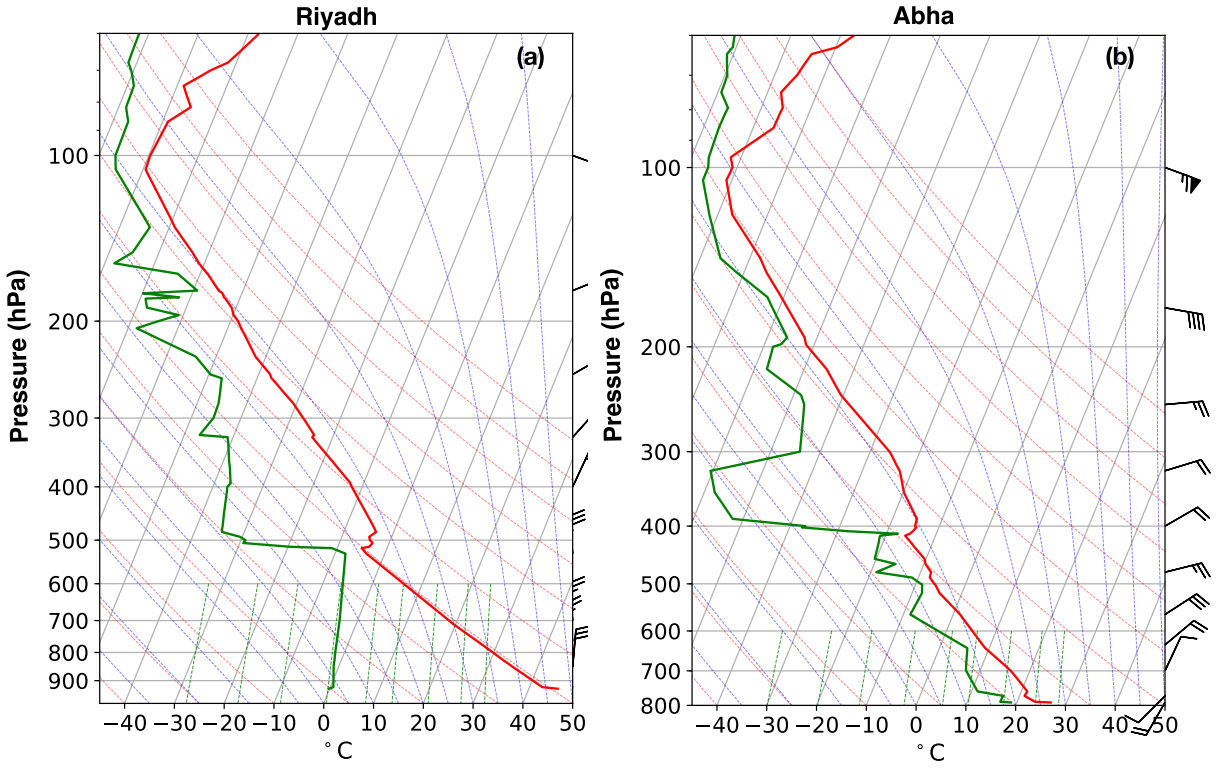

Figure 2.2) Skew-T diagrams for two radiosonde release sites in Saudi Arabia on 3 August 2016 at 12:00 UTC for an inland location (a) and a location nearer to the coast (b).

Table 2.1) Summary of the WRF-Chem model options utilized and the simulation setup.

WRF-Chem Version 3.9.1.1	Parameterization/model option
Simulation start	2 August 2016, 00:00:00 UTC
Simulation end	5 August 2016, 00:00:00 UTC
Domains	$dx = dy = 45$ km/15 km/3 km
Nesting	One-way
Vertical levels	50 stretched
Initialization	GDAS-FNL reanalysis
Aerosol module/erodible grid map	GOCART/Ginoux et al. (2001)
Microphysics	Morrison double-moment
Radiation	RRTMG longwave and Goddard shortwave
Land surface	Noah-MP land surface model
Cumulus schemes	Betts–Miller–Janjic (BMJ)
(45 and 15 km grids only)	Kain–Fritsch (KF)
	Grell 3-D ensemble (GD)
	Tiedtke scheme (TD)
	Simplified Arakawa–Schubert (AS)
Boundary layer/surface layer	MYNN level 3

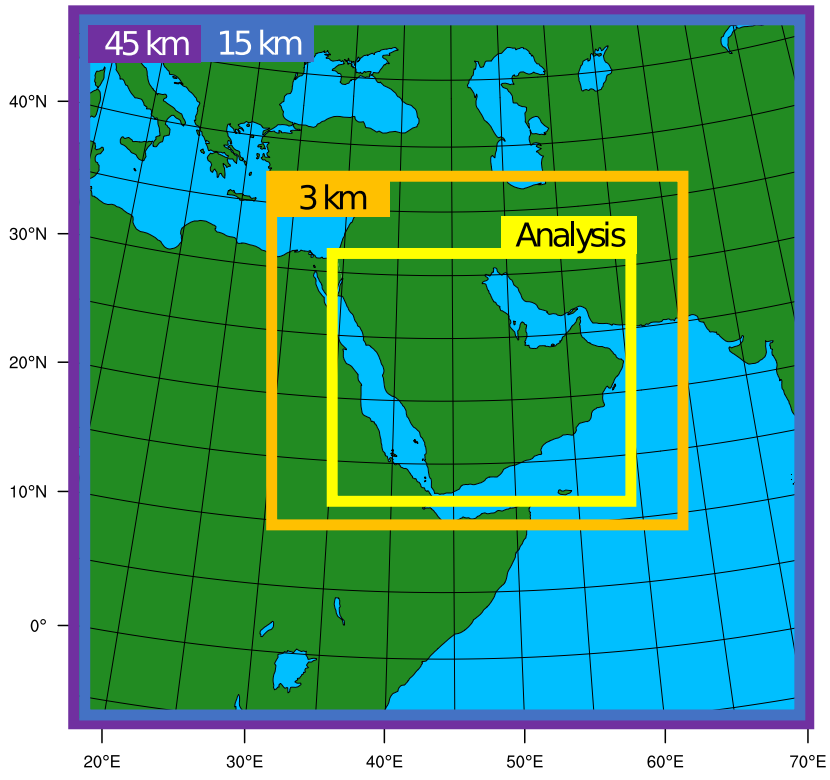

Figure 2.3) Model domain setup and analysis region for the 45 km (purple) and 15 km (blue) independent simulations with cumulus parameterizations as well as the 3 km nested convection-permitting simulation (orange). The averaging region for the analysis is denoted in yellow.

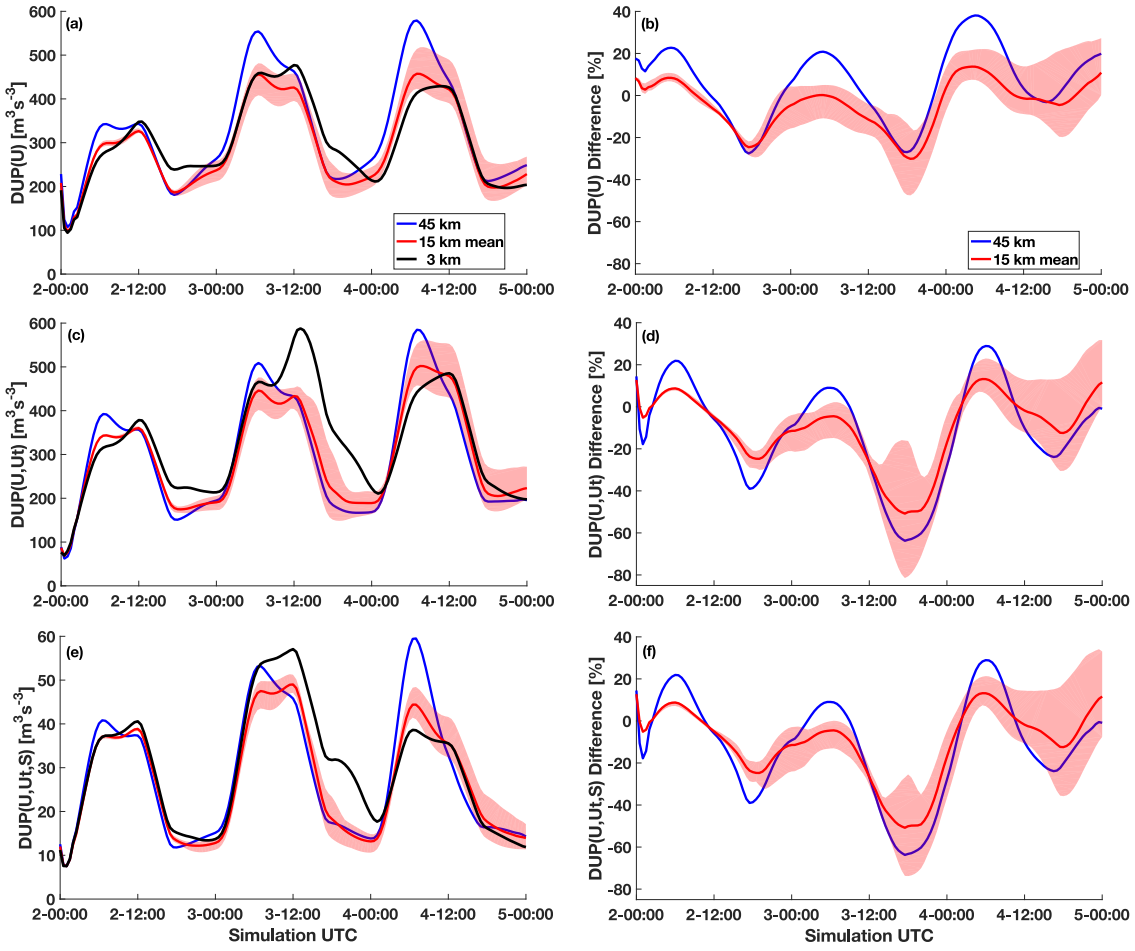

Figure 2.4) The spatially averaged dust uplift potential for (a) DUP(U), (c) DUP(U,U_t), and (e) DUP(U,U_t,S) for the 45 km (blue), 15 km mean (red), and 3 km (black) simulations with the maximum and minimum spread across the 15 km simulations indicated in light red shading. Note that there is a change in scale in the ordinate in panel (e)**.** (b, d, f) The percent difference between the 3 km convection-permitting simulation and the simulations employing cumulus parameterizations for the different DUP parameters.

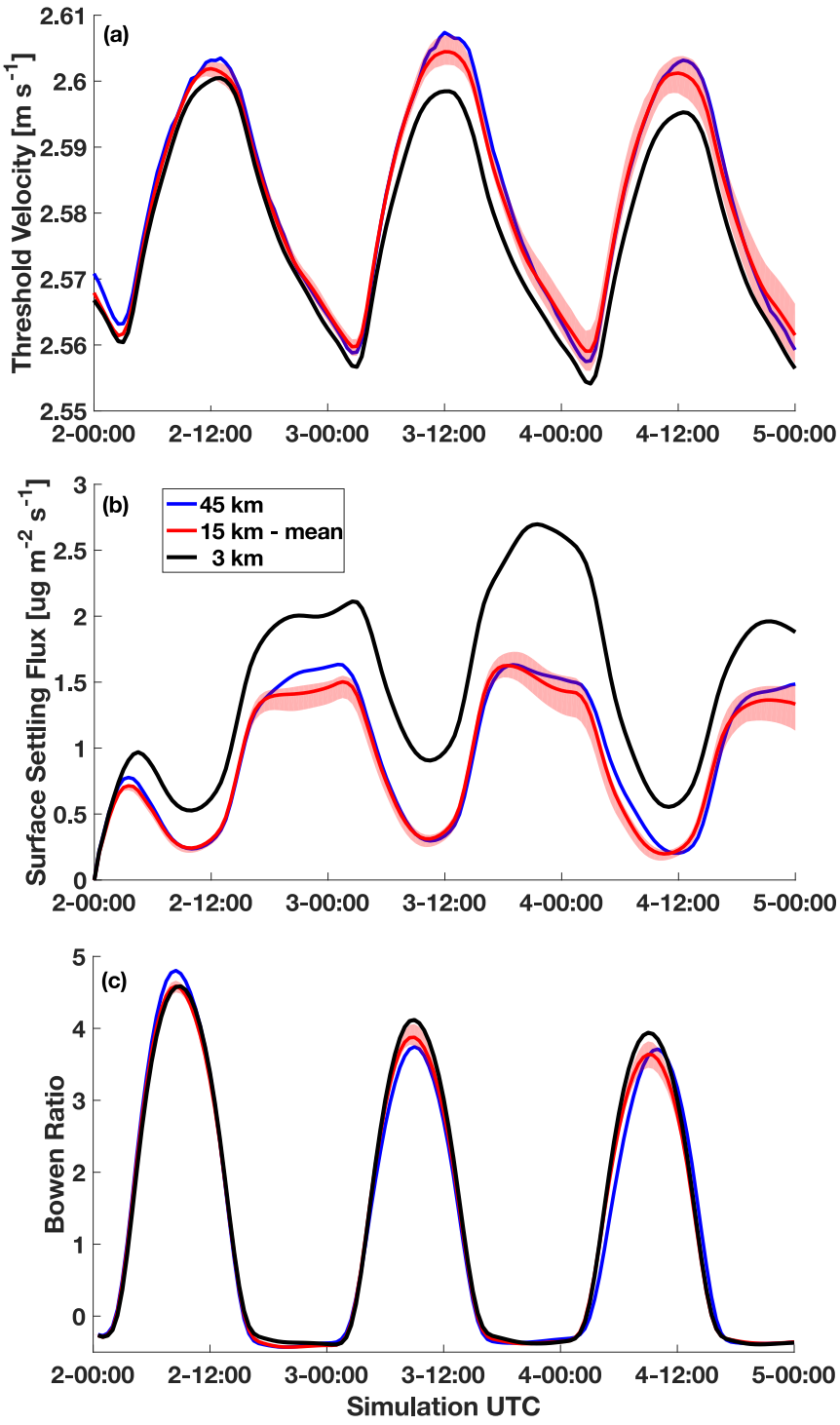

Figure 2.5) Spatially averaged (a) dust uplift threshold velocity, (b) dust surface settling flux, and (c) the Bowen ratio of sensible to latent heat flux. Colors and shading are the same as in Fig. 2.4.

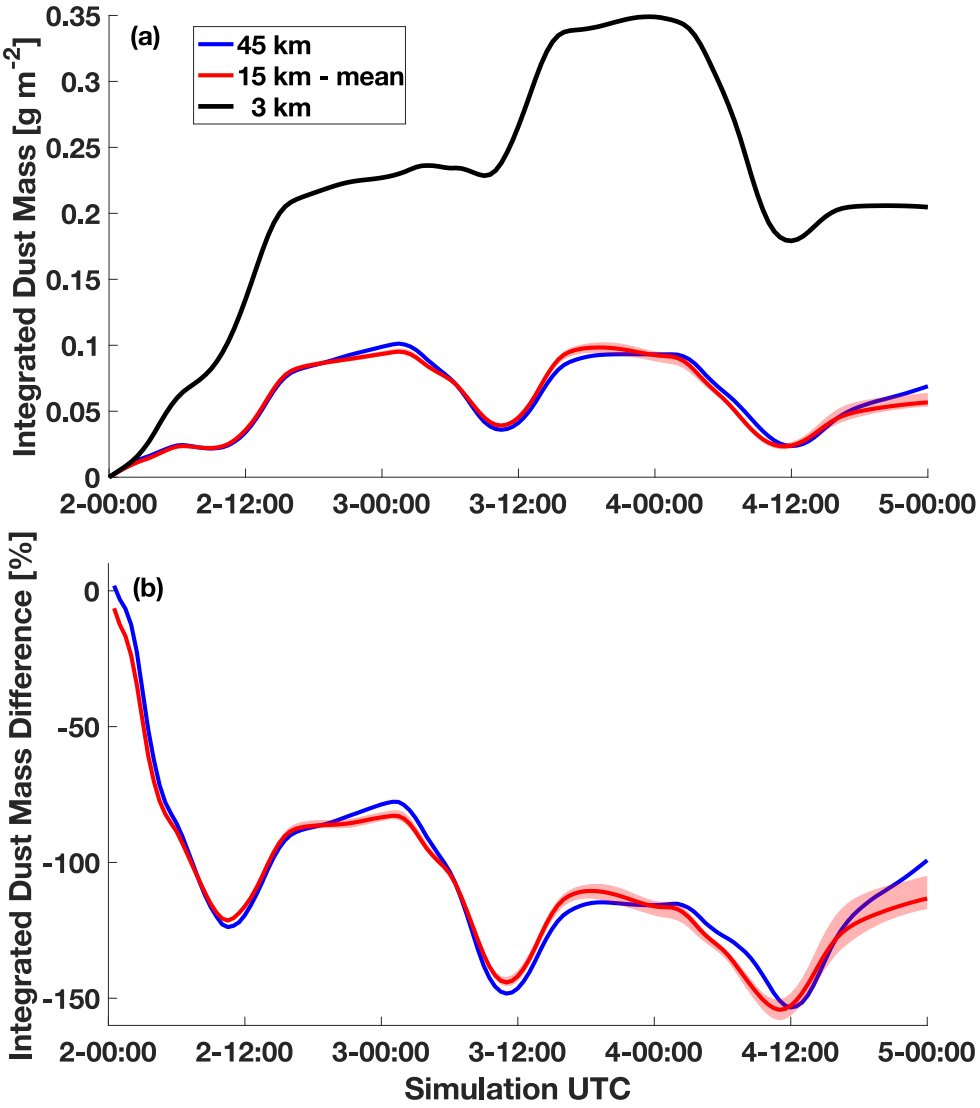

Figure 2.6) Spatially averaged, vertically integrated dust mass. Colors and shading are identical to those used previous figures.

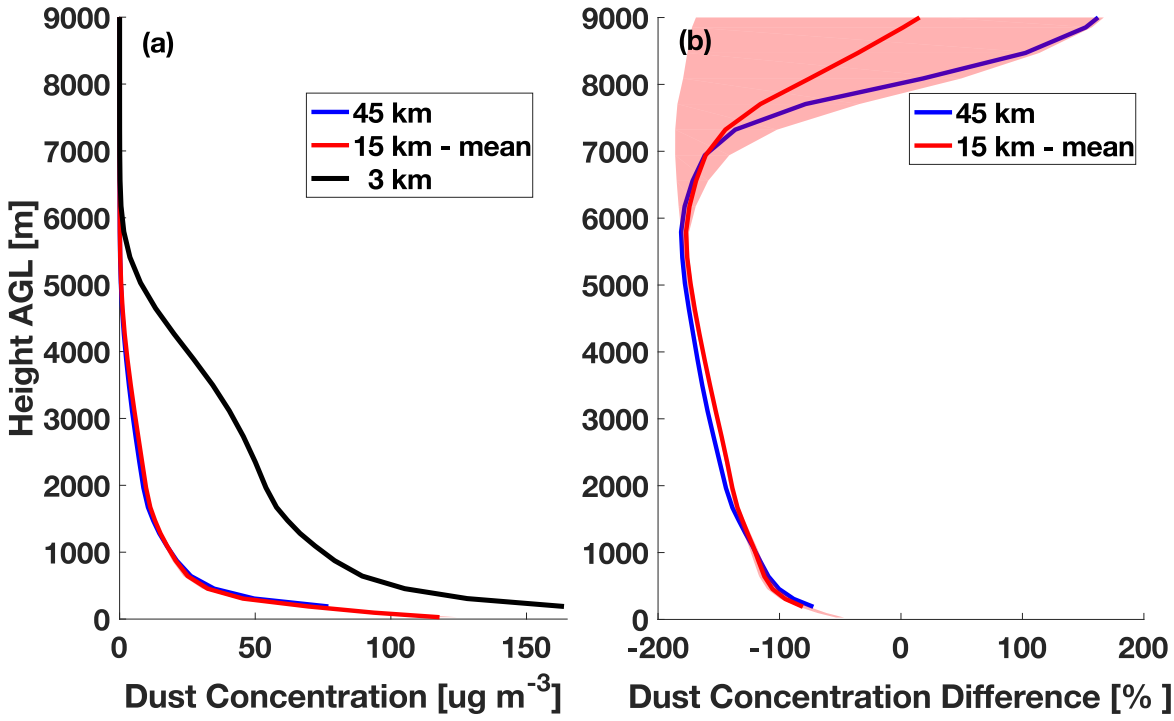

Figure 2.7) (a) Spatially and temporally averaged vertical dust concentrations as well as **(b)** the percent difference between the 3 km convection-permitting simulation and the simulations employing cumulus parameterizations. Plots are truncated at 9 km as the values above this height do not significantly vary from what is shown here. Colors and shading are identical to those used in previous figures.

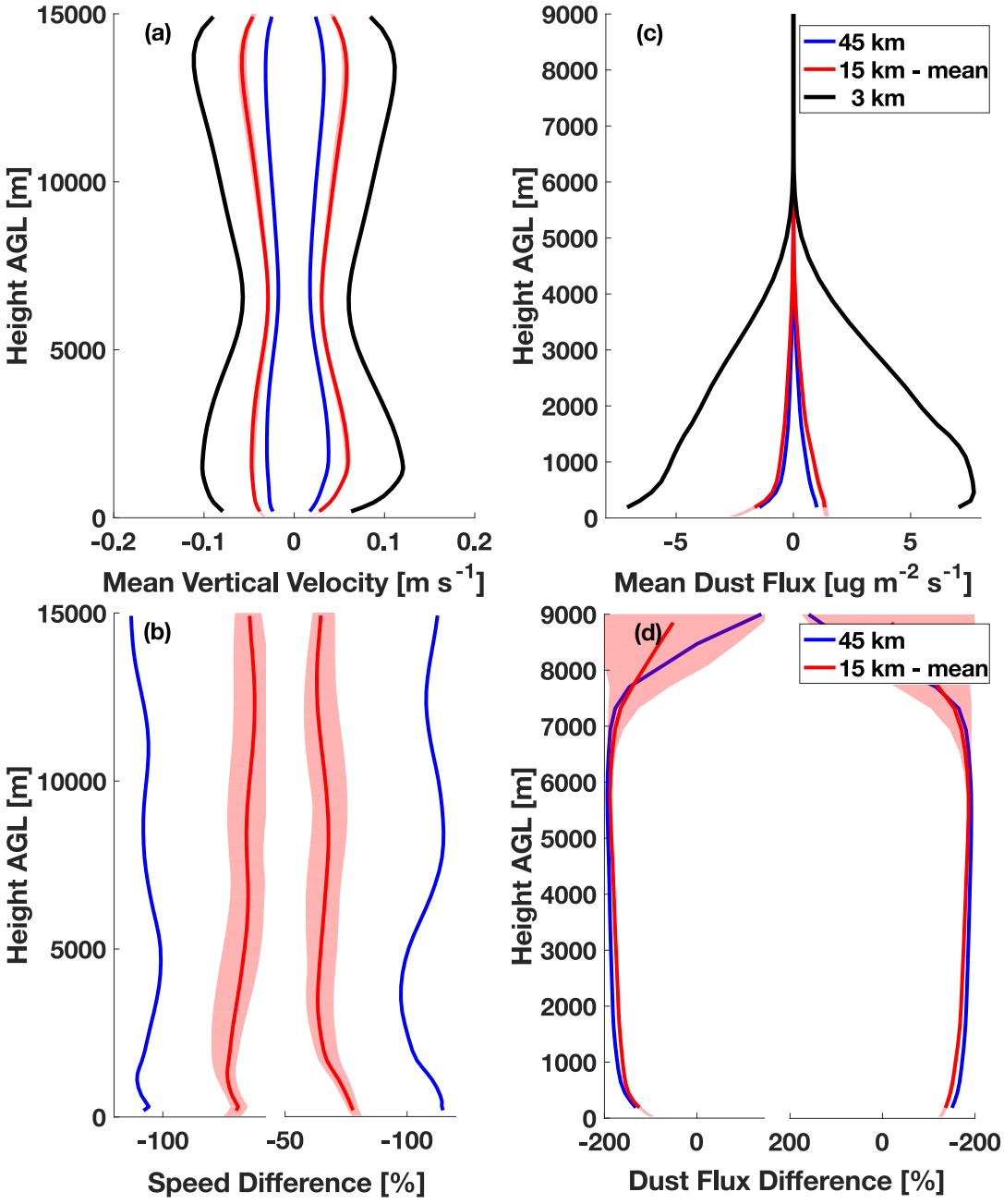

Figure 2.8) (a) Spatially and temporally averaged vertical velocities as well as (b) the percent difference between the 3 km convection-permitting simulation and the simulations employing cumulus parameterizations. All velocities above or below zero were considered. Colors and shading are identical to those used previous figures. Panels (c) and (d) are the same as panels (a) and (b) but represent the vertical dust mass flux. Note that the vertical axes are truncated at 9 km in panels (c) and (d) as the values above this height do not vary significantly from what is shown here.

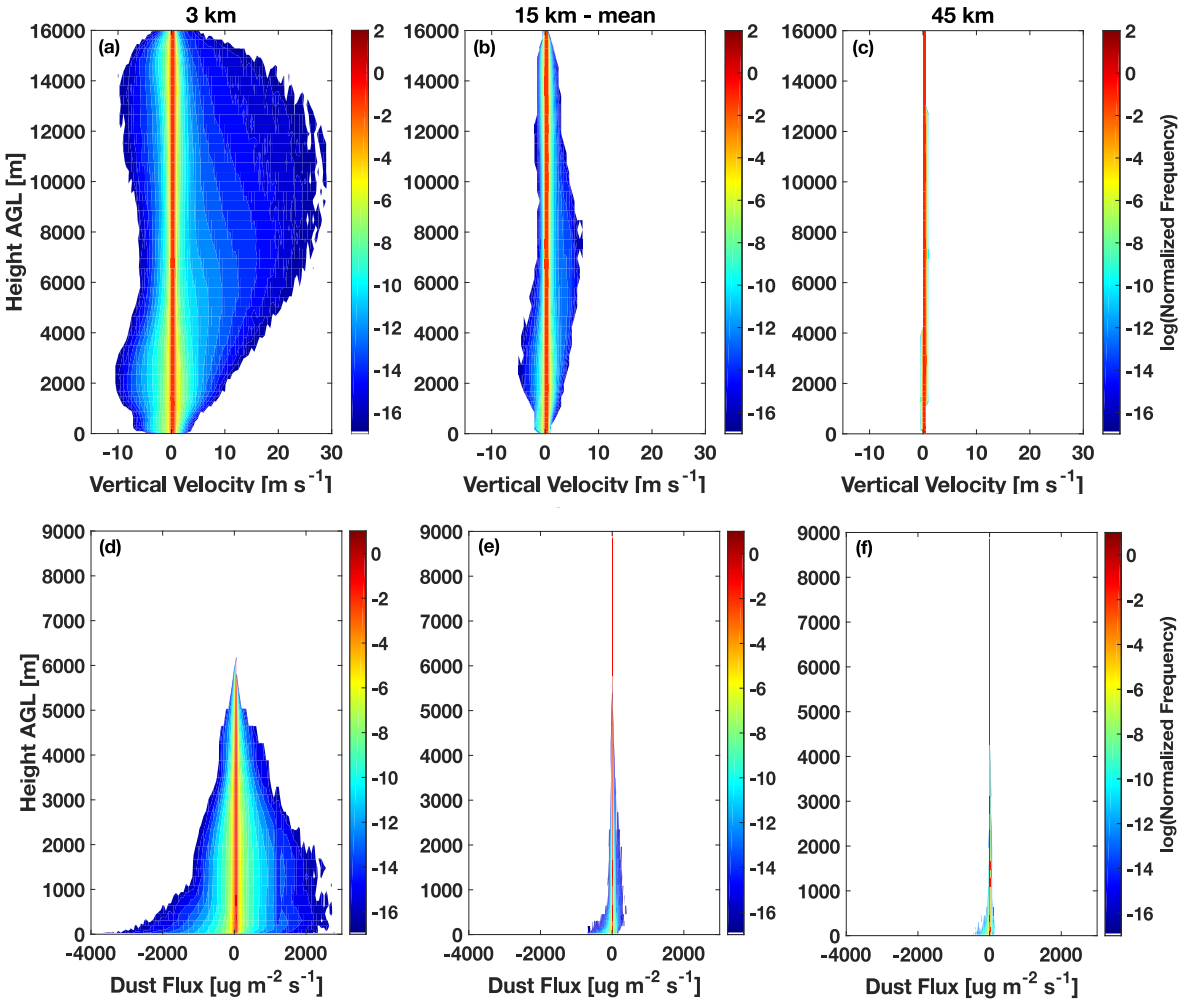

Figure 2.9) (a, b, c) Contoured frequency by altitude diagrams (CFADs) for vertical velocity, normalized by the number of grid points in each respective simulation. The contours are computed on a log scale to highlight the variances away from zero. Panels (d), (e), and (f) show the same but for vertical dust mass flux. Note that panels (d), (e), and (f) are truncated at 9 km as the values above this height do not significantly vary from what is shown here.

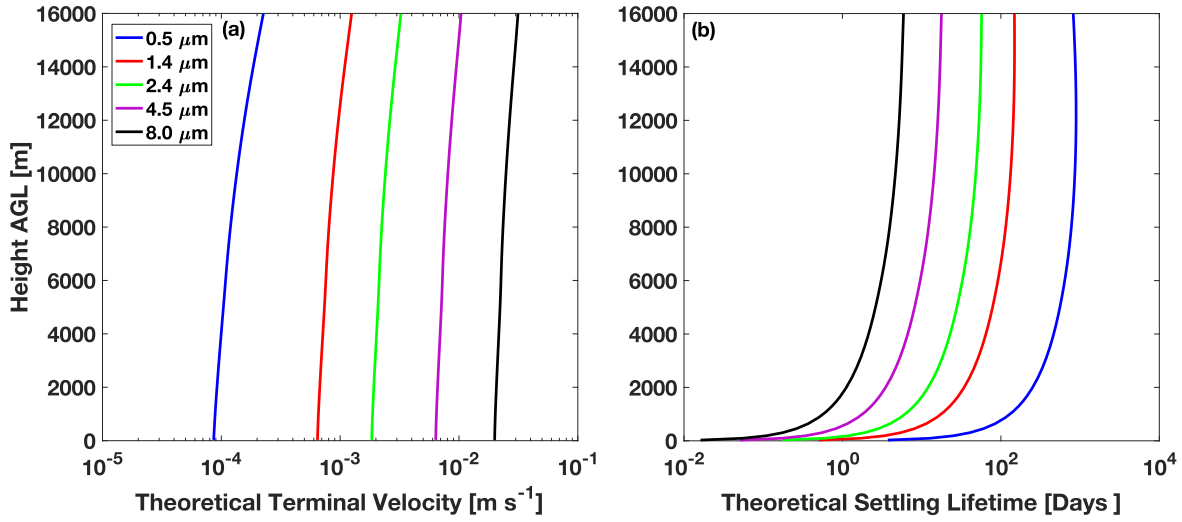

Figure 2.10) (a) Theoretical terminal velocity of dust particles based on Stokes settling velocity with slip correction for pressure dependence for the five effective radii of dust particles in WRF-Chem. The calculations assume no vertical motion, advection, deposition, coagulation, or condensation. (b) The lifetime of these theoretical dust particles based on their height in the atmosphere.

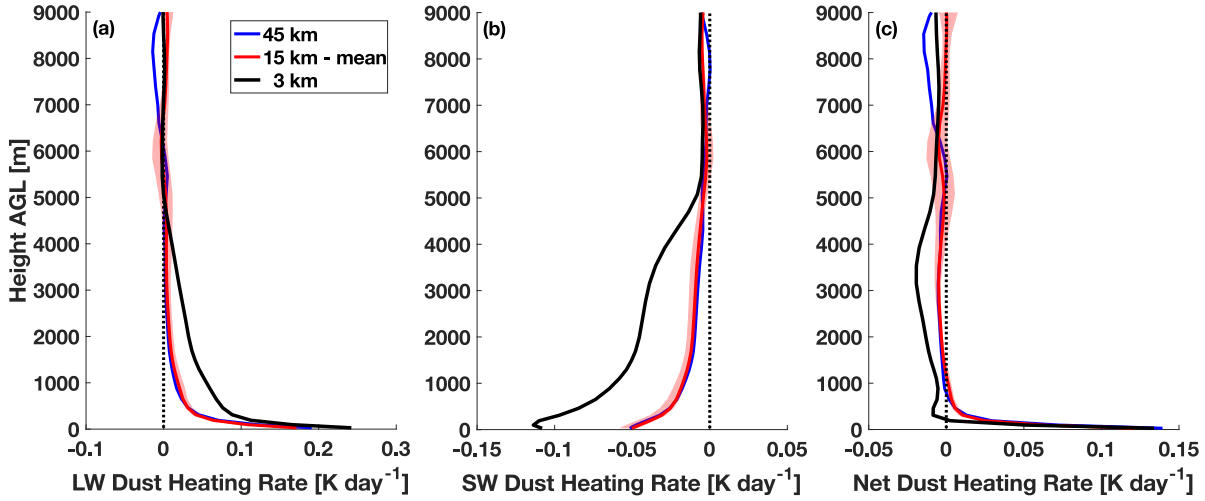

Figure 2.11) Spatially and temporally averaged longwave (a), shortwave (b), and net (c) dust heating rate profile for the 45 km (blue), 15 km mean (red), and 3 km (black) simulations with the maximum and minimum spread across the 15 km simulations indicated in light red shading. Plots are truncated at 9 km as the values above this height do not significantly vary from what is shown here.

CHAPTER 3 – DIRECT RADIATIVE EFFECTS IN HABOOBS

3.1) Introduction

As seen in Chapter 2, mineral dust is lofted from the surface to the atmosphere by strong winds. The most dramatic and dangerous instance of this occurs in association with convective dust storms, whereby visibility can be reduced to near zero in a matter of seconds (Chen and Fryrear, 2002; Zhang and Wang, 1997; Leys et al., 2011) (Fig. 3.1). Convective dust storms are the result of dust lofting in and at the outflow boundary of a cold pool, or density current, which forms as precipitation evaporates below the cloud base of a mature convective cell or convective system. The air, now cooler and therefore denser than its surroundings, is negatively buoyant and sinks until it hits the ground and spreads out as a distinct air mass, or cold pool. These convective downdrafts can produce intense surface winds and depending on the soil type and moisture content loft loose soils into the air (Membery, 1985; Roberts and Knippertz, 2012; Knippertz and Todd, 2012; Cowie et al. 2015; Pantillon et al., 2015; 2016; Huang et al. 2018) and produce a hazardous wall of dust known as a haboob (an Arabic word for 'strong wind').

Convective dust storms are a public safety hazard (Sprigg, 2016; Middleton and Kang, 2017), mainly due to the near instantaneous loss of visibility in the transportation sector (Baddock et al. 2013) and the respiratory effects of inhaling particulate matter (Goudie, 2014; Middleton, 2017). Despite the immediate threat of a dust storm residing on the mesoscale (~100 km), the influence of haboobs extends much further: they can move 85 metric tons of dust per kilometer per hour (Chen and Fryrear, 2002), comprise upwards of 30-40% of the regional dust budget (Miller et al., 2008; Pantillon et al., 2015; Heinhold et al., 2013), and can be remarkably

long-lived, having been observed to travel over 1000 km as an unambiguous entity (Flamant et al., 2007; Miller et al., 2008; Roberts and Knippertz, 2014).

Convectively generated dust storms pose a direct threat to human life and play an important role in the earth system, yet our knowledge of the physical mechanisms embodying such a phenomenon is deficient, making any sort of meaningful forecast of these systems implausible. Uncertainties and insufficiencies in the theory and numerical representation of cold pool dynamics, cloud microphysics, and aerosol feedbacks proliferate, making the research and forecasting of haboobs an outstanding challenge. This chapter serves as a first step in comprehending the feedbacks between cold pool properties and airborne mineral dust particulates inside a haboob at the process-level by singling out one of the three aerosol feedback mechanisms: the direct aerosol radiative effect.

The direct aerosol effect encompasses feedbacks on the system that result from mineral dust interacting with radiation. Dust scatters and absorbs in both the solar shortwave (SW) and terrestrial longwave (LW) parts of the electromagnetic spectrum, extinguishing and redirecting incoming and outgoing radiation in the process. Because dust modulates the earth's radiation budget and climate, many previous studies have concentrated on quantifying the vertical heating and cooling rates due to absorption and scattering from both observations (Heintzenberg, 2009; Banks et al., 2014; Mishra et al., 2014) and radiative transfer modeling (Carlson and Benjamin, 1980; Quijano et al., 2000; Lemaître et al., 2010; Meloni et al., 2015; Peris-Ferrús et al., 2017). Regardless of the vertical location of a dust layer, during the day dust scatters incoming solar SW radiation and decreases net insolation at the surface, leading to a decrease in surface temperature. In a major dust storm, this decrease in insolation has been measured to be on the

order of 300 Wm^{-2} (Slingo et al., 2006; Banks et al., 2014), with an associated -13 °C change in near-surface temperature (Slingo et al., 2006).

Complicating matters, in addition to SW scattering, dust also absorbs in the SW and LW, emitting infrared radiation and heating the atmosphere throughout the dusty layer which, when vertically integrated, can have an opposite response of near-equal magnitude to that observed at the surface (Slingo et al., 2006; Hansell et al., 2010; Marsham et al., 2016; Alamirew et al., 2017). The combined effect of cooling at the surface and heating aloft is to decrease the atmospheric lapse rate and increase static stability, both locally and throughout the atmospheric column, consequently priming the atmosphere to resist vertical convective motions. In addition to enhanced static stability, these changes to the thermodynamic profile will also alter the amount of convective available potential energy, convective inhibition, and the probability of initiating new convection along the cold pool boundary.

Concertedly, as surface temperatures decrease during the day due to the presence of dust, sensible heat fluxes (SHFs) from the ground to the air are diminished (Fan et al. 2008, Jiang and Feingold, 2006; Mallet et al., 2009; Miller et al., 2004; Perez et al. 2006; Heinold et al., 2007; Alamirew et al., 2017, Saleeby et al. 2019) and turbulence kinetic energy (TKE) is suppressed, thereby further enhancing atmospheric stability. A reduction in TKE points fundamentally to reduced vertical mixing, downward transport of momentum, and near-surface wind speeds. Several modeling studies have investigated changes to the structure and properties of the planetary boundary layer (PBL) due to the mineral dust direct effect. The consensus across studies is that including scattering aerosol (Jacobson and Kaufman, 2006) or a dusty near-surface layer in a numerical simulation will reduce TKE and increase atmospheric stability during the daytime (Miller et al., 2004; Perlwitz et al., 2001; Barbaro et al., 2013; Chen et al., 2017;

Bukowski and van den Heever, 2020). Previous work has involved modeling TKE due to the dust radiative effect on low level jets, near-surface wind speeds (Jacobson and Kaufman, 2006; Heinold et al., 2008; Alizadeh Choobari et al., 2013), and cold fronts (Rémy et al. 2015), but there is not always agreement on the sign of the response and these mechanisms are unclear in the case of convective outflow boundaries.

Daytime radiative effects in dusty environments have been the focus of most previous studies, while the longwave-only nighttime regime has received relatively less attention outside of low level jets, with those studies that have examined the latter generally finding that there is warming at night, or less efficient cooling of the nocturnal boundary layer (e.g. Miller et al., 2004; Mallet et al., 2009; Marsham et al., 2016; Saleeby et al. 2019). This nighttime effect could possibly increase SHFs and TKE (Miller et al. 2004; Liu et al., 2016) or have little effect (Saleeby et al. 2019). Notably, the complicated evening transition between a SW-dominated to a LW-dominated regime has been understudied in the literature. Considering that haboobs can be exceptionally long-lived (Flamant et al. 2007; Miller et al., 2008; Roberts and Knippertz, 2014) and that continental convective storms often initialize in the late afternoon to early evening (Heinold et al., 2013), the response of these interim cases is anticipated to be less straightforward than those distinctly centered in one radiative regime. Moreover, dust radiative feedbacks are likely to be highly sensitive to the ambient conditions and dust concentrations in such an environment.

Independent of their potential to loft and transport aerosol species, cold pools are an important component of weather and remain an active topic in research: density currents transport momentum and thermodynamic perturbations, producing vigorous surface winds in the process (Vescio and Johnson, 1992). Moreover, cold pools are capable of sustaining squall line

thunderstorms (Thorpe et al., 1982; Rotunno et al., 1988; Weisman and Rotunno, 2004) and can initiate convection through forced ascent at their leading edge (Purdom, 1982; Weaver and Nelson, 1982; Wilson and Schreiber, 1986; Moncrieff and Liu, 1999;2000; Tompkins, 2001; Torri et al., 2015). Cold pools also play an important role in the lofting of environmental dust into deep convection, and pathways of transporting dust from within cold pools to the updrafts have also been explored (Takemi, 2005; Seigel and van den Heever, 2012b), as has the indirect connection between dust, cloud microphysics, and cold pools (van den Heever et al., 2006; Knippertz et al., 2009; Seigel et al., 2013; Grant and van den Heever, 2015).

Prior research has also investigated the connection between pristine density currents and the land surface, including soil moisture (Fast et al., 2019; Drager et al., 2020) and surface heat fluxes (Bryan and Rotunno, 2014; Grant and van den Heever, 2016; 2018; Gentine et al., 2016; Drager and van den Heever, 2017; Kurowski et al. 2018). Both surface heat fluxes and TKE both play an important role in cold pool dissipation rates and therefore any changes to these quantities due to the dust direct effect will alter cold pool lifetimes. Furthermore, the impacts of static stability on cold pool depth and intensity (Liu and Moncrieff, 2000; Seigel and van den Heever, 2012a), could also be altered by dust in and around a haboob. The higher order feedbacks due to a potential dust radiative effect on stability, SHFs, and TKE will alter mixing and entrainment of environmental air into the haboob, further modifying cold pool intensity, lifetime, and dust emissions in an abstruse way.

Haboobs are a unique variety of density current in that they dynamically loft copious amounts of dust into themselves, simultaneously spawning particles and responding to their presence. In essence, haboobs induce their own aerosol feedbacks. Because of this added complexity of aerosol interactions, most previous research has focused on understanding either

pristine cold pool dynamics or direct dust radiative effects separately, making literature combining the two sparse outside of microphysical indirect effects. Few studies have investigated how the dust particles inside a haboob feed back on the parent cold pool dynamics, let alone the evolution of radiative aerosol perturbations throughout the density current lifecycle through a SW, LW, and SW/LW intermediate environment. Here, we seek to quantify the direct radiative effect inside a haboob on cold pool properties, strength, and feedbacks on dust emissions and deposition. In order to understand this phenomenon, we will revisit the same Arabian Peninsula dust event from Bukowski and van den Heever (2020) (described in Chapter 2) and simulate a single convective event that produces a convective dust storm with multiple interacting cold pools at higher resolution.

3.2) Case study, model description, and analysis methods

3.2.1) Case study overview

An overview of the large-scale environment across the Arabian Peninsula for the day of and following this case study can be found in Bukowski and van den Heever (2020) and is also described in Chapter 2. However, the focus is now on the conditions on August 2nd that allow convection to develop later in the day including a sea-breeze (Fig. 3.1b) aided by a heat low in the interior of the peninsula near Kuwait and along the Persian Gulf (Fig. 3.1a) that moves humid air (Fig. 3.1c) from the Indian Ocean inland. This moist air meets large-scale downslope winds from northern Saudi Arabia, Iraq, Jordan, and Syria that is also moving toward the regional heat lows, thereby producing a convergence line. Along this line, aided by coastal topography, several pockets of convection initiate during the local afternoon around 09:00:00 UTC (12:00:00 Local) and develop through the afternoon and evening (Fig. 3.1c-f). One of these convective clusters

was chosen for the fine grid simulations conducted here and is designated by the red boxes in Figs. 3.1 and 3.2. This storm was selected because it is located far enough from steep terrain that orographic forcing does not unnecessarily confound the analysis, and is relatively isolated compared to other storms in the domain, thereby simplifying the analysis. Additionally, the storm system initializes in the drier interior region where dust can be expected to loft and is representative of a typical haboob conducive environment.

The genesis and development of the selected convective system is shown Figure 3.4. The convection initially develops as a linear feature along the convergence line, and is comprised of numerous cells (Fig. 3.4a,d), each individually producing cold pools, which are evident by their signature circular divergent winds at the surface (Fig. 3.4g). Strong winds in the density currents loft dust (Fig. 3.4j), with especially high dust concentrations at and behind gust front boundaries (Fig. 3.4m). As the storm develops, the convective cells and cold pools interact to form a more unified convective complex, where discrete cells and individual cold pools become more difficult to identify (Fig. 3.4 – center column). Later in the mature phase of the storm's lifetime, a clear, collective gust front is visible north and south of the convective line, with sufficient vertical motion at the outflow boundary to produce light precipitation (Fig. 3.4c) that removes dust from the atmosphere (Fig. 3.4o). In later time periods, the location of maximum dust concentrations correlates with the location of maximum wind speed behind the gust front and outside of the areas of precipitation (Fig. 3.4 – right column).

It is important to note that while the storm and airborne dust concentrations develop, there is a simultaneous change in radiation occurring, both in response to the diurnal cycle and the lofting of dust. The early initiation of the storm lifecycle occurs under a daytime SW-dominated regime, while storm strengthening takes place during a SW to LW transition in the

early evening, reaching a mature storm phase in a LW-only regime at night (See Section 3.2.4.a). It is impossible to deconvolve the radiation and the storm lifecycle as they are both being perturbed concurrently. This is a limitation of the case study and experimental design of Chapter 3 and this challenge warrants future study outside of this dissertation.

3.2.2) WRF-Chem model description and physics

For consistency, the setup and parameterizations are almost identical to that used in Bukowski and van den Heever (2020) (and shown in Chapter 2, Table 2.1), including WRF-Chem version 3.9.1.1 (Skamarock et al., 2008; Grell et al., 2005; Fast et al., 2006) coupled to the GOCART module (Ginoux et al., 2001) and initialized with the same boundary conditions from the GDAS-FNL database (National Centers for Environmental Prediction/National Weather Service/NOAA/U.S. Department of Commerce, 2015). All physics parameterizations are the same, including Morrison double-moment microphysics (Morrison et al., 2005, 2009), RRTMG longwave radiation (Iacono et al., 2008), Goddard shortwave radiation (Chou and Suarez, 1999), the interactive Noah land surface model (Niu et al., 2011; Yang et al., 2011), and MYNN level 3 boundary layer representation (Nakanishi and Niino, 2006; 2009). While the GOCART module is used for dust, the dust parameterization differs from Bukowski and van den Heever (2020) in that the Ginoux et al. (2001) soil erodibility map is replaced with an idealized surface where each grid box is capable of lofting dust and is not multiplied by a scaling factor as was done in Bukowski and van den Heever (2020). Using a more idealized surface removes a degree of freedom in the analysis related to the erodibility map, for which there are multiple approaches (e.g. Ginoux et al. 2001; Prospero et al., 2002; Schepanski et al., 2007; Walker et al. 2009) of what is known to be a highly sensitive model parameter (Uno et al., 2006; Saleeby et al., 2019;

Bukowski and van den Heever; 2020).This simplification to the analysis implies that the results in this paper are an upper bound that overestimates the regions capable of lofting dust, but removes the chance for misleading interpretations of results due to the erodibility map.

The model was run from 00:00:00 UTC on 2 August 2016 to 18:00:00 UTC on 2 August 2016 with output analyzed at 5 minute intervals. A one-way triple nest at 15:5:1.666 km was used (Figure 3.2). This grid setup is similar to Bukowski and van den Heever (2020) with boundaries of the two coarser grids being the same, but were run at 15:5 km instead of 45:15 or 15:3 km. The innermost nest was run at a resolution of 1.666 km and was centered around the specific storm in this case study and was not part of the Bukowski and van den Heever (2020) analysis. To better resolve cold pool processes near the surface, the vertical resolution was doubled from 50 stretched layers in Bukowski and van den Heever (2020) to 100 stretched layers. Better representation of low-level winds (e.g. turbulent energy cascade, cold pool height and environmental stability) will also lead to led to more realistic dust emissions and vertical distribution.

Similar to Bukowski and van den Heever (2020), the dust radiative effect was determined by holding all variables and model settings constant and running two simulations: one with active dust aerosol radiation (RAD) and one without (NORAD). In the NORAD simulation, radiation is still active in the environment and impacts the meteorology and cloud microphysics, but specifically excludes interactions with aerosol. The simulations were otherwise identical.

To remove additional degrees of freedom in the analysis, dust emissions in the GOCART module and the aerosol radiation scheme are only executed in the code after the first downdrafts are identified in the convective storm system at 10:00:00 UTC. Waiting for the cold pools to form in this manner eliminates uncertainties related to dust impacts on the storm structure, semi-

direct effects, and initial formation of the density currents, as well as effects from diffuse airborne dust lingering in the atmosphere from other sources and ensures that the analysis is focused solely on the cold pool lofted dust. By prescribing dust emissions in this way, the only aerosol modifying the environment will be dust lofted by the haboob itself.

3.2.3) Dust feature identification and tracking

The convective system in this case study produces numerous cold pools that collide and interact with each other throughout the simulation (Fig. 3.4g-i). These cold pools loft dust, but also contain areas of active precipitation that scavenge dust aerosol (Fig. 3.4a-c,m-o). To track the boundaries and mergers of these outflow elements and determine which portions of the outflow boundary contain dust requires the use of an identification algorithm to follow features throughout the simulation. Here, the offline postprocessing Tracking and Object-Based Analysis of Clouds version 1.2 (TOBAC - Heikenfeld et al., 2019) framework was employed. TOBAC was originally developed to track convective updrafts and cloud volumes but is highly customizable and I modified the code here to identify and track dust within the density currents.

TOBAC works in three steps. Firstly, it detects similar features of a 2D data field based on multiple threshold levels and attributes an area-weighted mean center to each. Including several thresholds rather than a single limit permits the algorithm to detect weak features while also assigning a more representative center to stronger features that meet the multiple thresholds. For this study, surface dust concentration was selected as the 2D identification field, with thresholds of 1200, 2000, 3000, and 4000 ug/m^3. These thresholds result in most of the dusty cold pool regions being identified while ignoring lower ambient dust concentrations outside of the haboob.

Several 2D input variables for the TOBAC framework were tested for this experiment, including other more commonly tracked cold pool properties like potential temperature and vertical velocity (e.g., Drager and van den Heever, 2017). However, these properties do not specifically identify which regions of the cold pool contain dust. Feature identification using surface dust ensures that only the dusty regions of the cold pools are included in the analysis, which is inherently necessary for studying dust radiative effects and hence addressing the science goals of this research. The decision to track on dust versus cold pool properties results in two competing yet incomplete outcomes: either non-dusty portions of the cold pool are included in an analysis meant to describe dust interactions, or dusty regions are analyzed as if they represent the entire density current when significant portions of the cold pool are pristine. To concentrate on dust effects, the latter option was chosen in that dust was selected as the tracking variable with the caveat that it does not represent the entirety of the cold pool, or the interactions between dusty and pristine portions of the storm. A comparison of the dust features identified by TOBAC relative to the full outflow boundary is found in Fig. 3.5.

After locating dust features and their center points, the second step in the TOBAC framework involves segmenting 3D volumes, in this case dust concentrations at the surface and aloft, with each identified feature using a watershedding technique to connect and detach features that overlap, merge, or separate during their lifetime. Lastly, TOBAC tracks the 3D feature volumes and their centers in time by checking if the same feature exists in the previous time step and then records its location. In the end, TOBAC produces a database of independent 3D dust features within the haboob that have been tracked in time (Fig. 3.5a-c). This allows for composite and mean statistics to be performed on the database, which will be presented in Section 3.2.4. A full list of detailed TOBAC parameters can be found in Table 3.2.

3.2.4) Analysis Methods

3.2.4.a) Radiative Regimes

Because the dust radiative effect will depend on the wavelength and intensity of radiation, the results are broken into three radiative regimes (Fig. 3.6a). This includes a daytime period with strong SW insolation at the surface, a transitional early evening period with low values of incoming SW, and a final LW-only period at night. The cutoff between day and evening is designated here at the time when domain averaged incoming SW at the surface reaches half its initial value. To test if the daytime and / or evening results are sensitive to the exact temporal boundary, the threshold was moved 30 minutes backward and forward, but the sign of the responses did not change. The placement of the nighttime boundary is more straightforward and is set where the domain averaged incoming SW reaches zero.

3.2.4.b) Focus on Surface and Near-Surface Values

Considering this study focuses on outflow boundaries that are dense, stable, near-surface features, the analysis will not examine the full vertical thermodynamic or dust profile. After examining mean profiles of cold pool temperature, as well as dust and aerosol heating rates from the surface to 4 km AGL (Fig. 3.7), it is clear that the maximum dust concentrations, and consequently the strongest radiative feedbacks, are contained within a shallow layer near the surface below 1.0-1.5 km AGL. Cold pool temperature as well as dust concentrations and its direct effects decrease exponentially away from the surface as shown in Bukowski and van den Heever (2020), although can be important from an integrated standpoint. As such, outside of integrated dust values, the analysis in Section 3.3 below will focus on surface quantities or lowest model level quantities where appropriate.

3.2.4.c) Normalization and Detection Differences

Despite running TOBAC identically on both the RAD and NORAD simulations to produce two databases of tracked cold pool features, dissimilarities in the detection between the two simulations are apparent and are expected from theory and previous work. The dust radiative effect alters the environment, which leads to differences in the physical processes and dust concentrations. As dust concentrations change, they affect the area of the domain that meets the feature detection threshold. TOBAC correctly identifies these differences and tracks the unique feature horizontal and vertical velocities, cold pool movements, and the merging of features in each simulation. Nonetheless, the distinct detections in each case prevents a one-to-one / feature-to-feature comparison due to the specific feature number and area identified in the RAD and NORAD case (Fig. 3.6b). The most significant difference in the area of identified features occurs around 15:00:00 UTC, with more dust area in the RAD simulation, but are otherwise close between the two simulations. Because of the detection differences, all results are presented from either a mean perspective (Figs. 3.6-3.7) or a composite framework via histograms normalized by the number of identified points in each time block (Section 3.3).

In general, the difference in the number of points does not change the results when normalized, except for surface dust concentrations and integrated dust at the latter portion of the evening and the full nighttime period. Not accounting for feature area, there is more dust in the RAD case for all time periods (Fig. 3.6c,e). However, when the feature area is included, the sign reverses in the transitional case and at night, with the NORAD case producing higher dust concentrations (Fig. 3.5d,f) for roughly 1 hour between 15-16 UTC before returning to the original trend. Therefore, the results for evening and nighttime surface dust concentration and

integrated dust are ambiguous for the transition period. All variables were tested for this dubious inversion from the normalization process, but it was only present in these two dust variables.

All TOBAC-identified data points from the RAD and NORAD simulations are collected into three bins based on the day, transition, and night classification and represented as histograms throughout this paper.

3.3) Results

When dust aerosol is lofted off the surface by cold pools, it goes on to interact with solar and terrestrial radiation. It will scatter and absorb radiation, leading to changes in the properties of several variables, including the haboob's dynamics. The catalyst of the dust radiative feedback mechanism is the aerosol heating rate of the atmosphere (Sec. 3.3.1). This heating imbalance will alter SW and LW radiation at the surface (Sec. 3.3.2) and go on to modify surface temperatures (Sec. 3.3.3). This difference in temperature affects surface heat fluxes (Sec. 3.3.4), turbulence, winds, the cold pool propagation speed, and stability (Sec. 3.3.5), which directly alters the amount of dust lofted and deposited by the cold pools (Sec. 3.3.6). This chain reaction of feedbacks culminates in the dust concentration of the haboob, which is the net inequality between emission and settling rates (Sec. 3.3.7). The effect dust has on these physical mechanisms will depend on the wavelength of radiation, the dust concentrations, and the environmental conditions. Each part of this direct dust radiative mechanism is split into day / evening / night and is described below. A conceptual schematic of the processes in a density current that are directly or indirectly altered by the dust radiative effect can be found in Figure 3.8.

3.3.1) Aerosol Heating Rates

During the day, dust in the cold pools will scatter SW radiation, preventing it from reaching the surface. Simultaneously, dust absorbs some of the incoming SW and heats dusty layers aloft. The absorption of SW is represented by positive perturbations to atmospheric heating rates and is evident by the increase in the SW heating rate in the RAD simulation of the TOBAC-tracked cold pool dust (Fig. 3.9a). This increase reaches a maximum of 0.5 K hr^{-1} in the density currents, although the median of the distribution is closer to 0.1 K hr^{-1}. The maximum and median heating rates constrain the length of time a haboob must exist for the dust effects to be felt by the local atmosphere. Weak effects must either exist in greater number or for a longer period of time to have an effect. Additionally, dust absorbs and emits in the LW, which corresponds to a negative heating (cooling) rate as the atmosphere radiates more energy to achieve balance. In the daytime, the RAD simulation has lower values (Fig. 3.9c), or more LW absorption and emission than the NORAD simulation. The same results are evident in the evening transition, with higher SW heating rates (Fig.3. 9b) and more LW emission (Fig. 3.9d) in the RAD compared with the NORAD case, while the relative importance of each effect reverses; in the daytime, the SW aerosol heating rate is higher, while in the evening the LW component dominates.

At night the SW is zero, but the LW effect is at its strongest (Fig. 3.9e), with the absolute value of the median nighttime LW heating rate being higher than the SW rate during the day. While SW effects may have been found to be relatively more important for large-scale dust sources (Saleeby et al., 2019; Bukowski and van den Heever, 2020), the LW effect appears to be just as, if not more important than the SW effects on the mesoscales of the gust front case.

3.3.2) Shortwave and longwave radiation at the surface

The scattering and absorbing of SW radiation in the dusty cold pool leads to less SW being transmitted to the surface in both the daytime and evening periods of the RAD case (Fig. 3.10a,b). Additionally, there is a shift toward more LW directed downward to surface in all three time periods (Fig. 3.10c-e) due to the SW/LW absorption and emission, which radiates in three dimensions and results in some portion of radiation being directed downward. Due to the competition between the reduction in SW and the increase of LW downward at the surface during the day, terrestrial radiative fluxes between the surface and the atmosphere change in both directions and do not present a clear shift (Fig 3.10.f), which has been noted in other studies as well (Miller et al., 2004; Mallet et al., 2009; Marsham et al., 2016; Saleeby et al., 2019). However, in the evening as the SW effect becomes less important, the LW dust effect again begins to dominate and increases in the RAD case (Fig. 3.10.g). This same shift in LW is also apparent at night after the SW component no longer contributes (Fig. 3.10h).

3.3.3) Surface and near-surface air temperature

Daytime SW scattering by haboob dust in the RAD case exceeds LW absorption / emission when incoming SW is high, leading to lower surface temperatures being more likely (Fig. 3.11a). Because the surface temperatures are lower, the air above the surface is also cooler when dust radiative effects are present (Fig. 3.11d). Density currents are driven by the temperature (and hence density) difference between cold pool air and the environmental air around it. The theoretical cold pool strength, is often calculated with the following equation (Benjamin, 1968; Rotunno et al., 1988):

$$V^2 = 2\int_0^H -g\frac{\theta'}{\theta_{env}}dz \qquad \text{[Eq. 3.1]}$$

where V is the theoretical cold pool speed (m s^{-1}), or intensity, H is the cold pool depth (m) defined by a buoyancy threshold, g is gravitational acceleration (m s^{-2}), dz is the model vertical grid spacing (m), θ' is the cold pool perturbation potential temperature (K) relative to the mean air outside the density current, θ_{env} (K), with θ' calculated as a simple difference between the environmental air and the cold pool air ($\theta' = \theta_{env} - \theta_{cold\ pool}$). It is evident from Eq. 3.1 that a larger gradient between cold pool air and environmental air ($\frac{\theta'}{\theta_{env}}$) leads to a more intense cold pool that will travel faster, assuming all else equal. When dust radiation is therefore included, scattering leads to colder temperatures in the cold pool compared to the less-dusty ambient environment. This implies that the density current is stronger, or more intense, when dust is present during the day, and these cold pools will spread away from their parent storms more rapidly.

Nevertheless, the trend reverses in the evening and nighttime when the LW effect dominates. With LW absorption and emission, surface temperatures and air temperatures near the surface do not cool as rapidly as they normally would in a clear-sky scenario. Thus, nocturnal cold pools are warmer when laden with dust (Fig. 3.11b-c,e-f) than a pristine cold pool would be. Because the temperature differential between the cold pool and the large-scale environment is reduced, the haboob is weaker, or less intense at night, and as a result will propagate more slowly.

3.3.4) Surface heat flux

As the dust radiative effect modifies surface and near-surface air temperatures, SHFs also change. SHFs are often represented by the following equation:

$$SHF = C_d C_p \varrho_{air} U(T_{sfc} - T_{air}) \qquad \text{[Eq. 3.2]}$$

where C_d is an aerodynamic bulk transfer coefficient, C_p is the heat capacity of dry air at constant pressure (J kg^{-1} K^{-1}), ρ_{air} is the density of air (kg m^{-3}), U is the near-surface wind speed (m s^{-1}), and T_{sfc} and T_{air} are the temperature of the surface, or skin temperature, and the near-surface air, or 2-m temperature(K^{-1}) respectively.

The daytime haboob is colder and therefore denser when accounting for dust radiative effects, which leads to higher windspeeds (Section 3.3.5). Because of SW scattering, the distribution for surface temperature and the near-surface air both shift toward lower temperatures (Fig. 3.11a,d). However, there is a reduction in the magnitude of the T_{sfc}-T_{air} difference (Fig. 3.12a) between the RAD and NORAD simulations. As a consequence, the positive and negative contributions cancel leading to little change in the daytime SHFs. This outcome is inconsistent with other studies that show a reduction in SHF during the day due to suppressed surface temperatures from the dust scattering effect (Fan et al. 2008, Jiang and Feingold, 2006; Mallet et al., 2009; Miller et al., 2004; Perez et al., 2006; Heinold et al., 2007; Alamirew et al., 2017, Saleeby et al., 2019). This discrepancy appears to stem from the fact that previous studies have focused on large-scale synoptic or climate-scale dust cases, whereas this study specifically investigates cold pools. In a cold pool the significant temperature shift that increases SHFs is absent in large-scale circulations in the Arabian Peninsula, such as heat lows or downslope winds, but may be similar to features like cold fronts. Here, the land surface must respond concurrently to the cold air perturbation from the density current and dust aerosol effects. The abrupt drop in T_{air} as the density current passes produces a strong positive SHF response, or fluxes directed from the surface to the air, that dominate over the SHF decrease from the daytime SW feedback.

In the day, the SW effect first leads to a cooler surface, which in turn prevents the air above it from warming through longwave heating. Conversely, in the evening and nighttime, the LW aerosol effect traps heat aloft first, which then warms the surface. In the transitional evening case, the surface begins to cool as the incoming solar radiation vanishes. Terrestrial radiation is however trapped by dust, which radiates downward and prevents the surface from cooling as rapidly as it would in a pristine aerosol case. Both T_{air} and T_{sfc} increase because of this LW effect, but T_{air} increases faster than T_{sfc}, leading to a reduction in the surface-air temperature difference (Fig. 3.12b). Coupled with the warmer, weaker and less dense cold pool in the RAD case, SHFs are reduced during the evening and are more likely to be negative, or directed from the air to the ground, than in the NORAD simulations.

After the sun has set, both the surface and the near-surface air are warmer due to the dust LW effect. However, there is now a larger surface-air difference in the RAD nighttime case as the terrestrial radiation is trapped and the layers above it cool as they flux towards and away from the surface. The relatively warmer dusty cold pools are less dense, but due to higher windspeeds at night (Section 3.3.5) SHFs increase.

3.3.5) Turbulence, Wind, and Low-Level Stability

Changes to the temperature of the density currents relative to the environment will drive changes to their intensity and their propagation speeds. In the daytime, the simulated cold pools are colder in the RAD experiment due to the dust scattering effect, which leads to stronger in-cold pool windspeeds (Fig. 3.13d), and thus higher values of TKE (Fig. 3.13a). This results in daytime cold pools being more intense and moving faster due to the impacts of dust radiative effects.

In the transitional period, LW absorption and emission by the dust leads to a warmer density current with lower windspeeds (Fig. 3.13e) and suppressed TKE (Fig. 3.13b) in the RAD simulation. The presence of the dust within the cold pool also enhances low-level stability (Fig. 3.13h) due to the air above the surface being warmer than the cooling surface from the trapping and emitting of LW radiation aloft (Section 3.3.4). Therefore, the evening portion of this case produces cold pools that are relatively weaker and move slower in the RAD case.

At night, dust radiative effects are less straightforward: the cold pool is warmer due to the LW effect (Fig 3.11c), but there are higher windspeeds (Fig. 3.13f) and enhanced turbulence (Fig. 13c) in the haboob. This result contradicts the theory that a reduced temperature gradient between a cold pool and its environment should lead to reduced windspeed and intensity based on Eq. 3.1 from Benjamin (1968) and Rotunno et al. (1988). However, when dust radiation is included, the LW effect prevents the surface from cooling as strongly as it would under clear conditions that typically stabilize the nocturnal boundary layer. The LW warming effect leads to a less stable surface layer (Fig. 3.13i) that retains some of the buoyant contribution to TKE and windspeed that were already depleted in the pristine case.

While the dusty portions of the cold pool are less stable, the pristine desert environment around the haboob cools rapidly, leading to a strong inversion and statically stable conditions. It has previously been shown that the stability of the environment into which a density current propagates affects its height and propagation speed (Liu and Moncrieff, 2000; Seigel and van den Heever, 2012a). Seigel and van den Heever (2012a) tested the effect of the static stability of a thin surface stable layer on cold pools, similar to the nocturnal desert environment in this study. They found that a stronger statically stratified environment surrounding a cold pool leads to a shallower and faster moving density current due to an increased horizontal pressure gradient

behind the gust front. We hypothesize that in the dust radiation case, the difference between the less statically stable haboob and the more stable, pristine environmental air around it leads to the observed increase in windspeed and turbulence as in Seigel and van den Heever (2012a) as the pressure gradient force between the two increases, thus increasing propagation speed. This hypothesis requires further testing and we speculate that this effect would be highly sensitive to the depth and strength of the nocturnal inversion layer in different environments.

3.3.6) Dust emission and settling rates

The modifications to wind and stability near the surface will feedback on dust emissions and settling rates. As seen in Bukowski and van den Heever (2020), and described in Chapter 2, dust flux to the atmosphere is primarily a function of wind speed [Eq. 2.3 Chapter 2] but can be strongly modified by soil erodibility and soil wetness [Eq. 2.4-2.5 Chapter 2]. Here, because soil erodibility is set to a constant value by design and the parent storm is not affected by dust radiation to significantly alter precipitation effects, changes in windspeed drive the observed changes in dust emission rates. Higher windspeeds in the day enhance dust emissions, lower windspeeds in the evening lead to lower dust emissions, and stronger winds at night support stronger emissions (Fig. 3.14a-c).

Dust fluxes from the air to the surface, or dust removal from the atmosphere, depends on the combination of turbulent transfer toward the surface and gravitational settling, the latter of which is inversely proportional to the viscosity of air and therefore inversely proportional to temperature. In the day, lower temperatures and higher TKE in the RAD simulations leads to more dust being removed from the atmosphere (Fig. 3.14d). In the evening, warmer temperatures and suppressed TKE both support lower dust fluxes to the surface (Fig. 3.14e), while at night

warmer temperatures compete with enhanced TKE, but ultimately dust fluxes to the surface are reduced (Fig. 3.14f).

3.3.7) Dust concentrations

Dust concentrations at any given point are a balance between emissions, transport, and deposition, and the self-imposed feedback of dust radiation on dust concentrations is the culmination of a cascade of processes altered by the dust radiative effect, as represented by the schematic in Figure 3.8. At the surface, there is an increase in dust concentrations during the day from higher dust emissions and lower dust deposition rates and a slight increase in integrated dust as well (Fig. 3.15a,d). From the mean plots in Figure 3.6, this trend of higher dust concentrations would hold for the entire simulation period and is supported by the fact that more cells are identified over the dust threshold of 1200 [ug m^{-3}] in the RAD simulation. Nevertheless, when normalized by detected area, the distributions are inconclusive or may present an opposite result (Section 3.2.4; Fig. 3.15b-c,e-f).

From the balance between dust emission and deposition rates, the SW-dominated period would have robustly higher dust concentrations, the evening could be either higher or lower, and the nighttime would have higher concentrations. The identification and analysis techniques used in this study do, however, break down for the dust-dust feedbacks and are insufficient for reaching a conclusion for this case study. However, this feedback mechanism will be addressed further in Chapter 4 with a more straightforward idealized modeling experimental design.

3.4) Discussion and conclusions

This chapter examine the impacts of dust-radiation interactions on cold pool processes and associated feedbacks. To quantify these effects, an Arabian Peninsula convective outflow dust event was simulated using WRF-Chem with (RAD) and without (NORAD) dust radiation interactions. The TOBAC framework was used to track and identify the dusty regions of the numerous cold pool boundaries and create histograms of cold pool properties for both the RAD and NORAD simulations as a function of three distinct radiative regimes based on insolation: daytime (high SW, LW), evening transition (low SW,LW), and night (LW only). A summary of the direct dust feedbacks on cold pool processes can be found in the schematic in Figure 3.8, and the impact the dust radiative effect has on each mechanism can be found in Table 3.3.

During the day, dust scatters the SW radiation and reduces insolation at the surface, cools the surface and the air above it, and increases the temperature gradient between the cold pools and their parent environment. This leads to stronger density currents with higher windspeeds, enhanced turbulence, and increased dust emissions and concentrations. Unlike the synoptic-scale dust events previously examined in the literature, SHFs during the day are not reduced by the SW scattering effect because the surface response is dominated by a strong positive SHF response due to the cold air perturbation from the density current and enhanced windspeeds. In the evening transition between day and night, dust LW absorption aloft and emission toward the surface becomes more important and leads to a warmer surface and warmer cold pools with a reduced temperature gradient between cold pool air and the environment, which results in weaker density currents with suppressed TKE, windspeeds, dust lofting, and SHFs. At night, the LW warming persists, but the trapped LW leads to a less stable nocturnal cold pool than if radiative cooling had occurred in a pristine environment. Therefore, the outflow boundary is

warmer, but not necessarily weaker according to Eq. 3.1 because it contains stronger windspeeds, enhanced TKE and SHFs, and higher dust emissions, which we hypothesize is due to the less stable haboob air moving into the pristine and statically stable nocturnal boundary layer.

These results will need to be expanded to different storms and environments and may be highly sensitive to timing, insolation, ambient dust concentrations and dust mineralogy, surface properties (Chapter 4), and model parameters such as the refractive index, spherical dust assumptions, and the size partitioning of dust mass (see remarks in Sec. 2.6). A continuation of this work that explores the parameter space will be discussed in Chapter 4, but more case studies and understanding the higher order effects such as dusty / pristine collisions and understanding the ambiguous dust-on-dust feedback will require further study.

Nonetheless, the results here can be applied to the forecasting of haboobs. To first order, dust radiative feedbacks will lead to a colder, dustier, faster moving cold pool in the day. In the early evening, haboobs can be expected to be warmer, slower, and will loft less dust as they travel, whereas at night, a haboob will be warmer, but gustier in the more stable nocturnal surface layer. These identified feedbacks of dust radiation on cold pool properties are a first step in a larger picture to understand dust radiative effects in mesoscale dust events, such as convective outflow boundaries, and the effect that different radiative regimes have on this phenomenon.

3.5) Figures and tables

Figure 3.1) An advancing dust-laden cold pool or haboob on 16-June-1997 in Big Spring, TX (after Chen & Fryrear, 2002)

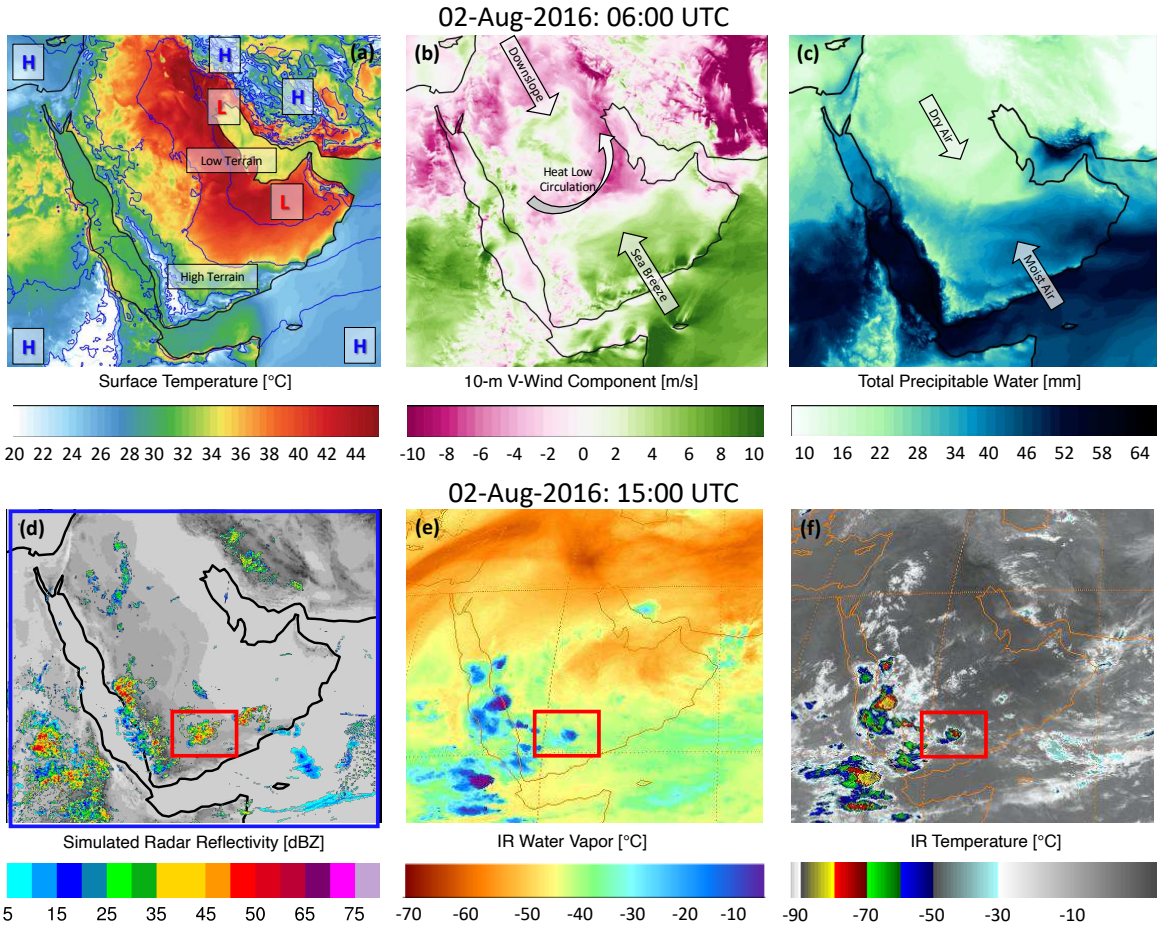

Figure 3.2) (Top) – Pre-storm case study meteorology setup for 02 August 2016 at 06:00 UTC from the 5 km WRF-Chem RAD simulation: (a) surface temperature and relative low and high pressure regions, (b) 10 m V-wind component, (c) total precipitable water. (Bottom) – Snapshot of the convective storm at 02 August 2016 at 15:00 UTC: (d) simulated radar reflectivity from the 5 km WRF-Chem RAD simulation, (e) IR water vapor temperature from METEOSAT-7, (f) IR temperature from METEOSAT-7. The storm analyzed in the 1.7 km inner-nest simulations (Fig. 3.3) is outlined in the red boxes in the bottom row (see Figure 3.4).

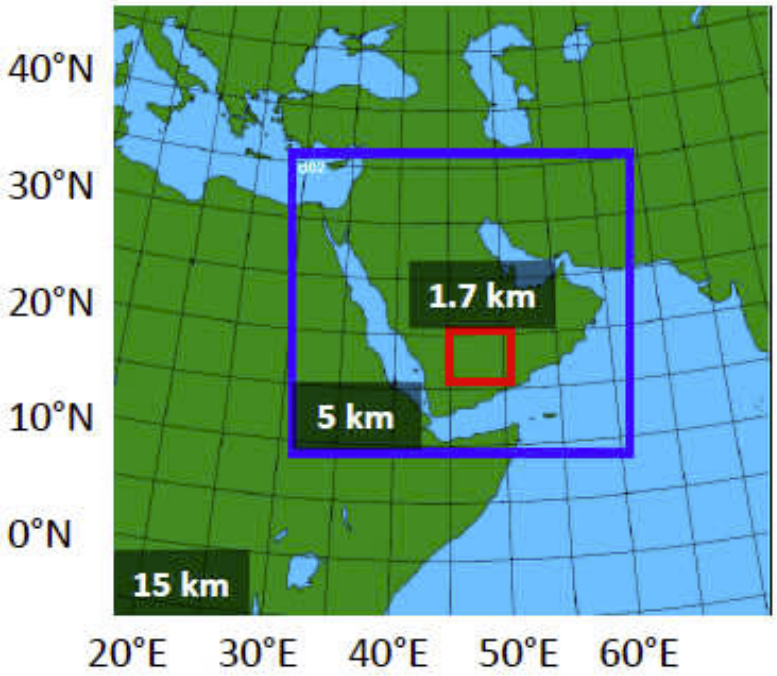

Figure 3.3) Model domain setup for the 15 km (full image), 5 km (blue), and 1.7 km (red) one-way nested simulations.

Table 3.1) Summary of the WRF-Chem model options utilized and the simulation setup.

WRF-Chem Version 3.9.1.1	Parameterization/model option
Simulation start	2 August 2016, 00:00:00 UTC
Simulation end	2 August 2016, 18:00:00 UTC
Dust lofting start	2 August 2016, 10:00:00 UTC
Domains	dx = dy = 15 km / 5 km / 1.7 km
Nesting	One-way
Vertical levels	100 stretched
Initialization	GDAS-FNL
Aerosol module	GOCART
Erodible grid map	Idealized
Microphysics	Morrison double-moment
Radiation	RRTMG longwave & Goddard shortwave
Land surface	Noah MP Land Surface model
Cumulus	BMJ on 15 km grid only
Boundary layer	MYNN level 3

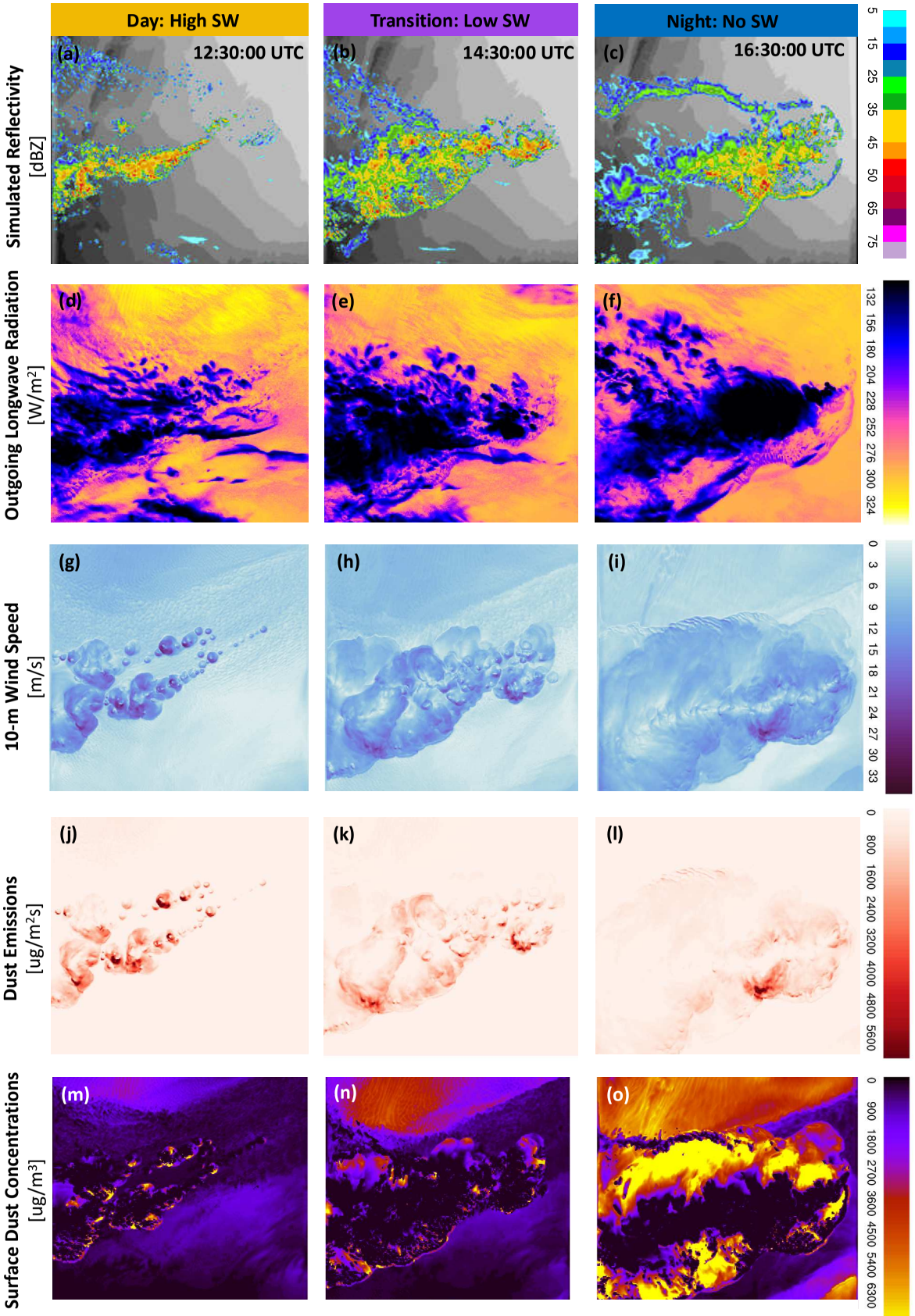
Day: High SW
Transition: Low SW
Night: No SW
(a)
12:30:00 UTC
(b)
14:30:00 UTC
(c)
16:30:00 UTC
Simulated Reflectivity [dBZ]
5 15 25 35 45 50 65 75
(d)
(e)
(f)
Outgoing Longwave Radiation [W/m²]
132 156 180 204 228 252 276 300 324
(g)
(h)
(i)
10-m Wind Speed [m/s]
0 3 6 9 12 15 18 21 24 27 30 33
(j)
(k)
(l)
Dust Emissions [ug/m²s]
0 800 1600 2400 3200 4000 4800 5600
(m)
(n)
(o)
Surface Dust Concentrations [ug/m³]
0 900 1800 2700 3600 4500 5400 6300

Figure 3.4) Dust storm progression during the 3 analysis time periods (day, transition, and night) for the RAD simulation: (a-c) simulated radar reflectivity, (d-f) outgoing longwave radiation, (g-i) 10 m windspeed, (j-l) dust emission rate from the surface to the atmosphere, (m-o) surface dust concentrations.

Table 3.2) Summary of TOBAC parameters used to identify and track dusty portions of the cold pools.

TOBAC Version 1.2	Option	Description
Center position threshold	Weighted difference	Threshold-weighted center for tracking
Sigma threshold	4	Standard deviation for initial filtering step
Minimum number	10	Min. number of identified features
Erosion threshold	0	No removal of ridges in connected features
Target	Maximum	Thresholds increase in value
Feature thresholds	1200, 2000, 3000, 4000 ug/m^3	Dust thresholds for feature detection and weighting
Segmentation method	Watershed	Use watershedding to connect related features
Segmentation threshold	1200 ug/m^3	Min. value for detection
Track method	Predictive	Trajectory linking using predicted motion
Vmax	30	Max. speed features can move and be predictively tracked
Order	0	Order of polynomial used to extrapolate trajectory
Extrapolate	1	Number of timesteps to extrapolate trajectories
Memory	0	Features not allowed to vanish and still be tracked
Time cell minimum	10	Cells must exist for 10 consecutive minutes to track
Adaptive stop / start	0.2 / 0.95	Default search radius limits
Subnetwork size	150	Max. number of grid boxes in a linked subnetwork

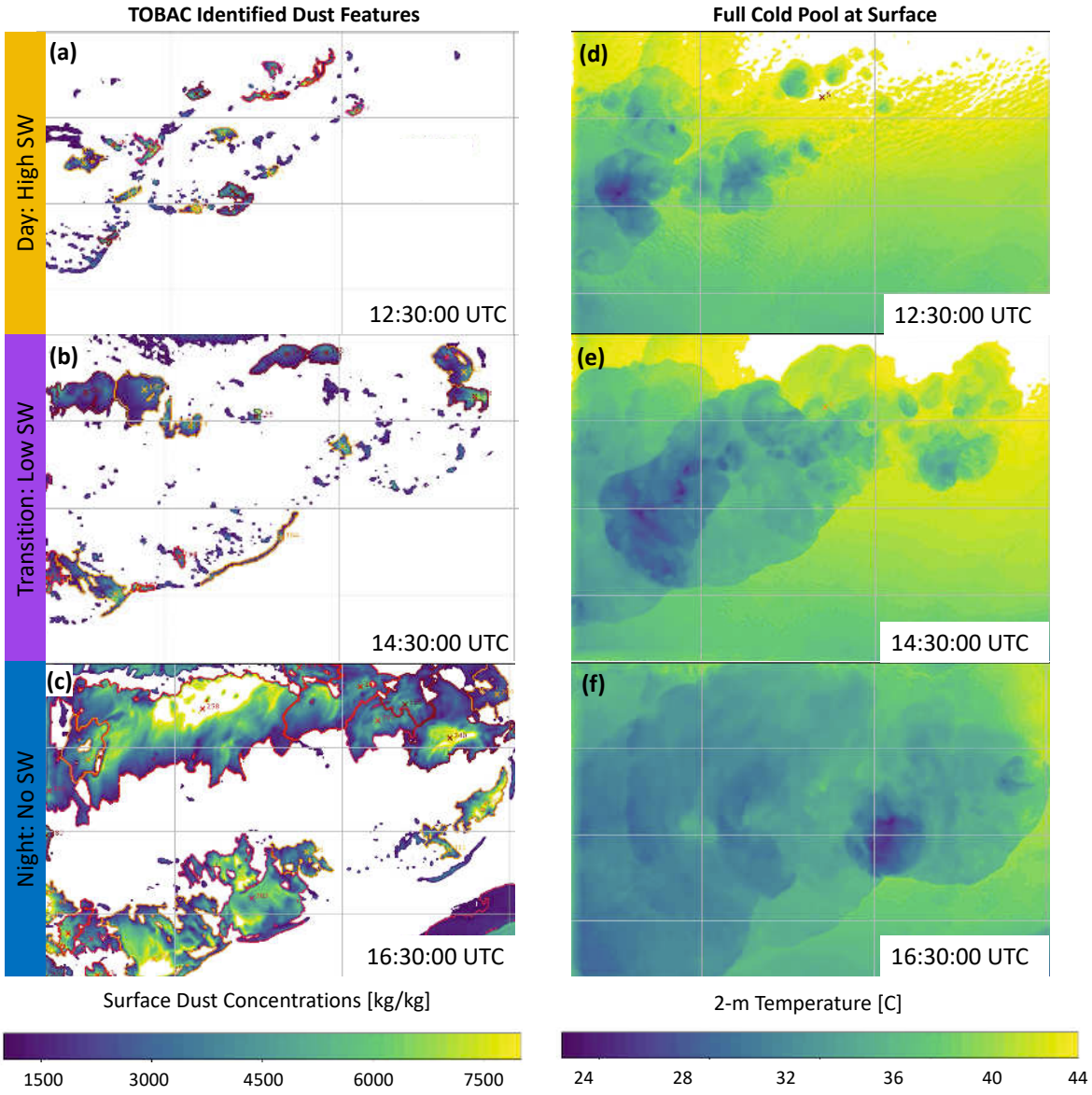

Figure 3.5) (Left) – Outlines of TOBAC-identified dust-laden boundaries (red lines) layered over surface dust concentrations for the three analysis times (day, transition, and night) from the RAD simulation. These outlines represent only the dusty parts of the cold pool, with the threshold weighted center of each figure marked with and 'X.' (Right) – 2 m temperature for the three analysis times. The right-side panels represent the full outflow boundary.

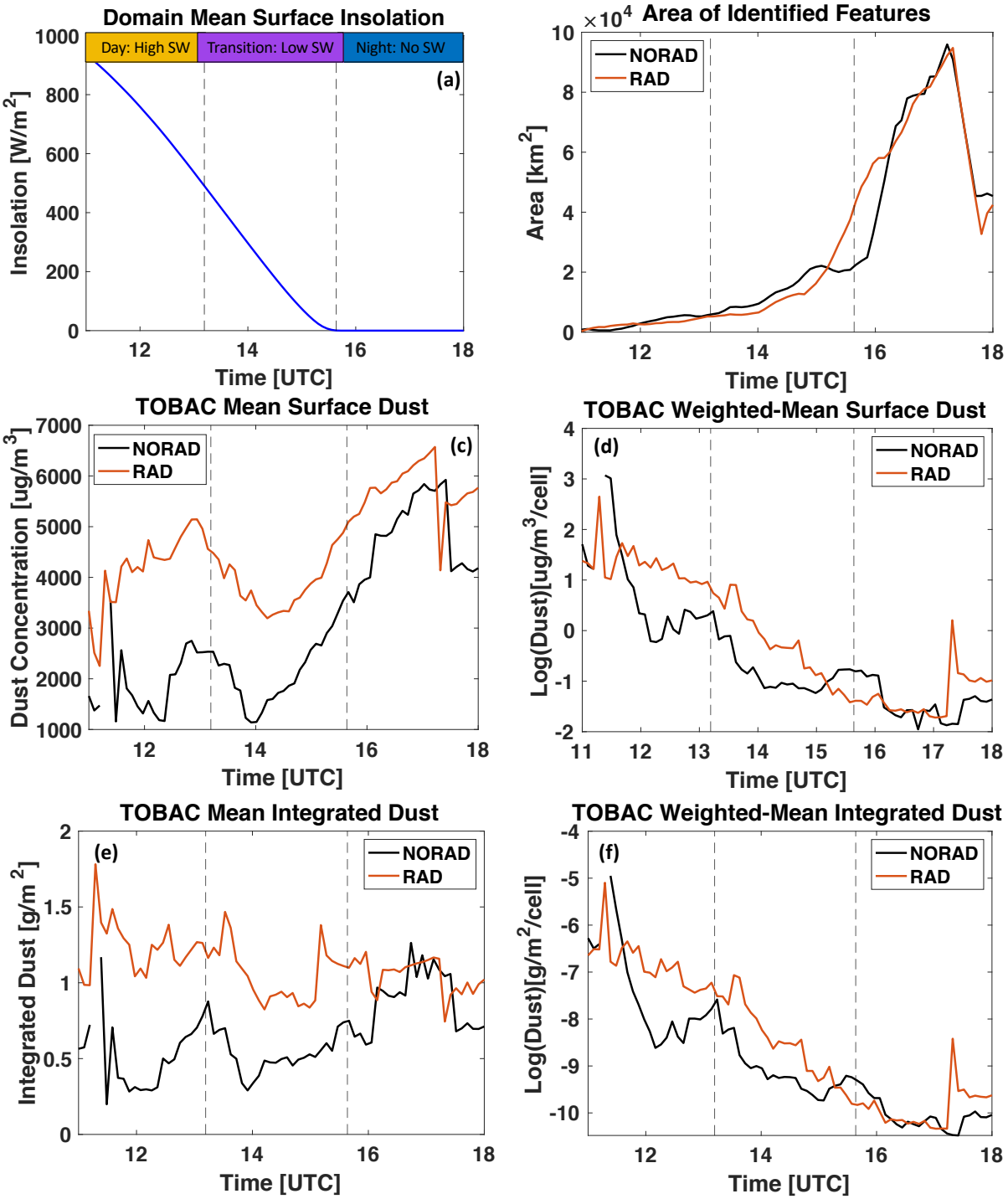

Figure 3.6) (a) Domain mean surface insolation timeseries and designation of the three radiation regimes for analysis: day / high SW (orange), transition / low SW (purple), night / no SW (blue). (b) timeseries of the dust feature area identified by TOBAC for the NORAD (black) and RAD (brown) simulations. Panels (c-f) are averages of dust quantities inside the TOBAC-identified features for the NORAD (black) and RAD (brown) simulations. (c) Mean surface dust concentrations, (e) mean integrated dust, (d) log of area-weighted mean surface dust concentrations, (f) log of area-weighted mean integrated dust.

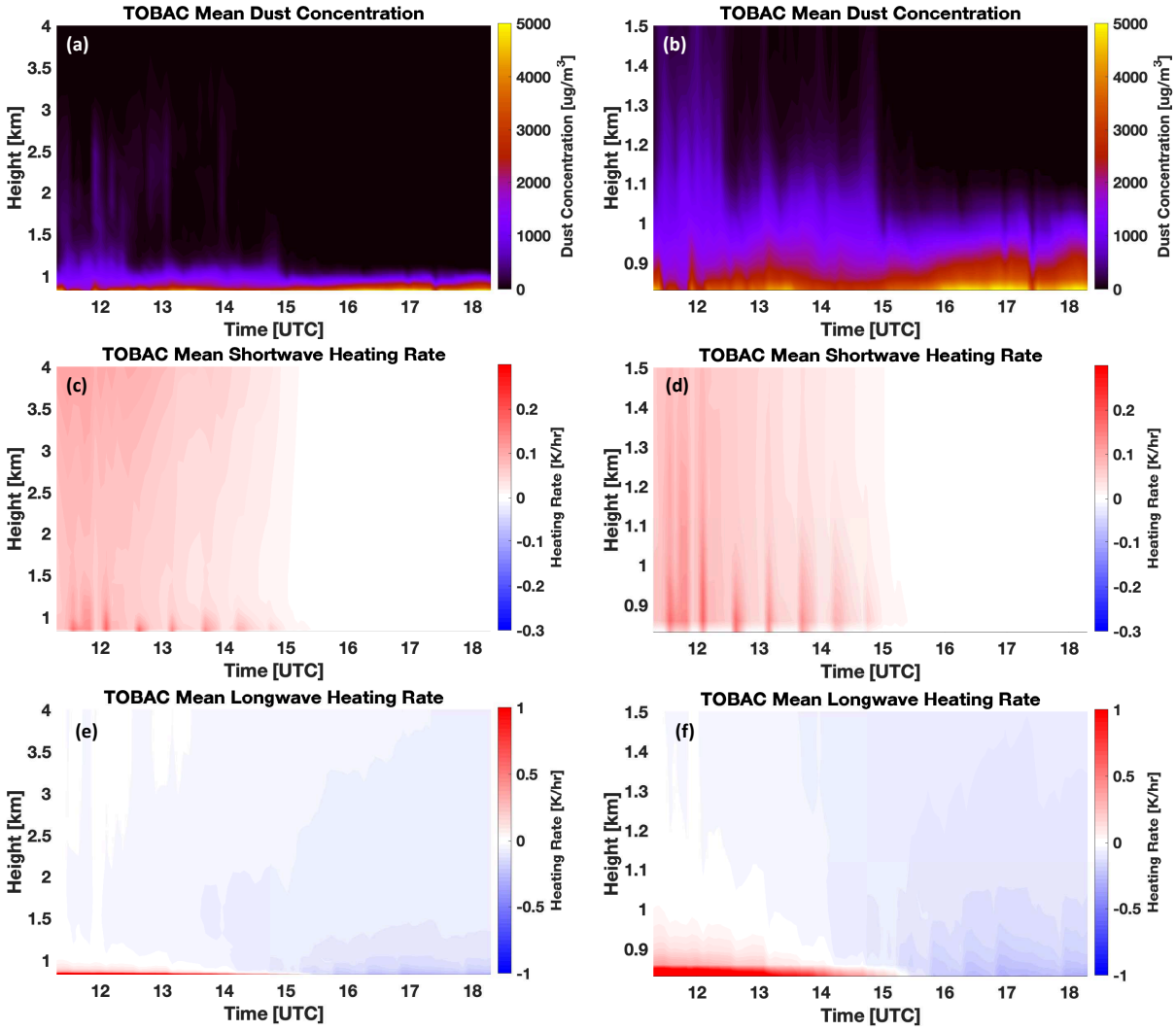

Figure 3.7) Profile timeseries of mean TOBAC (a-b) surface dust concentrations, (c-d) shortwave heating rate, and (e-f) longwave heating rate. The left panels range from the surface to 4 km, whereas the right panels zoom in on the lowest 1.5 km.

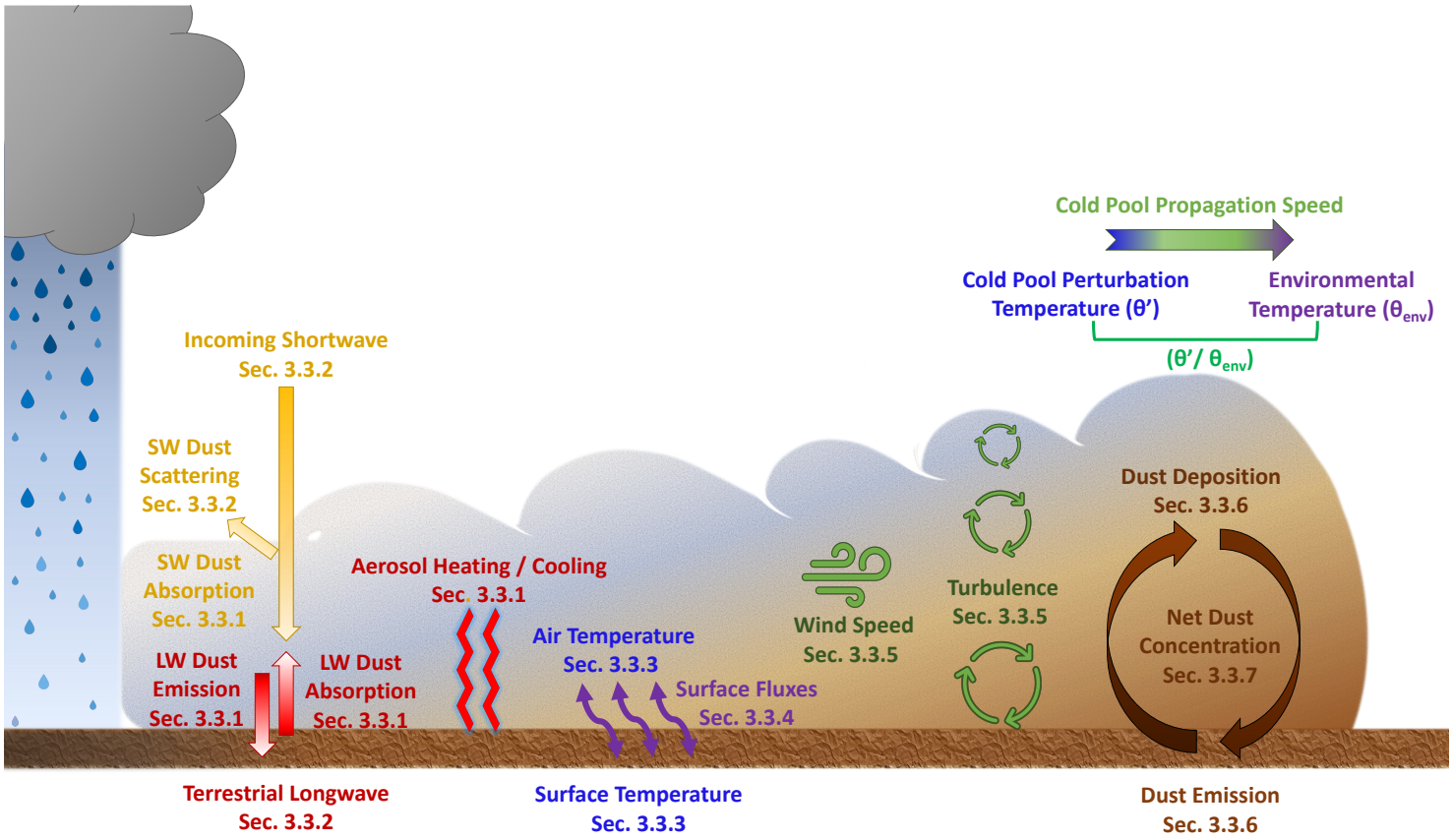

Figure 3.8) A conceptual schematic representing the physical processes impacted by the dust radiative effect in a cold pool. The numbers refer to the section where the mechanism is discussed.

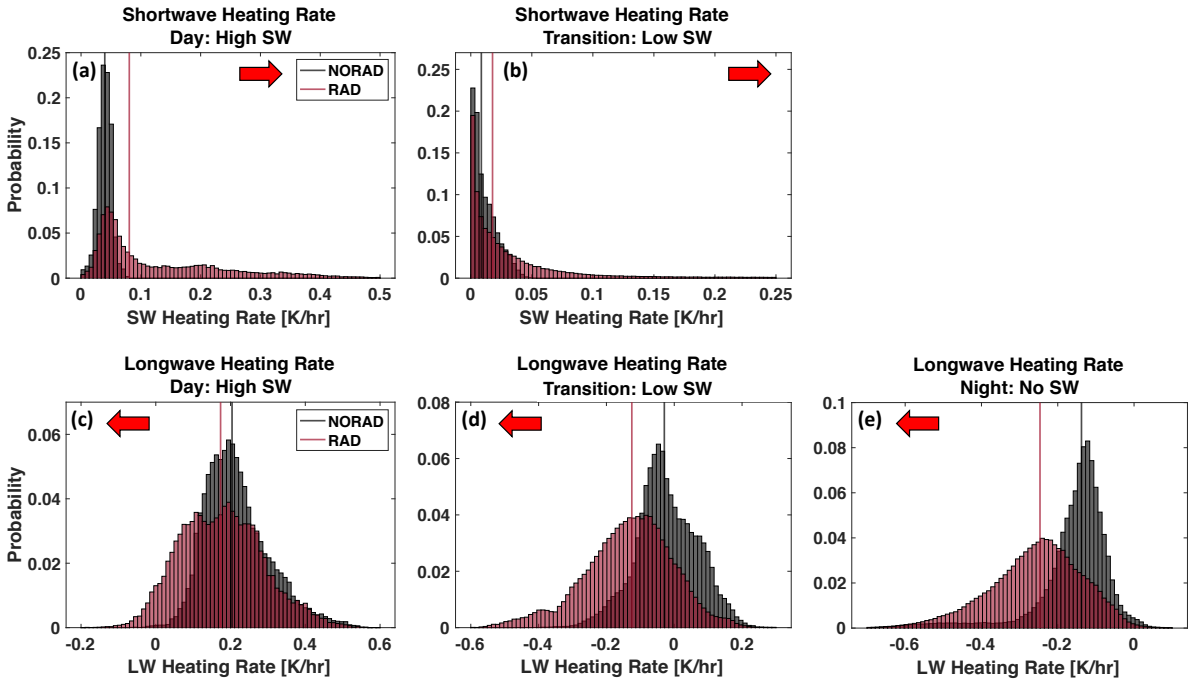

Figure 3.9) Normalized probability histograms of the shortwave (a-b) and longwave (c-e) heating rates for the 3 analysis time periods for the TOBAC-tracked dust features in the NORAD (gray) and RAD (dark red) simulations. The vertical lines represent the median of each distribution. Arrows pointing toward the left indicates a shift in the distribution to lower values (decrease) when dust radiation is included, with the opposite arrow orientation indicating a shift towards higher values (increase) from including aerosol radiative interactions.

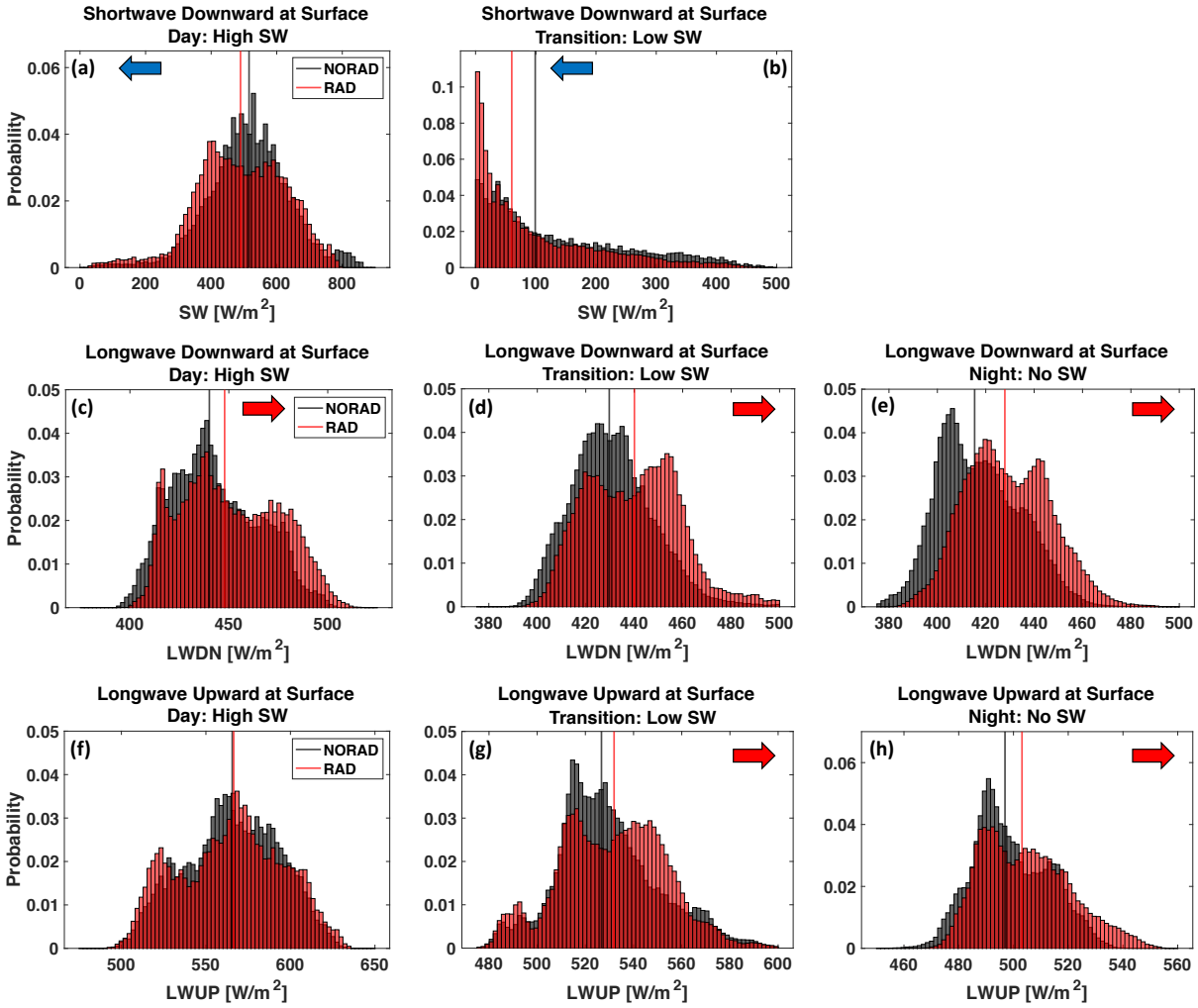

Figure 3.10) Same as Figure 3.9, but for surface (a-c) downward SW radiation**, (d-f)** downward LW radiation, and (f-h) upward LW radiation.

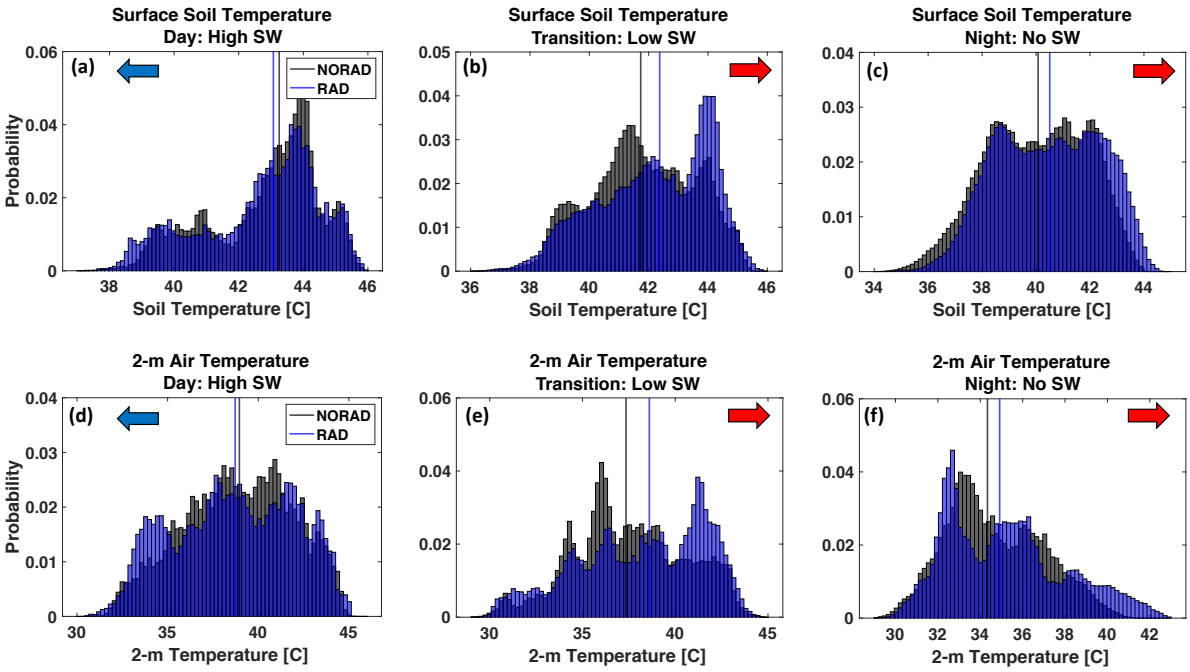

Figure 3.11) Same as Figure 3.9, but for surface (a-c) soil temperature and (d-f) 2 m air temperature.

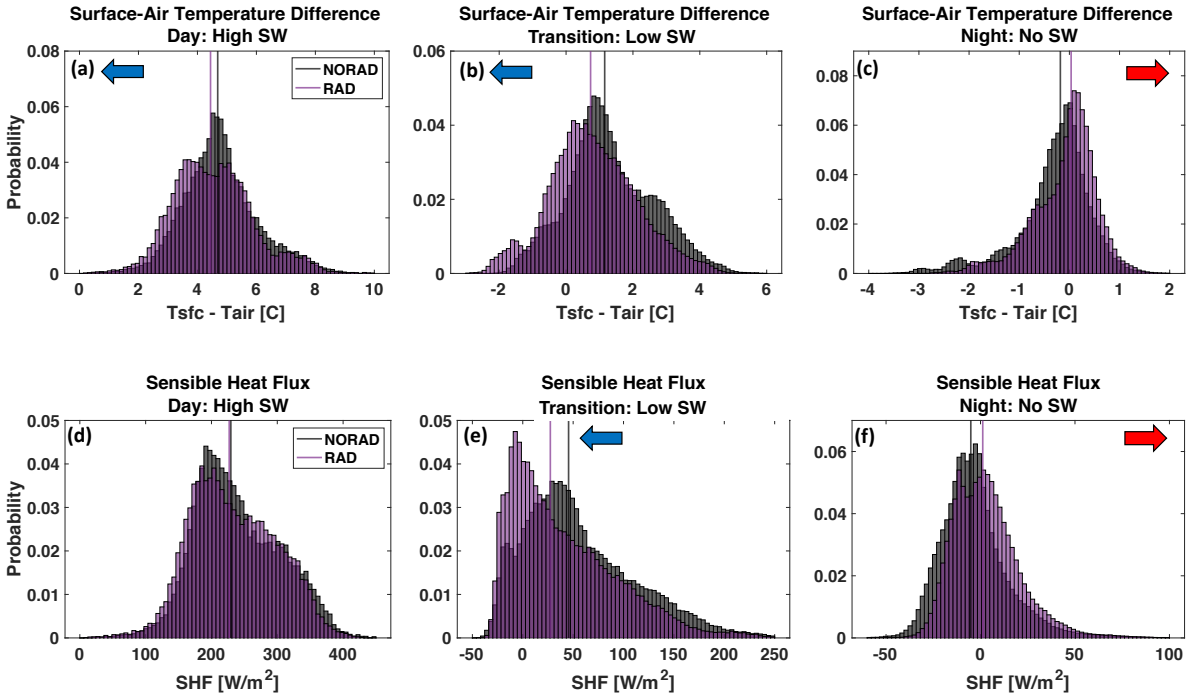

Figure 3.12) Same as Figure 3.9, but for (a-c) surface-air temperature difference and (d-f) sensible heat flux.

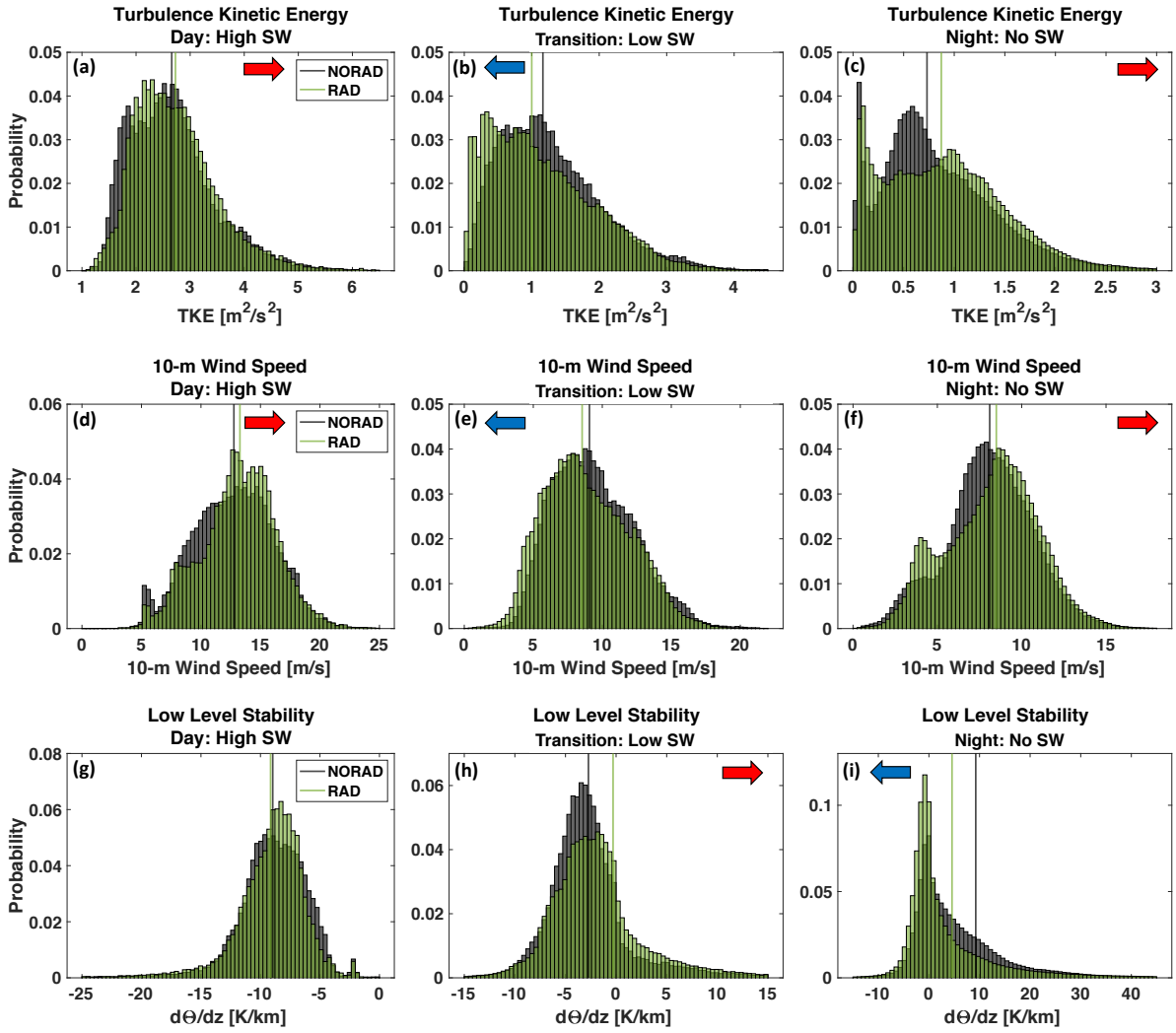

Figure 3.13) Same as Figure 3.9, but for surface (a-c) turbulence kinetic energy, (d-f) 10-m windspeed, and (g-i) stability.

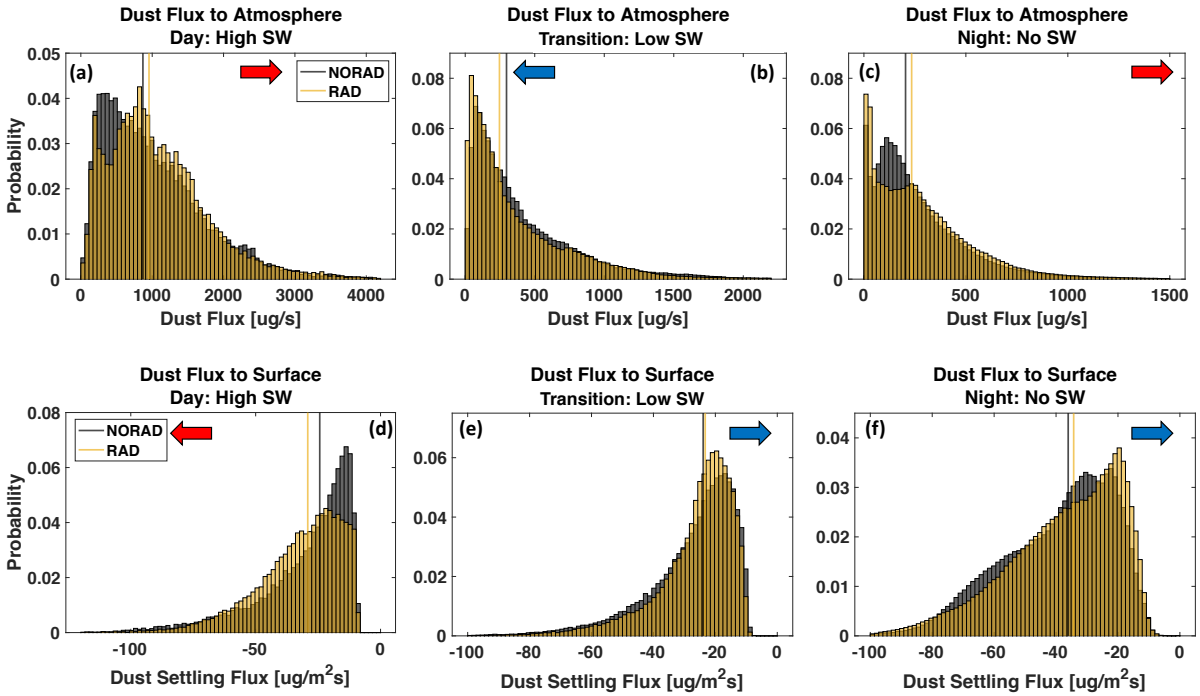

Figure 3.14) Same as Figure 3.9, but for surface (a-c) dust flux to atmosphere and (d-f) dust settling flux. Note that the arrows in panels (d-f) are the opposite of the other figures because dust settling flux is designated as a negative value (i.e. settling removes dust from the air).

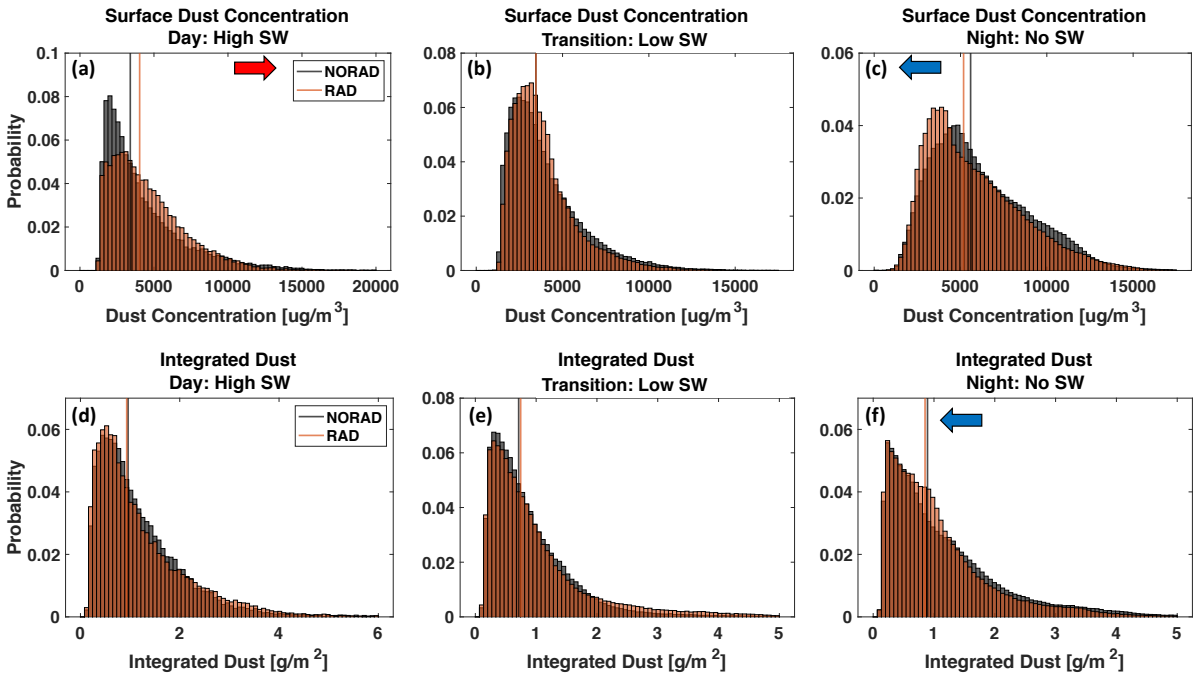

Figure 3.15) Same as Figure 3.9, but for surface (a-c) dust concentrations and (d-f) integrated dust.

Table 3.3) Summary of the mean direct dust radiative response in the simulated density currents. The start next to responses indicates that the normalization procedure affects the results (see Section 3.2.4).

Parameter	Day (High SW)	Transition (Low SW)	Night (No SW)
SW Heating Rate	Increase	Increase	None
LW Heating Rate	Increase	Increase	Increase
Surface SW Downward	Decrease	Decrease	None
Surface LW Downward	Increase	Increase	Increase
Surface LW Upward	Null	Increase	Increase
2-m Air Temperature	Decrease	Increase	Increase
Soil Temperature	Decrease	Increase	Increase
T_{sfc} - T_{air}	Decrease	Decrease	Increase
Sensible Heat Flux	Null	Decrease	Increase
Turbulence Kinetic Energy	Increase	Decrease	Increase
10-m Windspeed	Increase	Decrease	Increase
Low-Level Stability	Null	Increase	Decrease
Dust Emission Rate	Increase	Decrease	Increase
Dust Settling Rate	Increase	Decrease	Decrease
Surface Dust Concentration	Increase	N/A*	N/A*
Integrated Dust	Increase	N/A*	N/A*

CHAPTER 4 – THE IMPACT OF LAND SURFACE PROPERTIES ON HABOOBS

4.1) Introduction

In Chapter 3 we investigated the importance of mineral dust inside a convectively generated dust storm from the perspective of radiative feedbacks to the haboob. However, haboobs can interact with their environment not only through atmospheric dust radiative effects, but also through their connection to the land surface. While wind speed is a major driver of dust emissions, these emissions are modified by the underlying surface (Marticorena and Bergametti, 1995; Shao et al., 1996; 2002; Shao and Lu, 2000; Ginoux et al., 2001; Darmenova et al., 2009; LeGrand et al. 2019; Saleeby et al., 2019; Bukowski and van den Heever, 2020). The physics of dust mobilization from the surface to the atmosphere is immensely complex. Through the years, researchers have taken several different paths in an attempt to meticulously identify and quantify these processes and a comprehensive review of this arduous endeavor and its references can be found in Kok et al. (2012).

The physical mechanisms driving dust mobilization from the surface are reduced in their complexity for parameterized representation in numerical models that differ in their details, although bulk dust models almost always scale emissions based on three major factors: soil erodibility and surface type, soil type, and soil moisture content (e.g. Marticorena and Bergametti, 1995; Shao et al., 1996; 2002; Shao and Lu, 2000; Ginoux et al., 2001). Darmenova et al. (2009) has tested the direct impact of these different scaling factors on dust emissions and reviewed the different approaches to this process in detail, as has LeGrand et al. (2019). Yet, these surface parameters are not only important for dust emissions: they are also an integral factor in cold pool dynamics and properties. In this way, land surface properties affect both the

mechanics of dust mobilization and the cold pool simultaneously, and this synchronous coupling can feed back on dust emissions and the density current in indirect ways. Thus, this study has two objectives. First, to identify which surface parameters, specifically surface type, soil moisture, and soil type, are most significant in predicting haboob dust and propagation. Second, to understand the physical mechanisms that explain why and how these surface properties, important to both dust mobilization and cold pools, affect and feedback on haboob dust and processes.

4.2) Previous Work

Convective dust storms have been studied because of their threat to safety (Baddock et al., 2013; Sprigg, 2016; Middleton and Kang, 2017) and dangers to health (Goudie, 2014; Middleton, 2017). Scientists have also sought to quantify synoptic to global dust budgets and their radiative impacts; because haboobs can loft immense amounts of dust and be long-lived (Flamant et al., 2007; Miller et al., 2008; Roberts and Knippertz, 2014), researchers seek to quantify the contribution of convective dust storms to regional and global dust budgets. Results vary widely and include ranges lower than 10 % in Australia to possibly more than 60 % (Bou Karam et al., 2009) in the western Sahel with a strong seasonal component to dust uplift (Heinhold et al., 2013; Bergametti et al., 2017). Estimations and forecasts of haboob dust concentrations from models depend on accurate representation of cold pools, dust uplift, and surface factors, and remain challenging (Knippertz and Todd, 2012) due to interacting variables. In Chapter 2 we investigated some of the interactions of the dust parameterizations with the environment and convective transport, and in Chapter 3 we examined how radiation feeds back

onto haboob properties. Here, we will now explore another interaction: the connection between surface properties that affect both dust lofting and cold pool dynamics.

As seen in Chapter 3, most previous literature has focused on either dust or cold pools, but not both, and surprisingly little work has been done on correlating the parameters that affect dust mobilization (soil type, soil moisture, and surface type) to the effect on parent convection or outflow boundaries. Soil type is often studied from the perspective of the clay content, whereby soils with higher clay fractions are estimated to loft more dust (Fecan et al., 1999), affect the partitioning of coarse and fine particles (Marticorena and Bergametti, 1995; Shao et al., 1996; Mokhtari et al., 2012), and has been shown to be important for radiative effects and atmospheric residence time (Kok, 2011; Mahowald et al., 2014). Nonetheless, the clay fraction of soil affects its composition, which affects its thermal conductivity and moisture-retention (Abu-Hamdeh, 2003) and therefore its interaction with the atmosphere via surface fluxes, which is known to be important for dust uplift (Huang et al., 2018) and cold pool dissipation (Bryan and Rotunno, 2014; Grant and van den Heever, 2016; 2018; Gentine et al., 2016*;* Drager and van den Heever, 2017; Kurowski et al., 2018).

Soil moisture will also affect the partitioning of surface fluxes and cold pools (Fast et al., 2019; Drager et al., 2020) and scales dust emissions so that less dust lofts when soil is moist. However, the influence and importance of soil moisture on haboobs is less clear. It has been shown previously that soil moisture effects reduce cold pool emissions of dust by 15 % (Heinold et al., 2013), and on a larger scale, the combined precipitation effect of wet scavenging and soil moisture only affects 9-25 % of total dust uplift potential in the Sahara (Heinhold et al., 2013; Bergemetti et al., 2017). Furthermore, desert topsoil dries fast during day (Belnap et al., 2004) and a large fraction of the precipitation evaporates in the dry air before reaching the surface

(Heinhold et al., 2013). As a consequence, in theory soil moisture may be important, but the practical significance of soil moisture in desert cold pools and dust uplift is still uncertain. While some studies have considered soil type and moisture, literature considering the effect of surface type on haboobs outside of identifying erodible surface maps is sparse. It is true that erodibility maps can drastically alter dust emissions and radiation (Saleeby et al., 2019; Bukowski and van den Heever, 2020) especially on the mesoscale (Walker et al., 2009). Other than scaling by erodibility, surface type is only directly included in some, but not all dust emission equations through a roughness length factor that represents the decrease in dust emissions with taller and/or more roughness elements due to drag and sheltering (Marticorena and Bergametti, 1995; MacKinnon et al., 2004; Pierre et al., 2012). Additionally, roughness length has been shown to have an effect on cold pools via changes to sensible and latent heat fluxes (Gentine et al., 2016) and the underlying surface vegetation, as well as soil moisture, will also have an effect on surface fluxes.

Many erroneously presume that deserts or desert-like environments are the only surface types of interest when considering dust emissions. Nevertheless, drylands such as short grasslands and cropland / agricultural / grazing rangelands are also significant local sources of dust (Stout, 2001; Lee et al., 2012). In fact, Ginoux et al. (2012) found that 20 % of global dust emissions originate from surfaces with vegetation and that anthropogenic dust sources, mainly from agricultural grasslands and croplands, contribute 25 % of the global dust budget. Anthropogenic climate change has already led to the desertification drylands (Burrell et al., 2020) and dust is correlated with drought (Reheis and Urban, 2011), which has increased and is projected to continue to increase as temperatures warm (Bell et al., 2018). Furthermore, there is evidence of a doubling of desert dust during the last century (Mahowald et al., 2010) and dust

emissions have been increasing in non-desert regions due to climate change and anthropogenic activities, which includes short grasslands (Munson et al., 2011) and agricultural regions (Neff et al., 2008; Brahney et al., 2013). Research on dust emissions in expanded dryland ecosystems is already underrepresented in the literature; understanding how these different surface types loft and respond to dust in convective outflow boundaries is useful now, but will also be relevant to understanding the transition of surface environments and haboobs in a warming climate. Hence, it is clear that the many interactions between haboobs and the underlying surface require more investigation.

To complicate matters, as seen in Chapters 2 and 3, the time of day is also significant for determining surface heat fluxes and cold pool propagation (Liu and Moncrieff, 2000; Seigel and van den Heever, 2012a) and must be taken into consideration. Huang et al. 2018 has taken a first step in understanding haboob-surface interactions by investigating how dust uplift changes in response to prescribed and static daytime sensible heat fluxes under the cold pool. They found through idealized simulations that increasing the sensible heat flux warmed the cold pool, but actually increased wind speed and dust uplift due to enhanced mixing at the surface. While this experiment was only tested for a daytime case with non-interactive surface fluxes, it does provide insight for this study.

With numerous concurrent interactions between dust uplift, the cold pool, and the surface, it is challenging to distinguish which factors are most important for predicting dust concentrations and the properties / dynamics of the haboob. Identifying which factors are critical for predicting dust concentrations and understanding how these factors may interact with each other will provide a roadmap for interactive dust modeling, including considerations for model setup, as well as the necessary accuracy of model input data. This study seeks to quantify the

importance of surface type, soil moisture, and soil type in predicting haboob dust and propagation, and to understand the physics of these haboob-surface feedbacks. To achieve this, an ensemble of 120 idealized numerical simulations of daytime and nighttime haboobs of varying strengths and surface properties will be analyzed using a global sensitivity technique and one-at-a-time factor separation tests.

4.3) Case Study and Model Description

4.3.1) Model Description and Physics

Simulations are conducted using the open-source Regional Atmospheric Modeling System version 6.2.11 (Pielke et al., 1992; Cotton et al., 2003; Saleeby and van den Heever, 2013) on a single Arakawa C-grid (Mesinger and Arakawa, 1976). Typically, resolution O(~100 m) is necessary to model cold pools from a numerical convergence standpoint (Bryan et al., 2003; Lebo and Morrison, 2015; Jeevanjee, 2017), and to represent cold pool processes (Droegemeier and Wilhelmson, 1987; Straka et al., 1993; Bryan et al., 2003; Grant and van den Heever, 2016; Hirt et al., 2020), thus a horizontal grid spacing of 150 m is utilized on a 65 km x 67.5 km domain. The simulations are run in 3D to more accurately represent the turbulent energy cascade in the Kelvin-Helmholtz waves generated in the turbulent wake of the density current (Cantero et al., 2008; Bryan and Rotunno, 2014). The vertical grid includes 150 levels stretched at a ratio of 1.02 from a minimum of 50 m at the surface to a maximum of 150 m aloft. The model top is 19.3 km, where Rayleigh damping is applied across the upper 14 levels (2.1 km). Model parameterizations include a Smagorinsky turbulence scheme (Smagorinsky, 1963; Lilly, 1962; Hill, 1974) and the Harrington (1997) radiation scheme, which is updated every minute and can interact with atmospheric aerosol (Stokowski, 2005; Saleeby and van den Heever, 2013).

Model dust scatters and absorbs radiation and feedbacks to the dynamics and thermodynamics are based on observations from the Saharan Dust Experiment (Haywood et al., 2003) with an index of refraction of 1.53+0.0015i. RAMS is coupled to the Land Ecosystem-Atmosphere Feedback (LEAF3) surface model, version 3 (Walko et al., 2000). The surface vegetation and soil classes are initialized homogeneously but dynamically interact with the atmosphere via surface fluxes. To simplify the analysis and remove cloud and precipitation effects, no wet microphysics are included in the simulations. Water vapor is allowed to interact with the land surface and radiation in the model but it is not allowed to condense.

The lateral boundary conditions are cyclic in both the x and y direction, with the furthest extent of the cold pool front over 50 grid points from the boundaries after one hour of integration. Initial conditions for the atmosphere and soil temperature are from ERA-5 (C3S, 2017) and are initialized in a horizontally homogeneous manner with zero background wind and no topography. The reanalysis data are from the Arabian Peninsula on August 3rd 2016, at Riyadh. This specific case was selected because it represents a well-studied and previously modeled dust event, which is part of the special ACP/AMT issue "Holistic Analysis of Aerosol in Littoral Environments – A Multi-Disciplinary University Research Initiative (HAALE-MURI)." An overview of this case study can be found in Miller et al. (2019) and is the basis for Chapters 2-3 of this dissertation. Soundings from 06:00:00 UTC (09:00:00 local) and 18:00:00 UTC (21:00:00 local) were used to initialize the daytime and nighttime simulations, respectively (Fig. 4.1). The soundings are representative of the arid interior basin of the Arabian Peninsula, both exhibiting dry air aloft and at the surface, and a tall planetary boundary layer height that extends to 600-500 hPa. The soundings are similar for day and night, although the boundary layer is reduced and there is the onset of a stable nocturnal surface layer in the nighttime case.

The simulations are initially integrated for 3 hours, each with their respective initial surface conditions, from 09:00 to 12:00 and 18:00 to 21:00 local time, to allow the planetary boundary layer and surface fluxes to develop / decline. After 3 hours, a single cold bubble is released and the model is integrated for another 60 minutes. A limitation of the single, idealized cold bubble setup is that the cold pools are not continuously forced by a precipitation shaft or its associated downdraft. This setup is therefore an approximation for shorter lived, isolated precipitating systems. For longer-lived more organized systems, such as in Chapter 3, this assumption becomes less valid and will require more research in the future.

The cold bubble is centered horizontally in the domain with a horizontal diameter of 8 km. In the vertical, the bubble is initialized with its lower edge at 150 m AGL and its top at 6 km. In both the vertical and horizontal, the cold bubble perturbation is represented as a cosine squared function with the strongest perturbation in the center decaying away towards ambient conditions at the sphere's edges. The selected cold pool depth is characteristic of the deep planetary boundary layer and high-based convection typical of this region (Cuesta et al., 2009; Garcia-Carreras et al., 2015). All cold pools initially have a positive moisture perturbation of 5.0 g kg^{-1}, based on observations of Saharan density currents (Trzeciak et al., 2017). A summary of the initial cold pool features and the simulation setup and physics options can be found in Table 4.1.

The simulations are highly, although not perfectly, radially symmetric across the x-y plane (e.g. Fig. 4.2-4.3). The simulations were averaged radially from the center of the domain outward to create 2D cross-sections (e.g. Fig. 4.3-4.4). All values are reported as perturbations from the mean environmental state ahead of the cold pool to account for differences in the

development of the boundary layer and surrounding environment based on the surface conditions.

4.3.2) Dust Emission Parameterization

For this configuration of RAMS, dust is lofted from the surface to the atmosphere through a dust parameterization (Eq. 4.1) based on Marticorena and Bergametti (1995) and is similar to the GOCART dust scheme used in Chapters 2-3:

$$F_p = E_{Z0} C S s_p U^2 (U - Ut_{wet}) \quad if\ U > Ut_{wet}\ \&\ w_{soil} < 0.5 \qquad \text{[Eq. 4.1]}$$

In Eq. 4.1, F_p is the dust flux from the surface (kg m^{-2} s^{-1}) for the two dust bins (p), S is a soil erodibility scaling factor set here, as in Chapter 3, to have an idealized, homogeneous initialization set to 1. C is a tuning constant, also fixed to a value of 1 for this study. Lofted dust is partitioned into a supermicron coarse bin and a submicron fine mode bin by the fractional number s_p (0 to 1). The s_p fraction depends on the clay content of the soil, with smaller aerosol size and higher threshold wind velocities lofting more dust (Alfaro and Gomes, 2001; Shao, 2001). U is the 10 m wind speed (m s^{-1}), and Ut_{wet} is the threshold velocity of wind erosion, Ut (m s^{-1}), and includes a soil moisture correction. The dust parameterization in RAMS is only called if both the near-surface wind speed exceeds the threshold velocity and the total soil saturation fraction, w_{soil}, is below 0.5.

The near-surface threshold friction wind velocity, Ut (Eq. 4.2), is a function of soil particle size, D_p (cm), soil particle density, ρ_p (g cm^{-3}), air density, ρ_a (g cm^{-3}), gravitational acceleration, g (cm s^{-2}), and the Reynolds number, Re.

$$Ut = \begin{cases} \frac{0.129K}{\sqrt{1.928 * Re^{0.092} - 1}} & if < Re < 10 \\ 0.129K\left(1 - 0.0858 * e^{-0.0617*(Re-10)}\right) & if\ Re \geq 10 \end{cases} \qquad \text{[Eq. 4.2]}$$

$$K = \sqrt{\frac{\rho_p g D_p}{\rho_a}} \sqrt{1 + \frac{0.006}{\rho_p g D_p^{2.5}}}$$

$$Re = \frac{1331 * D_p^{1.56}}{0.38}$$

Ut_{wet} is a scaled version of Ut (Eq. 4.3) and depends on the volumetric soil moisture, w ($m^3\ m^{-3}$), and w' ($m^3\ m^{-3}$), which is the minimal volumetric soil moisture required to induce an increase in erosion threshold, and has been determined empirically to be relative to the clay percentage, $\%clay$, of the soil (Fecan et al., 1998).

$$Ut_{wet} = Ut * \begin{cases} \sqrt{1 + 1.21(w - w')^{0.68}} & if\ w \geq w' \\ 1 & if\ w < w' \end{cases} \quad \text{[Eq. 4.3]}$$

$$w' = 0.0014(\%clay)^2 + 0.17(\%clay)$$

In addition to the other scaling factors in Eq. 4.1, E_{Z0} is a surface roughness, and Z_0 (cm), is a scaling factor (Eq. 4.4) from Pierre et al. (2012). Physically, the roughness length affects dust lofting by shielding the erodible soil and reducing the wind momentum transferred to surface. Greater E_{Z0} leads to higher values of surface roughness, thereby increasing the threshold wind velocity and decreasing the dust flux to the atmosphere (Marticorena and Bergametti, 1995). Here, the $Z_0 \geq 3.10 * 10^{-3}\ cm$ threshold is met in all simulations and therefore the E_{Z0} scaling factor is employed for all surface types in this experiment (Sec. 4.4.1).

$$E_{Z0} = \begin{cases} 0.7304 - (0.0804 * log_{10}(Z_0)) & if\ Z_0 \geq 3.10 * 10^{-3}\ cm \\ 1 & if\ Z_0 < 3.10 * 10^{-3}\ cm \end{cases} \quad \text{[Eq. 4.4]}$$

Outside of the dust parameterization, roughness length also affects heat fluxes between the atmosphere and land surface. Higher roughness lengths enhance the downward momentum transfer at the surface, represented by the surface friction velocity, $u*$ ($m\ s^{-1}$), which increases

sensible (Eq. 4.5a) and latent (Eq. 4.5b) heat fluxes in the bulk aerodynamic formulae reiterated here from Chapter 3:

$$\mathrm{SHF} = \mathrm{C_d C_p \varrho_{air} U(T_{sfc} - T_{air})} \quad \text{[Eq. 5-a]}$$

$$\mathrm{LHF} = \mathrm{C_d C_p \varrho_{air} U(Q_{sfc} - Q_{air})} \quad \text{[Eq. 5-b]}$$

where C_d is an aerodynamic bulk transfer coefficient that increases as roughness height increases, C_p is the heat capacity of dry air at constant pressure (J kg^{-1} K^{-1}), ρ_{air} is the density of air (kg m^{-3}), U is the near-surface wind speed (m s^{-1}), and T_{sfc} / Q_{sfc} and T_{air} / Q_{air} are the temperature / water vapor mixing ratio of the surface and the near-surface air (K^{-1}, kg kg^{-1}) respectively.

Dust is removed from the atmosphere via dry deposition onto the surface due to gravitational settling and dynamical transport via downdrafts. To first order, stronger winds, drier soils, smoother surfaces, and higher clay fractions will lead to more dust flux to the atmosphere. Because of the U^2 term in Eq. 4.2, it is clear that windspeed is the most important parameter in parameterized dust emissions. Nevertheless, as seen in Bukowski and van den Heever (2020) and in Chapter 2, the higher order parameters, such as soil moisture, modulate the effect of windspeed. Together, these dust parameters and dynamical transport can work together to alter dust concentrations.

4.4) Ensemble Design

4.4.1) Factors of Interest

Based both on previous literature and on the RAMS dust parametrization in Section 4.3.2, the authors have selected 5 factors that are likely to influence haboob strength and properties: cold pool temperature, soil moisture, clay soil fraction, surface type, and day versus night. Each

of these variables will alter either the dust emissions and settling, and/or the interaction of the cold pool with surface fluxes and dust radiative effects. These input parameters are combined into a simulation ensemble using the Morris-one-at-a-Time (MOAT) technique (Morris, 1991; Campolongo et al., 2007), also known as the Elementary Effects method, and is described in detail in the following section and a summary of the ensemble design can be found in Table 4.2. Foremost, the strength of the cold pool relative to its environment determines the cold pool propagation and wind speed, which in turn will impact dust flux to the atmosphere (Eq. 4.1). Cold pool strength and propagation speed are driven by the temperature (and hence density) difference between cold pool air and the environmental air around it and can be estimated with the following equation (Benjamin, 1968; Rotunno et al., 1988) that was also explored in Chapter 3:

$$V^2 = 2\int_0^H -g\frac{\theta'}{\theta_{env}}dz \qquad \text{[Eq. 4.6]}$$

where V is the theoretical cold pool speed (m s^{-1}), or intensity, H is the cold pool depth (m) defined by a buoyancy threshold, g is gravitational acceleration (m s^{-2}), dz is the model vertical grid spacing (m), θ' is the cold pool perturbation potential temperature (K) relative to the mean air outside the density current, θ_{env} (K), with θ' calculated as a simple difference between the environmental air and the cold pool air ($\theta' = \theta_{env} - \theta_{cold\ pool}$).

The cold pool temperatures in this experiment range from an initial maximum perturbation aloft of -20 to -10 K. As the cold bubble sinks, it warms; by the time the cold pool reaches the surface, the initial temperature perturbation will decrease by ~5 K. This warming reduces the effective surface cold pool temperatures to a range of -15 to -5 K, which was designed to match observations and modeling studies of surface cold pool temperatures in the

Sahara (Lawson, 1971; Knippertz et al., 2007; 2009; Emmel et al., 2010; Bou Karam et al., 2014; Provod et al., 2016).

Two separate soil properties are tested, including soil moisture and soil clay fraction. Soil moisture was simulated as a percent of soil saturation and was set to the same value at all soil depths. The values were initialized between 20 % and 40 % and were selected because they represent conditions where cold pools are entering environments where it has and has not previously rained and moistened the soil and also encompass the range in RAMS where dust is allowed loft (15 % - 50 %). The clay fraction of soil was set to 65 % for clay type soil, 57 % for silty-clay-loam, 48 % for clay-loam, and 40 % for silty-loam. The range in values for the clay fraction were based on erodibility measurements from arid soils in the Middle East (Vaezi et al., 2016; Gyamfi et al., 2016), which show clay and silt type soils as most likely to erode.

Four different surface types capable of lofting dust were selected, including desert, semi-desert, short grasslands, and agricultural crop-grassland. The Arabian Peninsula is best represented by a desert or semi-desert scrub surface (Sayre et al., 2020), although other major dust sources of the world, including the Sahara in northern Africa, the Gobi Desert in China, and the western Australian deserts (Tanaka and Chiba, 2006) are bounded by grasslands and croplands (Sayre et al., 2020) that loft dust in transition zones, in addition to vegetated and agricultural lands being large sources of local dust (Ginoux et al., 2012; Stout, 2001; Lee et al., 2012). Each surface type has different representations in the LEAF3 interactive land surface model, including surface roughness (0.001, 0.066, 0.034, 0.100 m), which depends on the combination of soil roughness (0.001), vegetation height (0.0, 0.7, 0.3, 1.0 m) and fractional vegetation coverage (0.0, 0.2, 0.75, 0.85), as well as albedo, evapotranspiration, and surface-air heat exchanges.

While the interactive land surface represents feedbacks between the land and the atmosphere, one limitation of this study is that the environment only responds to the land surface for the 3 hours of simulation time in an effort to adjust the boundary layer to the initial conditions. In reality, each surface type is representative of a distinct environment that may differ from the reference sounding used here. However, the same sounding was used for each surface type to remove an additional factor of influence and because it is also unclear how or if this factor could be combined with the MOAT technique. The higher order effects of environment-surface correlations should be tested under varying environmental conditions, but we leave this to future work.

Lastly, the difference resulting from the time of day was examined by running two separate suites of simulations to represent a daytime and a nighttime case. In the day, sensible heat fluxes will be positive (surface to air), whereas at night the sign can change to negative heat fluxes (air to surface), which can alter both the cold pool propagation and longevity. Additionally, environmental stability differs between day and night, with the nighttime case being more statically stable, and can affect cold pool intensity (Liu and Moncrieff, 2000; Seigel and van den Heever, 2012a). Lastly, as seen in Chapter 3, dust-radiation interactions can have opposite responses during the day and night, with dust scattering incoming solar radiation during the day and cooling the surface, while it absorbs and emits radiation during the during the night and has a warming effect.

4.4.2) Morris One-at-a-Time (MOAT) Sensitivity Analysis

The Morris One-at-a-Time (MOAT) method (Morris, 1991; Campolongo et al., 2007), also known as the Elementary Effects method, is used to rank which of the surface input factors

(cold pool temperature, soil moisture, clay soil fraction, and surface type) are most important for predicting different model output variables (e.g. wind speed, dust concentration, sensible heat flux, etc.) (Sec. 4.4.2.a,e). In addition to representing input-output relationships, MOAT is utilized to select appropriate combinations of surface factors and cold pool temperatures for the simulations to reduce the computational burden (Sec. 4.4.2.c) and to estimate the non-linearity in the relationship between input and output variables (Sec. 4.4.2.b). Each of these features of the MOAT method, and modifications to the statistical algorithm (Sec. 4.4.2.d), are discussed below.

4.4.2.a) Identifying and Ranking Input-Output Relationships

The MOAT method is a global sensitivity analysis technique, which relates uncertain input parameters in a system (e.g cold pool temperature, soil moisture, etc.) to output values (e.g. dust concentration) by perturbing only one input factor at a time. The statistical algorithm then quantifies the overall influence of the input factor on designated model output variables (μ) and ranks the input parameters in terms of their importance via the magnitude of μ, with higher values of μ designating stronger influence. It is important to reiterate that the purpose of MOAT, or global sensitivity methods, is to determine how an initial input factor's value affects the output of a variable. While the sensitivity can be calculated at different times in the simulation, these methods only reflect the effect of the initial values on the solution. Temporal correlations outside of initial values and attribution of physical mechanisms for the observed results in MOAT must be assessed by comparing the output of the one-at-a-time simulations to each other as shown below (Section 4.5.3).

4.4.2.b) Estimating the Non-Linearity of Input-Output Relationships

MOAT is unlike other one-at-a-time methods in that it is capable of estimating the non-linearity and interactions between input factors in the system (σ), with higher values of σ indicating a stronger dependency on the values of other input factors, or more interactions between factors. The σ/μ plane is used to visualize the results (Fig. 4.6), with each quadrant representing the four possible combinations of high / low importance (μ) and high / low non-linearity (σ) (Fig. 4.6a). The ratio of σ/μ also provides information on the correlation between the input parameter and the output variable (Garcia Sanchez et al., 2012) and whether the relationship is linear ($\sigma/\mu < 0.1$), monotonic ($0.1 < \sigma/\mu < 0.5$), almost monotonic ($0.5 < \sigma/\mu < 1.0$), or non-linear or non-monotonic ($\sigma/\mu > 1.0$) (Fig. 4.6b).

4.4.2.c) Reducing the Number of Simulations

In addition to estimating interactions across input factors, MOAT reduces the total number of model runs compared to traditional one-at-a-time factor analysis methods and is one of the most efficient global sensitivity techniques (Sarrazin et al., 2016). MOAT is classified as a multiple start perturbation method (Pianosi et al., 2016), where each "start," or initial condition, is randomly selected from the uniform grid of input parameter values and then follows a trajectory through the parameter value space by moving a discrete amount one factor at a time. This process is repeated R number of times to eliminate bias resulting from the initial condition influencing the trajectory. A local sensitivity is calculated for each trajectory and then all local sensitivities are combined, creating an estimation of the global sensitivity of the full input parameter space without testing all possible combinations. Twelve trajectories were run for this

study, which falls within the range of recommended trajectories required to reach solution convergence (Saltelli et al., 2004).

In traditional one-at-a-time methods, the number of simulations scales as N^k, where N is the number of input parameters and k is the number of values tested for each input parameter. Moreover, including a separate daytime and nighttime ensemble in this study expands the required simulations to $2N^k$. Here, N=4 input factors perturbed with k=4 values for a day and night case would require 512 simulations. Because of the trajectory approach, MOAT requires only R(N + 1) simulations, or 2R(N+1) for this study, and is independent of k. Thus, with R=12 trajectories MOAT reduces the sample size of this experiment from 512 to 120 simulations.

4.4.2.d) Modifications to the MOAT Algorithm

Both the MOAT trajectory selection and the calculation of the elementary effects for the Morris method were performed with the Sensitivity Analysis for Everybody (SAFE) toolbox (Pianosi et al., 2015), which uses the Campolongo et al. (2007) absolute value modification (μ^* instead of μ) to the calculations of Morris (1991) to reduce Type II errors based on the sign of the output variables. This is important for parameters like sensible heat flux, which can take on positive and negative values and artificially inflate the sensitivity without the Campolongo et al. (2007) edits. Because the units and the values of μ^* are unique to each output variable and are therefore arbitrary, I have created a modification of the μ^* output to report these values in a standardized form (μ_s^*) where μ^* values are scaled from 0 to 1. This is accomplished by dividing μ^* and σ by the maximum μ^* in each 10-minute time frame to yield μ_s^* and σ_s. While μ_s^* ranges from 0 to 1, the only limitation on σ_s is that it must be positive; highly non-linear situations will allow for $\sigma_s > 1$. By using this type of standardized framework, the arbitrary units can be

removed while simultaneously retaining the original σ/μ slope for the linearity analysis, with μ_s^* = 1 indicating the input parameter is the most important and μ_s^* = 0 indicating the parameter has no importance and zero prognostic significance on the output variable. Values of μ_s^* between 0 and 1 represent importance relative to 1 (e.g. μ_s^* = 0.9 signifies that the input factor is 90 % as important as the most important input parameter). *Unlike some other variance-based methods, the μ_s^* numbers are not intended to sum to 1 and multiple factors can have the same value if they are equally as important in predicting the output variable.*

4.4.2.e) Selection of Output Variables

While the MOAT algorithm can identify significant factors, it can only determine the predictive significance for a singular output value. Thus, a single number must be determined to represent the full spatial field of the output variable. This is a non-trivial task considering that haboobs are non-homogeneous in space and time (Figs. 4.2-4.5) and often have a distinct head and wake region. After several rounds of tests, we selected the average of the cold pool surface layer split into 10-minute intervals to retain the haboob's temporal progression. Originally, the haboob head and wake were identified separately and the analysis was run twice for the distinct features, but there was surprisingly little difference in which factors were important between the two. The same surface processes act on the head and the wake, thus allowing us to collapse the two and average over the full cold pool area. Surface values were selected to avoid the somewhat arbitrary method of identifying a haboob top when considering vertically-averaged values. Shorter and longer temporal windows were tested, but 10 minutes was found to capture the overall evolution of the results without repeating data.

4.5) Results

4.5.1) Haboob Characteristics

Figures 4.2-4.5 demonstrate the evolution of a 10 K haboob in the first 30 minutes of the simulations for a daytime (Figs. 4.2,4.4) and nighttime (Figs. 4.3,4.5) case. As described in Section 4.3.1, the cold pool is released in the center of the domain and spreads radially outward (Figs. 4.2, 4.3). The maximum wind and associated maximum in dust concentrations lie slightly behind the gust front boundary in the head region of the haboob, which has been noted elsewhere in observations (Marsham et al., 2013) and modeling (Huang et al., 2018). Due to weaker wind speeds in the trailing wake, less dust lofts in this portion of the cold pool and eventually begins to settle out through gravitational forcing. Dust is confined to the low-levels (Figs. 4.4,4.5 g-i), with most vertical transport occurring in the haboob head, which reaches 1.5 km during the day and 1.0 km at night. The depth of the dust wake increases with time due to turbulent mixing and dust entering the wake from reverse flow in the head's overturning billows (Figs. 4.4,4.5 j-l). Both the wake and head of the night haboob are shallower than the daytime haboob due to the statically stable nocturnal layer (Liu and Moncrieff, 2000; Seigel and van den Heever, 2012a).

Because of the hot and arid desert conditions, the cold pool weakens quickly due to surface fluxes and the entrainment of non-cold pool air through Kelvin-Helmholtz waves at its upper boundary. Dissipation occurs much faster in the daytime case than the nighttime case (Figs. 4.4,4.5 a-c) owing to the strong, positive surface sensible heat flux. For most of the nighttime cases, sensible heat fluxes in the cold pool are negative and prevent dissipation. Between the negative surface heat fluxes and stronger static stability, the nighttime density currents propagate faster (Figs. 4.4,4.5 d-f) and farther than those in the day and as a result produce stronger vertical velocities (Figs. 4.4,4.5 j-l) at the gust front.

4.5.2) Sensitivity Analysis

The MOAT sensitivity analysis allows us to determine how important an input factor is to a modeled output value. To fully understand dust uplift, it is also necessary to predict which factors are important for the parent cold pool. Thus, in this section we will consider which surface parameters are significant predictors of cold pool temperature / wind speed, surface heat fluxes, and lastly, dust concentrations.

4.5.2.a) Cold Pool Temperature and Wind Speed

In predicting surface cold pool temperature (Fig. 4.7) and horizontal wind speed (Fig. 4.8), which are related via Eq. 4.6, the initial cold pool temperature is the most important factor at the beginning of the simulations, a result that is perhaps expected. However, it fades in importance after interactions with the surface have had an opportunity to modify the density current. After the first 10-20 minutes, initial cold pool temperature is either replaced or matched in importance by the surface type. In the daytime simulations, soil moisture and soil type are more significant in predicting cold pool temperature and wind but are relatively unimportant at night. Interestingly, while wind speed and cold pool temperature are physically linked via Eq. 4.6, the factors are not perfect matches (Figs. 4.7,4.8 a-b). This indicates there are surface processes that affect either wind speed or cold pool temperature, or may affect them in different ways. Surface type and soil type are the most non-linear variables, while cold pool temperature and soil moisture are mostly linear (Figs. 4.7,4.8 c-d). During the day and night, the initial cold pool temperature and surface type are important for predicting haboob temperature and wind speed, although the soil type and soil moisture are important during the daytime and relatively

unimportant at night and is most likely related to the partitioning of sensible and latent heat fluxes.

4.5.2.b) Surface Heat Fluxes

Although the initial cold pool strength is significant for predicting haboob temperature and horizontal wind speed, it is less important for forecasting surface heat fluxes (Figs. 4.9,4.10). This is in spite of the wind velocity component in both equations (Eq. 4.5) and the temperature gradient term in the SHF equation (Eq. 4.5a). This implies that surface heat fluxes in a desert cold pool are more sensitive to variations in the roughness length or the moisture / temperature gradient than they are to changes in the wind speed. Even though the initial cold pool temperature is essentially unimportant during the day (and is dominated by surface type instead), SHFs depend more on cold pool temperature during the night than during the day, which is split between cold pool temperature and surface type being the principal factors.

LHF's are more complicated than SHF, with surface type again being most important during the day, but with soil type and soil moisture also playing a role. Physically, because LHF depends on the moisture gradient between the air and the surface, initial soil moisture and the amount of moisture each soil type can retain should also be important. In the nighttime LHF case, soil moisture and soil clay content are both more important than cold pool temperature and surface type.

4.5.2.c) Dust Concentration

Because cold pool temperature drives horizontal wind speed and dust is lofted based on that wind speed, the fact that dust concentrations are most dependent on cold pool temperature is

obvious (Fig. 4.11). Beyond cold pool temperature, the second most important parameter lofting dust is again surface type, which is followed by soil type and finally soil moisture. Despite the dust parameterization including a scaling factor for moisture [Eq. 4.1], it seems to have little effect in this case. The scaling factor in Eq. 4.1 only operates across a small range of soil moistures because soil is typically either dry enough to loft or moist enough to prevent lofting. For our experimental haboob case, soil moisture may matter more due to its effect on LHF than because of the emission scaling term, but it is relatively unimportant in both scenarios. Soil type is more important than soil moisture, and its effect is enhanced at night, possibly from the effect soil type has on moisture retention.

It can be seen from Figure 4.11-c,d that soil type and surface type exhibit highly non-linear behavior or interact with one another to predict dust concentrations. As a result, this makes explaining the physical mechanisms very difficult. Soil type can have a non-monotonic relationship to dust concentrations in that more clay content does not always correspond to more dust. A hypothesis for this non-monotonic behavior related to the intrinsic properties of soil types can be found in Sec. 4.5.3.b. Although the surface parameters exhibit non-linearity, the initial cold pool temperature is only slightly non-linear in its relationship to haboob dust (Fig. 4.11-c,d) in both the day and night. Based on where the cold pool temperature lies on the σ_s/μ_s* plane (Fig. 4.11-c,d), the relationship between cold pool temperature and haboob dust emissions must be higher than a first-degree linear polynomial, but lower than a quadratic or higher-degree polynomial, even though dust emissions scale as U^2 to U^3. I hypothesize that a relatively simple theoretical formulation could explain this relationship unearthed in the sensitivity analysis.

First, reduce Eq. 4.1 by removing the scaling factors (E_{Z0}, S, C), the bin partitioning term (s_p), and the soil moisture correction (Ut_{wet}), which was consistently ranked the lowest factor of importance in this analysis, to yield:

$$F \propto U^3 \quad \text{[Eq. 4.7]}$$

Eq. 4.7 indicates that the flux of dust to the atmosphere, F, is related to the third power of the near-surface wind, U. Then substitute the cold pool intensity, V^2, from Eq. 4.6 into Eq. 4.7:

$$F \propto V^{3/2} \quad \text{[Eq. 4.8]}$$

When Eq. 4.8 is expanded using Eq. 4.6, it results in Eq. 4.9:

$$F \propto \left[2 \int_0^{\mathrm{H}} -\mathrm{g} \frac{\theta'}{\theta_{\mathrm{env}}} \mathrm{dz})\right]^{3/2} \quad \text{[Eq. 4.9]}$$

Eq. 4.9 can be simplified into the proportionality statement in Eq. 4.10 that, to first order, relates dust flux (F) to the cold pool temperature (θ') relative to its environment (θ_{env}):

$$F \propto \left[\frac{\theta'}{\theta_{\mathrm{env}}}\right]^{3/2} \quad \text{[Eq. 4.10]}$$

In this relationship, dust flux is proportional to cold pool temperature and is within the range of exponents (~1-2) we would expect arising from the linearity analysis. There is a clear relationship between dust emissions in a convective outflow boundary and the temperature of the density current. This relationship implies that dust emissions can be predicted or based on cold pool temperatures, although more research is necessary to understand this idea further.

4.5.3) Physical Mechanisms

The MOAT sensitivity analysis in Section 4.5.2 identified the most important surface factors for predicting haboob temperature, dust, and surface heat fluxes. Nevertheless, MOAT can only distinguish significant factors from insignificant ones and cannot explain why these

factors are important or ascertain which underlying physical mechanisms are responsible for the effect. While the MOAT sampling strategy does not test all combinations of input factors, there are a limited number of trajectory combinations that perturb only one input factor and hold all others constant. Using this subsample of perturbed simulations allows for a more traditional one-at-a-time factor analysis, whereby processes can be examined and attributed. Within the 120 simulations, 24 (12 day and 12 night) exist in the subsample that represent three factors (soil moisture, soil type, and land surface type) with four value perturbations each. Although the traditional one-at-a-time analysis is important for understanding the mechanisms, it is important to note that the full sensitivity and non-linearity cannot be established with this method. The exact combination of factors can be important and may introduce non-monotonic behavior, hence the need for more sophisticated sensitivity algorithms such as MOAT in Section 4.5.2.

4.5.3.a) Soil Moisture

In the MOAT factor analysis, soil moisture was ranked consistently as the least important but most linear factor in its effects on the haboob processes of interest. Nonetheless, soil moisture still has an effect, whereby increasing soil moisture leads to lower dust concentrations in the haboob (Fig. 4.12-a,b) for both the day and night cases. From observational studies, it has been shown that that moister soils impede lofting by increasing soil cohesion, which is accounted for in Eq. 4.1 and will scale emissions accordingly.

Nonetheless, interactions with the cold pool are also responsible for the observed reduction in daytime dust in which the cold pool temperature becomes colder as soil moisture increases. This contrasts with the nighttime case where there is little change to the cold pool temperature (Fig. 4.12-c,d). However, theory suggests that a colder cold pool should lead to

stronger winds via Eq. 4.6 and subsequently enhance dust uplift. This discrepancy can be explained via the partitioning of the sensible and latent heat fluxes. The daytime LHFs are stronger with moist soils (Fig. 4.12-g,h) because energy is going into evaporating soil water, which cools the cold pool and prevents energy from heating the surface, consequently reducing SHFs (Fig. 4.12-e,f). When SHFs are reduced, there is less mixing and less dissipation of the density current, which results in the cold pool propagating faster across the domain. Yet conversely, decreased SHFs leads to less downward momentum transport, which diminishes the near-surface wind speed and reduces dust emissions. The latter finding is similar to that observed by Huang et al. 2018. Interestingly, during the day the density currents with moister soils propagate further (not pictured) than their dry counterparts because the SHFs dissipate the dry-soil cold pools faster. Despite the density currents being longer-lived in moister conditions, the wind speed near the end of their lifetime is weak and lofts significantly less dust than at the beginning of the simulation when the cold pools are intense and exhibit strong wind speeds. Nevertheless, the extended lifetime of dust lofting in the moist-soil case cannot overcome and replace the large soil moisture dust deficit from the beginning of the haboob's lifetime.

In the nighttime case, there is again more dust in the dry-soil haboobs (Fig. 4.12b) and higher surface concentrations of dust compared to the daytime case, but little change to the cold pool temperature (Fig. 4.12d). SHFs (Fig. 12f) do not change due to soil moisture at night because the surface is no longer absorbing incoming solar radiation and has cooled faster than the air above it. In fact, the surface is colder than the cold pool air, which is evident by the SHFs being negative in Fig, 4.12f. Additionally, LHFs at night are also negative in the haboob head, denoting that the surface is drier than the cold pool (Fig. 4.12h). Negative SHFs prevent the cold pool from dissipating and are almost identical across the different soil moisture values, thus

having little to no effect on temperature, momentum transfer, or wind speed. As such, the difference in dust concentrations must come from the soil moisture scaling factor in the dust emission equation (Eq. 4.1) for the nighttime case.

4.5.3.b) Soil Type and Clay Fraction

Soil type was identified by the MOAT sensitivity analysis to be the second most important factor in influencing cold pool temperature and haboob dust, demonstrating non-linear and non-monotonic behavior. From laboratory studies (Fecan et al., 1999), it has been shown that soils with high-clay fractions will loft more dust than low-clay fraction soils at the same soil moisture (Eq. 4.1-4.4). However, the non-monotonic nature of the soil type response indicates that increasing clay fraction does not always result in an increase in dust emissions, and the non-linear behavior suggests it interacts with other input parameters. Indeed, while the nighttime haboob follows the theory that high-clay fractions will loft more dust, the daytime haboob does not (Fig. 4.13-a,b): the 40 % clay fraction simulation has higher dust concentrations than the 48 % clay simulation.

Integral to the understanding of this non-monotonic response is the fact that changing the soil type in RAMS/LEAF3 inadvertently changes other soil properties. Soil textures are classified by their relative percentage of clay, loam, and silt soil. Since the total clay/loam/silt composition must equal 100 %, a decrease in the amount of clay must be matched by an increase silt or loam. The difference in soil texture leads to differences in other parameters such as porosity, water retention, and thermal conductivity, but it does not significantly alter the albedo or roughness length in this study. Clay and clay-loam soils have lower thermal conductivities, which means less energy will go into the ground and more will be transferred to the atmosphere

via SHFs (Fig. 4.13e) (Rempel and Rempel, 2016) and increase the canopy (near surface) temperature (Fig. 4.13i). Additionally, clay and clay-loam evaporate less and retain more water than silty soils (Fig. 4.13j) (Rempel and Rempel, 2016). When soil retains water rather than evaporating it, LHFs are reduced (Fig. 4.13g), which also reduces the canopy (near surface) water (Fig. 4.13k) and prevents evaporative cooling of the cold pool. Therefore, clay soil has the highest SHFs and warmest cold pool (Fig. 4.13c), but also the weakest wind speeds and lower dust emissions. This result is contrasts with the findings of Sec. 4.5.3.a where the stronger SHFs lead to stronger surface gusts. Here, there is likely an increase in downward momentum transfer due to SHFs, but it does not compensate for the silty soils producing a colder density current.

Returning to the non-monotonic dust results, there are two competing factors in the daytime haboob: the parameterized increase in dust emissions as clay fraction increases, versus silty soils producing colder and stronger cold pools. The balance of these complex and competing processes leads to non-monotonic results and has implications for modeling dust emissions in haboobs. Namely, the clay/loam/silt composition matters for surface fluxes and the interaction between the cold pool and the land surface. The USDA soil taxonomy classifies 12 different soil mixtures (USDA, 1999), each of which could elicit a different response to cold pools and dust emissions based on their thermal and moisture properties and the environment.

4.5.3.c) Land Surface Type

Besides initial cold pool temperature, surface type was identified as the most important factor on in predicting haboob dust concentrations and temperature, and like soil type, exhibited non-linear and non-monotonic behavior in that moving from a desert to a more vegetated surface type does not necessarily decrease dust amounts. Because the mobilization of dust is inhibited as

roughness length increases, this surface effect is represented in the dust parameterization through a roughness length scaling factor [Eq. 4.1,4.4]. Complicating matters, surface heat fluxes are also scaled by roughness length through the drag coefficient in Eq. 4.5, in which shorter roughness lengths decrease the drag coefficient and hence decrease the magnitude of the heat fluxes. Furthermore, there are higher order effects of the surface layer, such as surface albedo, that impact dust emissions via physical interactions with the cold pool.

In both the day and night, dust concentrations closely follow the trend of the roughness scaling factor (Fig. 4.14b) with the desert and grassland surface assigned the lowest roughness lengths and lofting the most dust (Fig. 4.15-a,b), while the simulations with higher vegetation heights loft less. This is despite the desert and grasslands not having the strongest cold pools (Fig. 4.15-c,d) and the desert having lower wind speeds during the day (Fig. 4.15-e,f). In the daytime case, the desert has the most dust, a warmer cold pool, as well as weaker outflow wind speeds (Fig. 4.15-e) due to the cold pool temperature and lower SHFs (Fig. 4.16a). This apparent contradiction arises because the increase in dust due to the shorter roughness length in the dust parameterization is strong enough to dominate over the roughness length reduction in SHFs and thus wind speed at the surface. Because the roughness length scales dust and heat fluxes simultaneously, it is almost impossible to deconvolve the summation of effects in Figures 4.15-4.16 and isolate the vegetation effects outside of the roughness parameter because it dominates the signal. Moreover, another factor to consider is the environmental stability, which has a lower stable layer in the daytime desert surfaces (Fig. 4.14c). The lowered location of the stable layer caps the cold pool and prevents vertical mixing, thus increasing surface dust concentrations.

It is therefore important to represent the vegetation height accurately to predict dust emissions. This is not a simple task when a single roughness height must be determined to

represent complicated landscapes with numerous sources of roughness. Additionally, land surface models like LEAF3 are often categorical and combine roughness height with vegetation interactions (e.g. albedo, transpiration) which go on to affect surface fluxes. Selecting the correct roughness length or vegetation cover may therefore come at the expense of other surface variables, or an accurate combination may not exist in the surface model. Thus, to understand the surface mechanisms, more tests are planned. First, the roughness length scaling factor must be removed from the dust equation so the heat flux signal is evident. Second, tests must be performed with the roughness length removed from the dust equation and set to the same constant value for all surface types in the heat flux equations to isolate the other land surface effects such as vegetation albedo and shading, heat and moisture retention, and impacts on stability. There is also concern for accurately representing roughness length scaling factors in dust parameterizations of surface mobilization. The scaling factor would have to match the surface type and cannot be set arbitrarily. Overall, surface type is the most significant surface parameter for haboobs, but needs further study to understand the exact mechanisms outside of roughness length.

4.6) Conclusions

In this study we conducted a suite of 120 idealized model simulations of daytime and nighttime haboobs to better understand feedbacks between dust producing cold pools and their underlying surface. The simulations covered a wide range of initial parameters, including varied initial cold pool temperatures, surface type, soil moisture, and soil type, based on previous work showing the importance of these factors for both dust mobilization and cold pool dynamics. The ensemble of simulations was analyzed with the Morris-one-at-a-Time (MOAT) sensitivity

method to identify which of the input surface parameters are most significant in predicting haboob temperature and dust uplift. Single simulations were then compared to each other in a traditional factor analysis to understand why the factors identified by the sensitivity analysis are significant or insignificant, and attribute physical mechanisms to the understanding of haboob physics.

The MOAT sensitivity analysis ranked the most important input factors for predicting haboob dust concentrations and properties as: initial cold pool temperature, surface type, soil type, and finally soil moisture.

Firstly, the initial cold pool temperature is the most significant parameter because cold pool temperature drives wind speeds, which drive dust emissions. Initial cold pool strength is important for the entire lifetime of nocturnal haboobs, but is important only at the beginning of the haboob's lifetime for daytime cases. In the day, positive sensible heat fluxes warm and dissipate the cold pool, but also increase gustiness and dust uplift due to the enhanced downward transport of momentum. Conversely, negative heat fluxes at night strengthen the cold pools, leading to nocturnal haboobs being stronger in terms of dust uplift and propagation distance and speed.

Surface type was identified as the second most important factor for predicting haboob properties and the effects are dominated by roughness length. Increased roughness length decreases dust emissions so that bare soil deserts loft more dust than surfaces with tall vegetation, such as semi-deserts or cropland. However, higher roughness lengths also increase heat fluxes, which can enhance wind speeds and dust uplift. These contrasting effects of roughness height dominate the signal, meaning we cannot ascertain the higher order surface

effects such as albedo or transpiration. More tests with the roughness length set as a constant would be necessary to deconvolve these processes further.

Soil type follows surface type in importance, and it generally follows the theory that a higher clay fraction of soil lofts more dust. But differences in thermal conductivity and moisture retention in clay versus silty soils has an effect in daytime haboobs due to the partitioning of sensible versus latent heat fluxes.

Soil moisture was consistently ranked as the least important parameter for predicting haboob dust, despite the soil moisture scaling factor in the dust parameterization. It was observed that moist-soil haboobs propagate further during the day because of the reduced sensible heat fluxes compared to dry-soil haboobs. However, moist-soil haboobs display relatively weaker wind speeds in the beginning of their lifetime, therefore lofting less dust overall compared to dry-soil cold pools.

Finally, a semi-linear relationship between haboob dust concentrations and cold pool temperature was observed in the sensitivity analysis. By combining the dust flux parameterization with the cold pool intensity equation, a relationship between dust flux and cold pool temperature was derived. This relationship provides an opportunity to relate haboob dust uplift to the thermodynamic environment.

The sensitivity analysis has provided insight into which parameters are most important for modeling dust emissions in convective outflow boundaries. Most important is modeling the correct cold pool temperature, which is challenging because of the complicated microphysical-dynamical-environmental feedbacks in convective downdrafts. An accurate roughness length is also crucial for predicting dust emissions and haboob propagation because it impacts both dust emission and surface fluxes. Soil moisture is generally unimportant, which is in agreement with

previous literature that suggests that erodible topsoil dries quickly in arid regions and may not be a significant parameter in practice.

Overall, despite this first attempt to identify factors most important to forecasting haboobs, challenges and future work is necessary. Namely, experiments representing more environments with dust-lofting ecosystems, such as dry grasslands, will help expand this knowledge. Furthermore, studies considering long-lived haboobs that will emit substantially more dust than the isolated convective outflows in this study are necessary for understanding haboobs, their intensity, and form better predictions in the future.

4.7) Figures

Table 4.1) Summary of the RAMS model physics and settings.

Model Aspect	Setting
Grid	Single Arakawa C-Grid (Mesinger and Arakawa, 1979) $\Delta x = \Delta y = 150$ m nx = 430; ny= 450 $\Delta z_{min} = 50$ m $\Delta z_{stretch\ ratio} = 1.02$ $\Delta z_{max} = 150$ m nz = 150
Model Top	19.3 km Rayleigh damping over top 14 layers (~2 km)
Time Step	0.5 s
Integration and Output	3 hours – boundary layer development 1 hour – cold pool 1 minute output
Model Start	06:00 UTC (09:00 Local) – Daytime 18:00 UTC (21:00 Local) – Nighttime
Microphysics	Water vapor physics only – no condensed water
Turbulence	Smagorinsky (1963) with stability modifications by Lilly (1962) and Hill (1974)
Radiation	Harrington (1997) with added aerosol sensitivity (Stokowski, 2005; Saleeby and van den Heever, 2013)
Land Surface	LEAF-3 (Walko et al., 2000) Constant and homogeneous erodible soil fraction
Lateral Boundary Conditions	Cyclical
Initialization	Horizontally homogeneous Zero background wind No topography
Initial and Surface Conditions	ERA-5 reanalysis from Riyadh, Saudi Arabia
Coriolis	None
Cold Pool Initialization	Center of domain Diameter = 8 km $\Delta z_{start} = 150$ m $\Delta z_{max} = 6$ km + 5.0 g/kg water vapor perturbation

Table 4.2) Summary of the values tested for the input parameters included in the ensemble.

RAMS / MOAT Simulation Ensemble				
Cold Pool Temperature [K]	-10 K	-13.33 K	-16.66 K	-20 K
Soil Moisture [% Saturated]	20 %	26.66 %	33.33 %	40 %
Soil Type / Clay Fraction [%]	Clay / 65 %	Silty-Clay-Loam / 57 %	Clay-Loam / 48 %	Silty-Loam / 40 %
Surface Type	Desert	Semi-Desert	Short Grasslands	Crop-Grassland
Day vs Night	12:00 Local Time	00:00 Local Time		

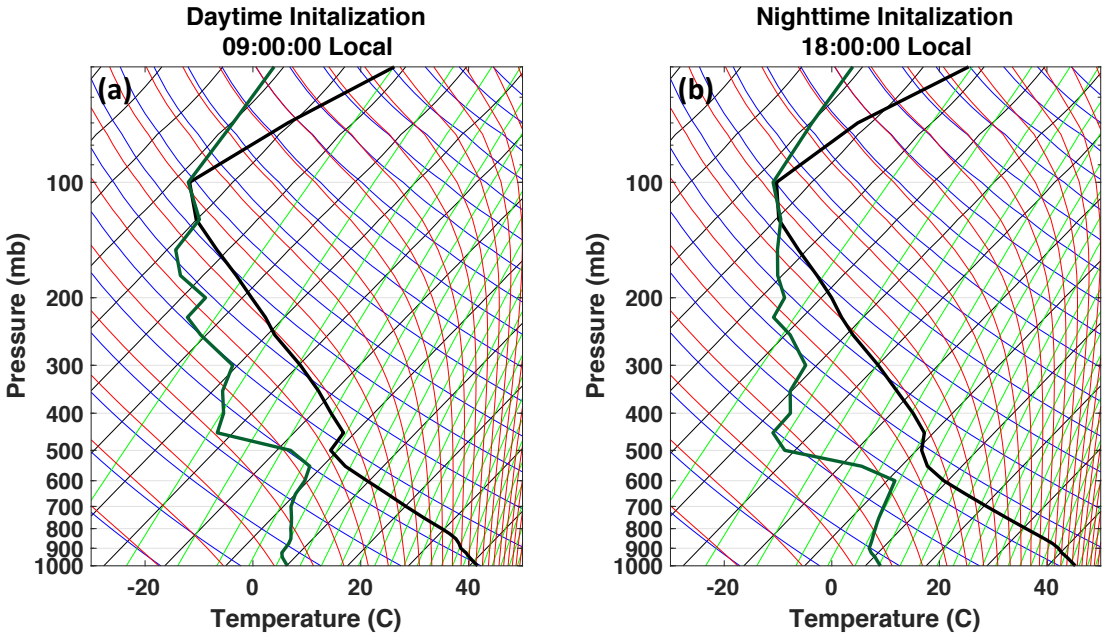

Figure 4.1) ERA-5 soundings from August 3rd 2016, at Riyadh, Saudi Arabia, used to initialize the model for the (a) daytime and (b) nighttime simulations.

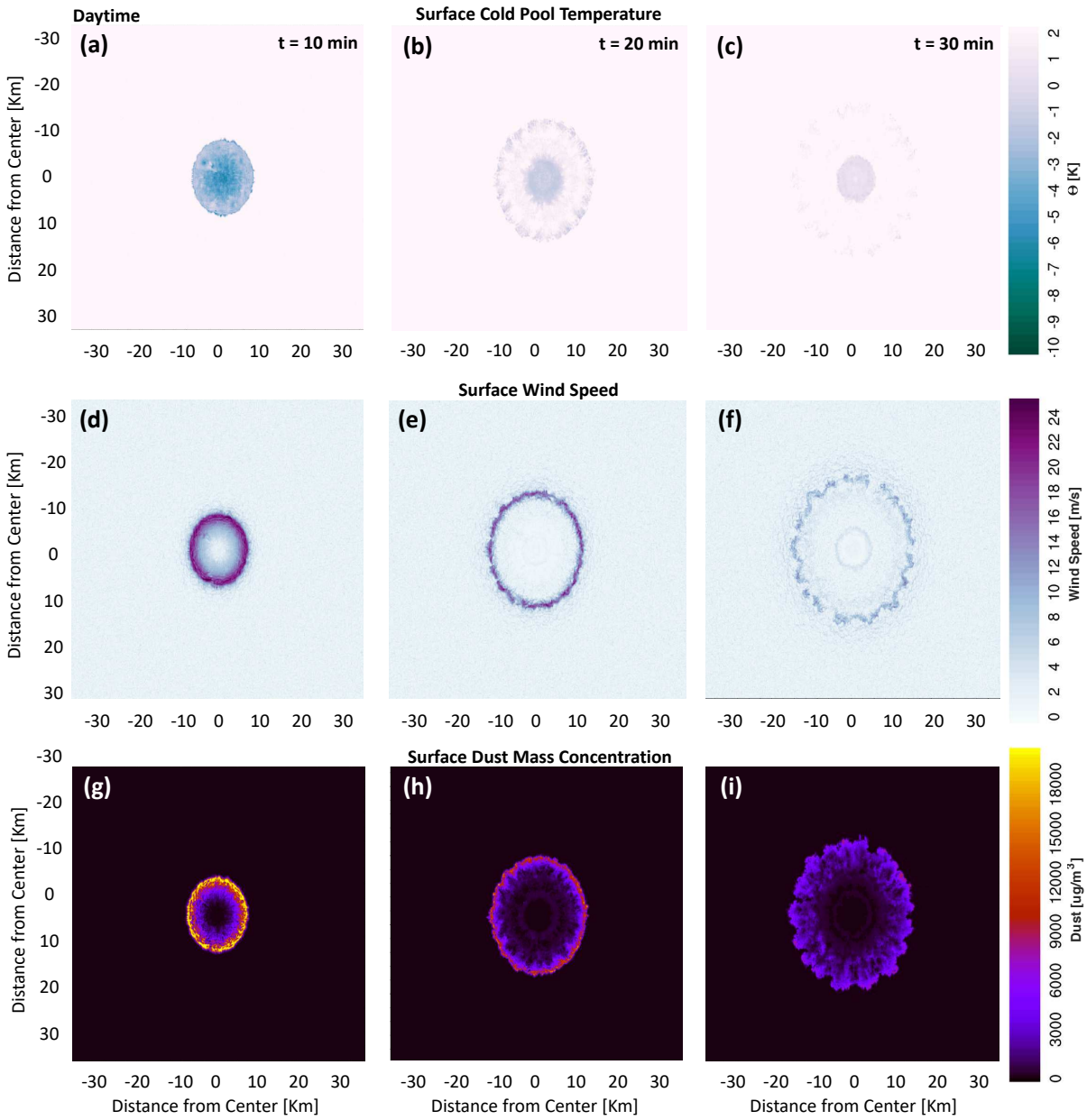

Figure 4.2) Plan view example of the first 30 minutes of the haboob's surface evolution for (a-c) cold pool perturbation temperature, (d-f) windspeed, and (g-i) dust concentrations for the daytime case. The surface values are approximated as the lowest-model level. The x-axis represents the distance from the center of the domain and therefore the center of the cold pool. This example represents the following initial conditions: 16.6 K cold pool, bare desert surface, clay type soil (65 %), and 20 % soil saturation.

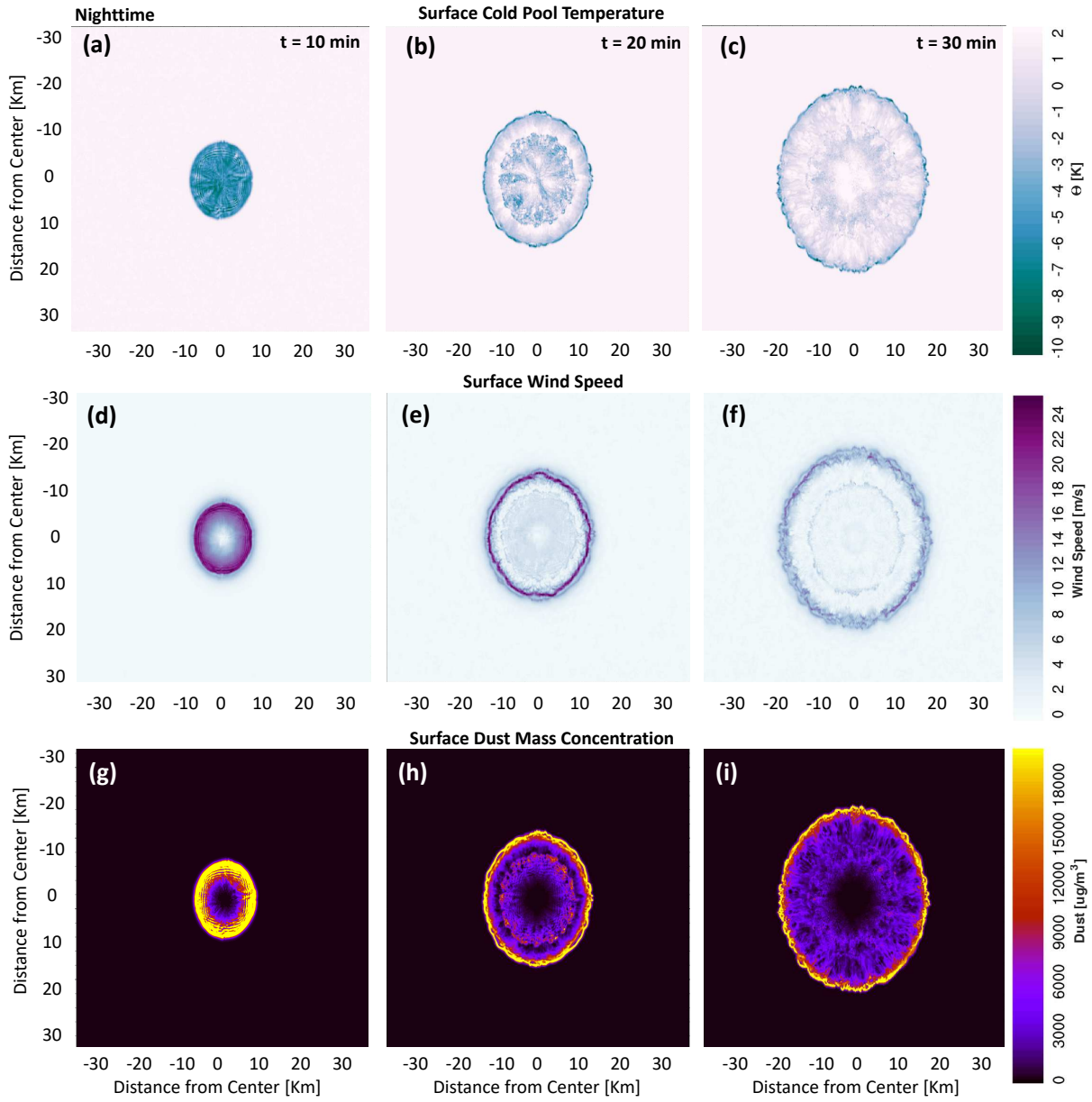

Figure 4.3) Same as Figure 4.2 but for the nighttime case.

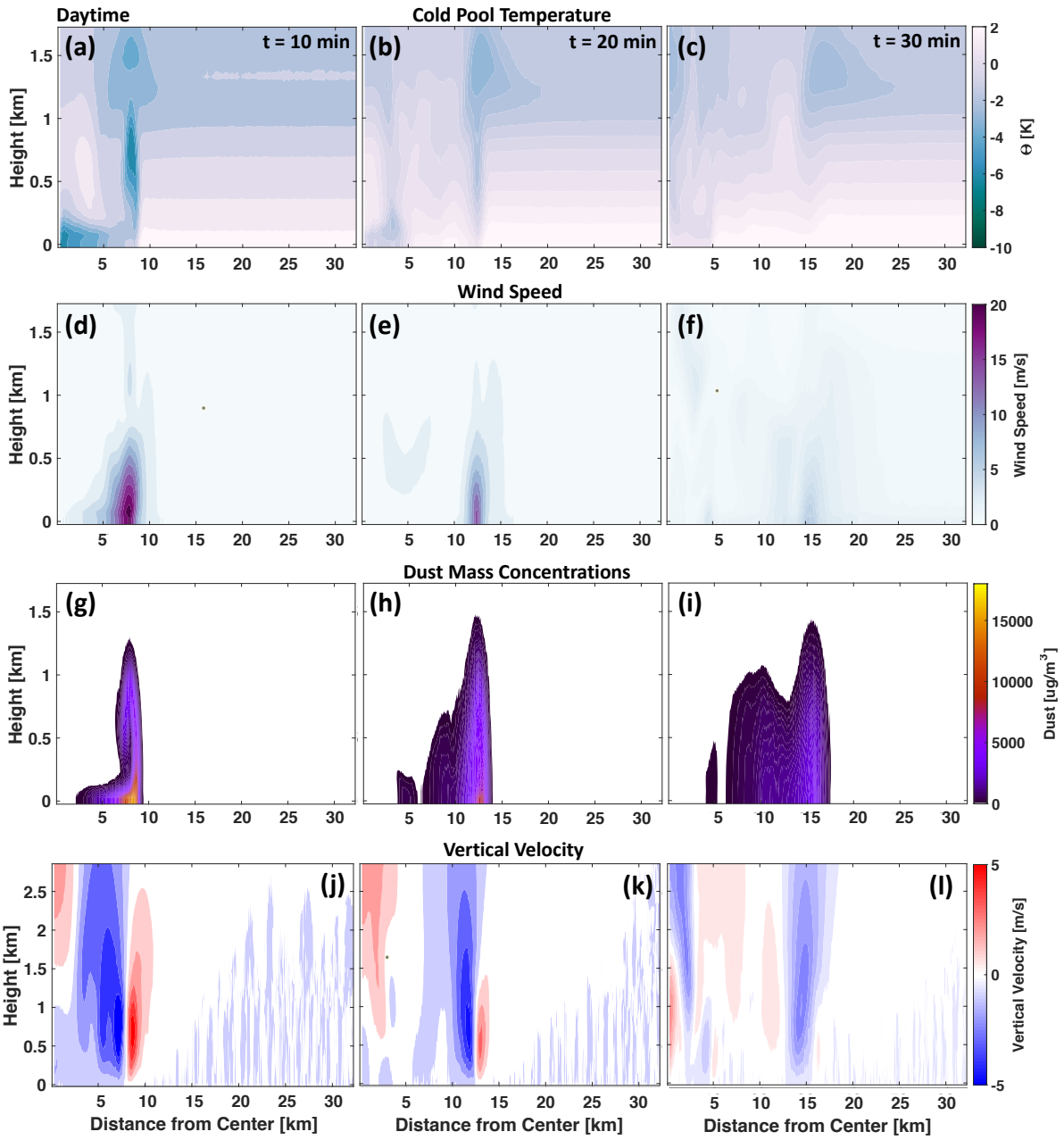

Figure 4.4) Similar to Figure 4.2, but a 2D radially averaged cross section instead of a plan view for the daytime case, with the addition of (j-l) vertical velocity.

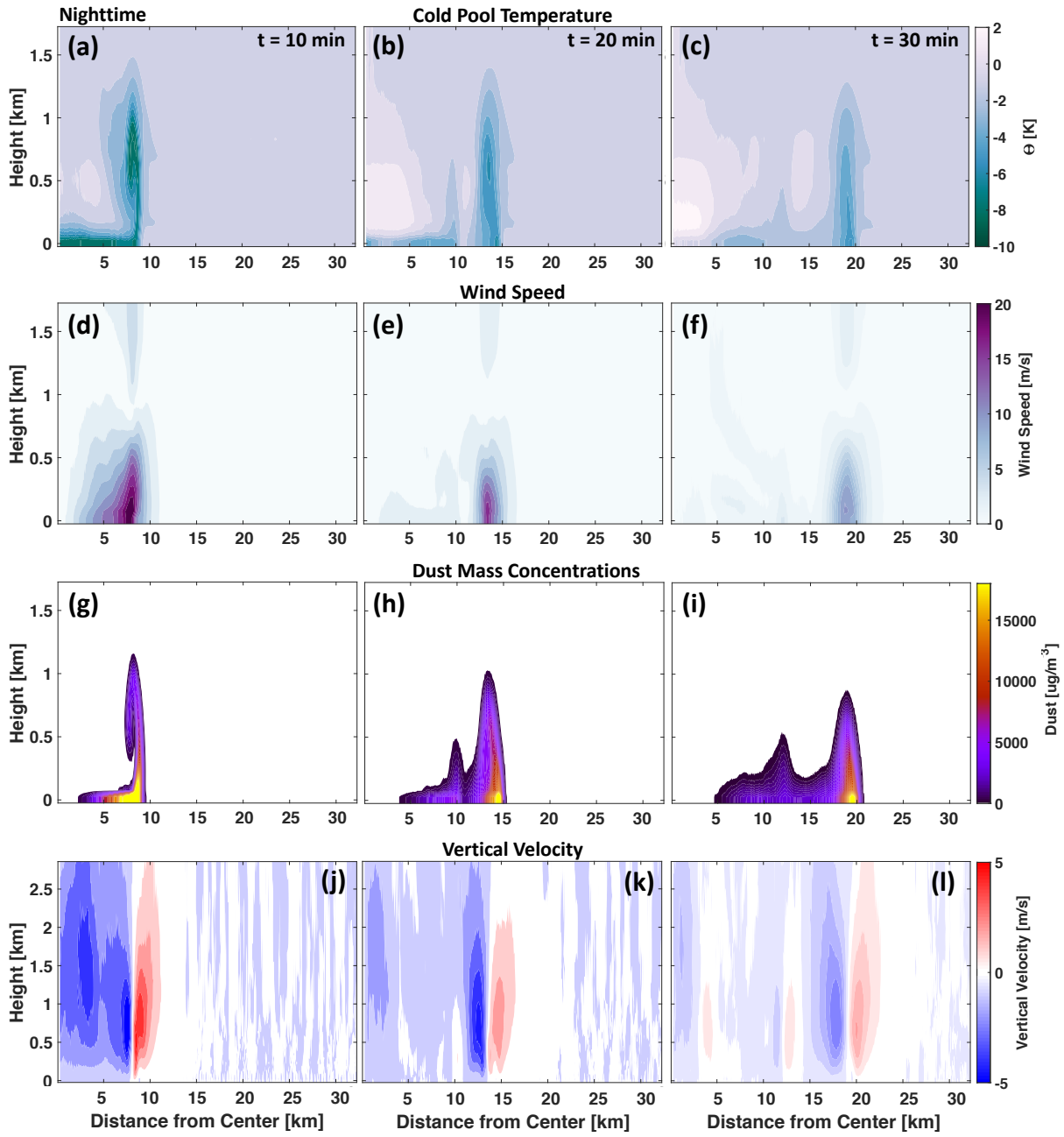

Figure 4.5) Similar to Figure 4.3, but a 2D radially averaged cross section instead of a plan view for the nighttime case, with the addition of (j-l) vertical velocity.

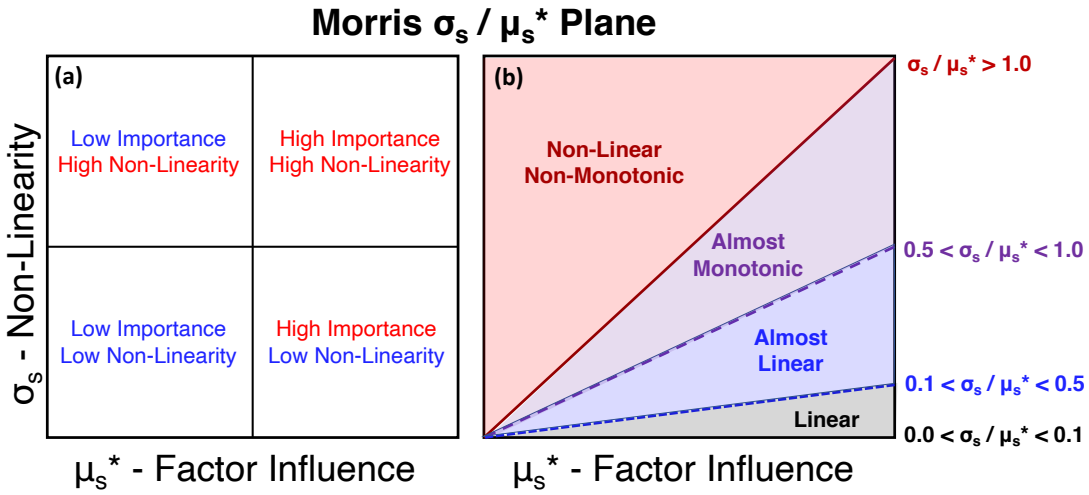

Figure 4.6) Interpretation and visualization of the MOAT sensitivity analysis standardized variables using the σ_s/μ_s^* plane for (a) the input factor importance (μ_s^*) and (b) the factor's non-linearity (σ_s), with each quadrant representing the four possible combinations of high / low importance (μ_s^*) and high / low non-linearity (σ_s). The right figure indicates how the slope (σ_s/μ_s^*) can represent the relationship between input factor and the output variable being linear (black), almost linear (blue), almost monotonic (purple), and non-linear and/or non-monotonic (red).

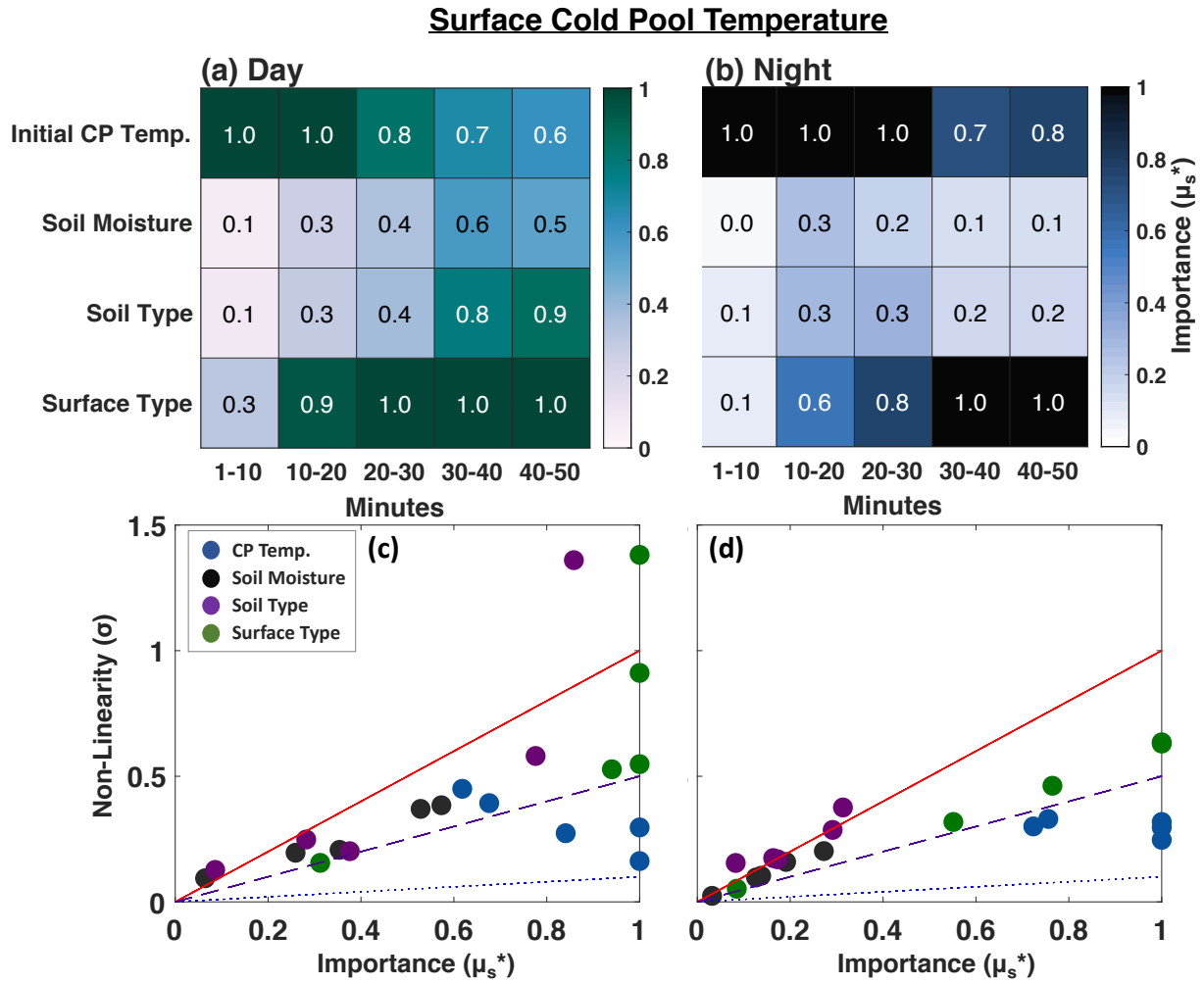

Figure 4.7) Top row: heatmap timeseries of μ_s^* values ranging from 0 (unimportant) to 1 (most important) in predicting surface cold pool temperature for the daytime (left) and nighttime (right) cases. The 4 rows represent the 4 surface input parameters (initial cold pool temperature, soil moisture, soil type / clay fraction, and surface type), while the x-axis is simulation time after initialization split into 10-minute averages. Bottom row: Morris σ_s/μ_s^* plane (Figure 4.6) for the heatmap above it. Each of the 4 surface types (cold pool temperature – blue; soil moisture – black; soil type – purple; surface type – green) have 5 data points that correspond to the 5 separate 10-minute time frame in the top row.

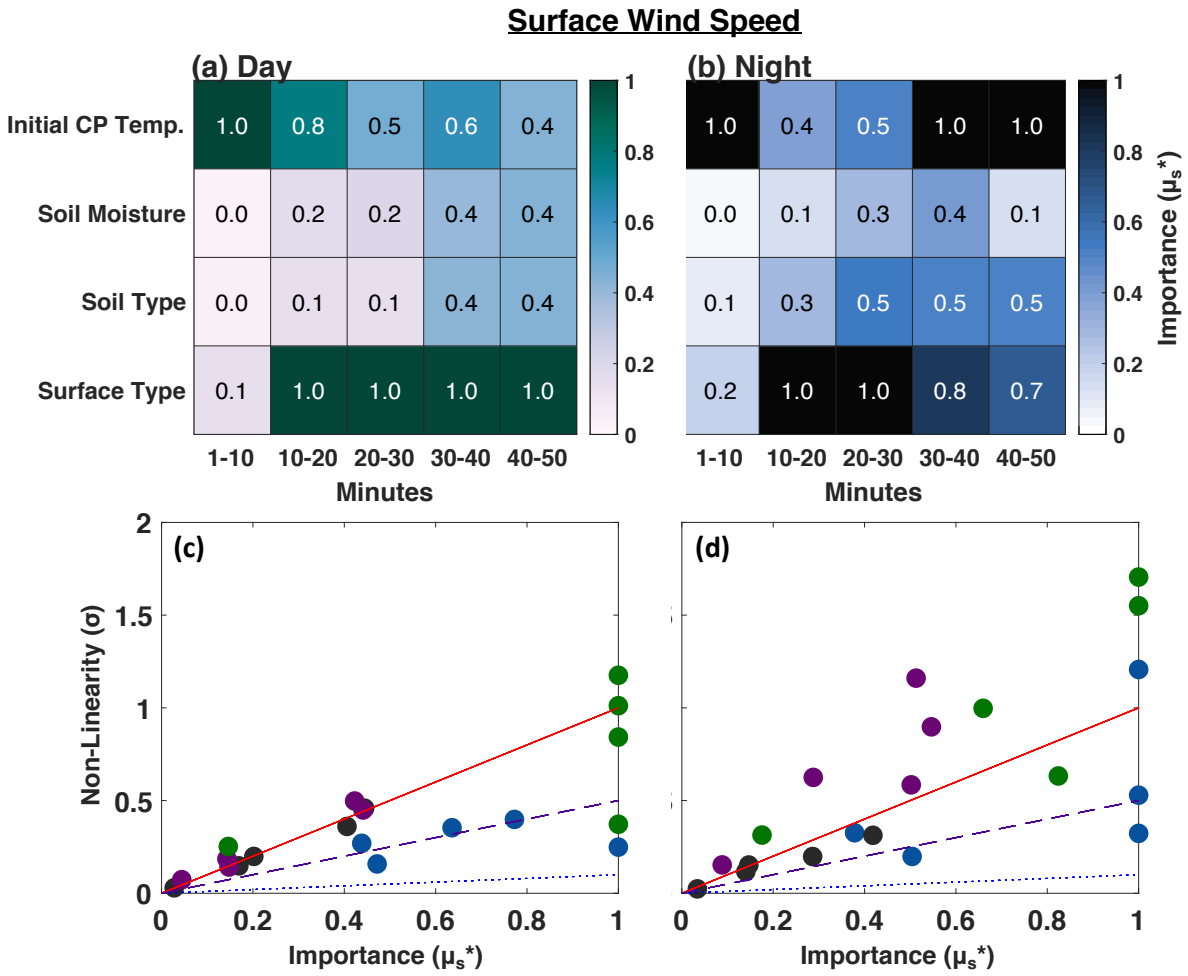

Figure 4.8) Same as Figure 4.7 but for surface wind speed.

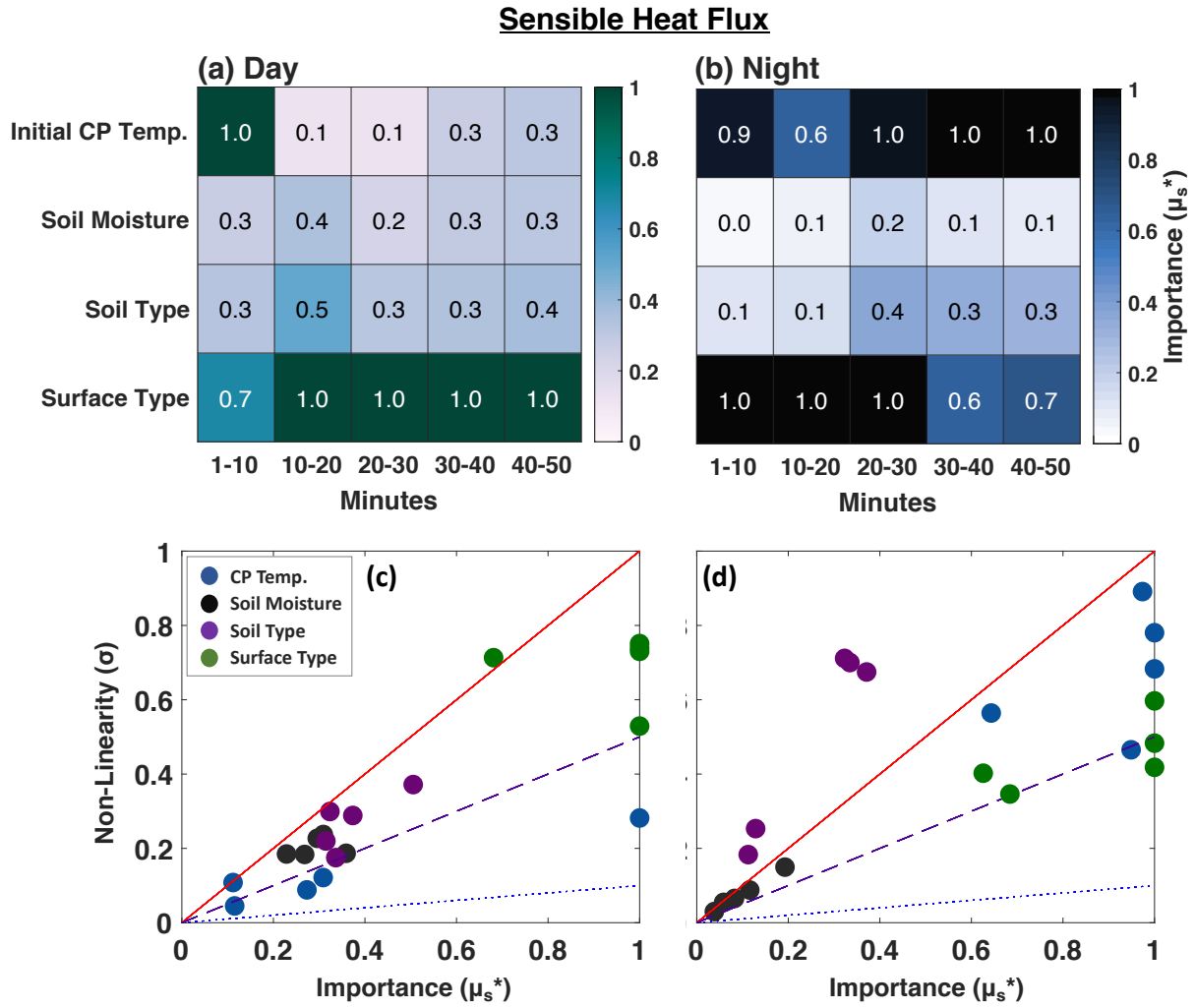

Figure 4.9) Same as Figure 4.7 but for sensible heat flux.

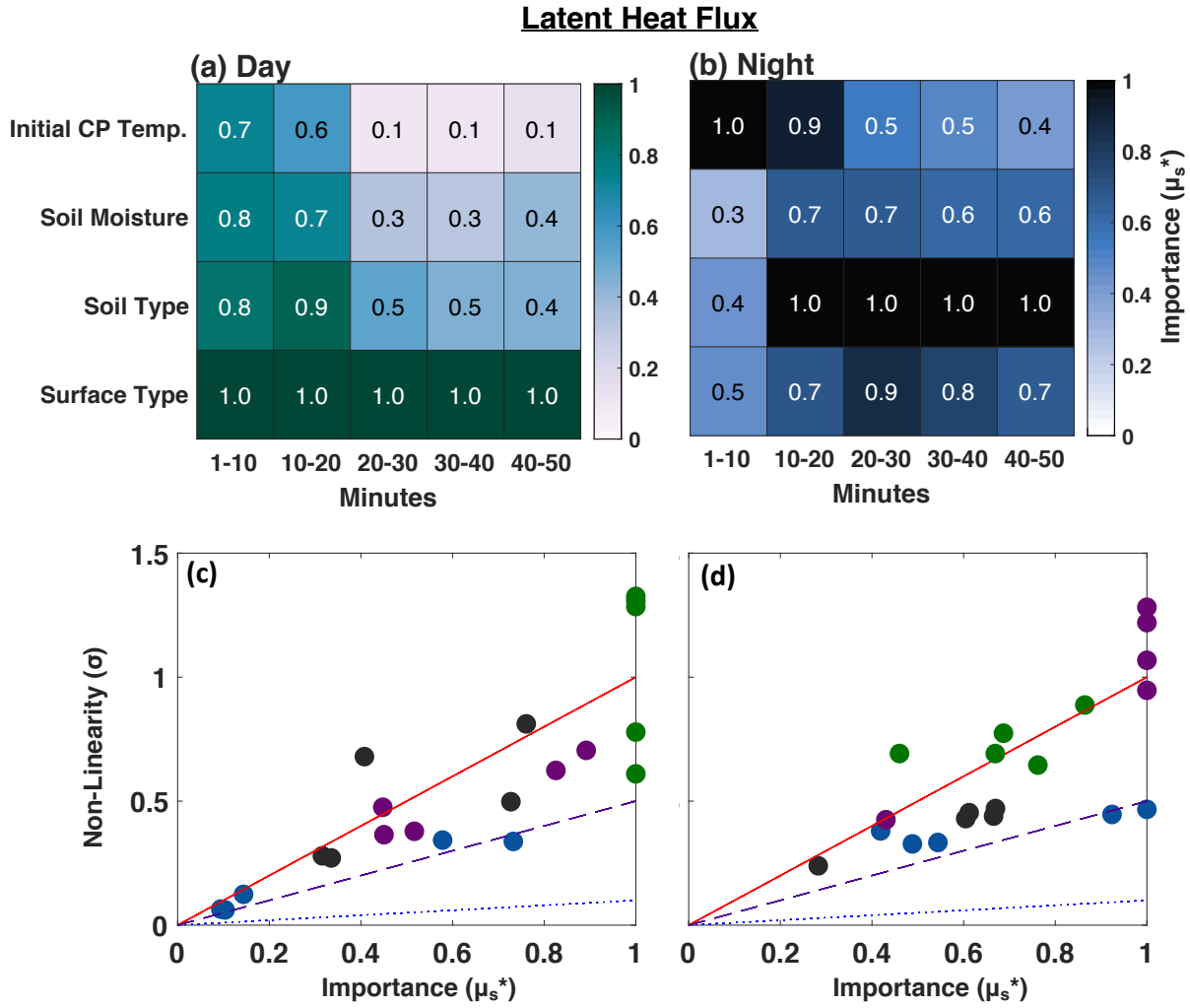

Figure 4.10) Same as Figure 4.7 but for latent heat flux

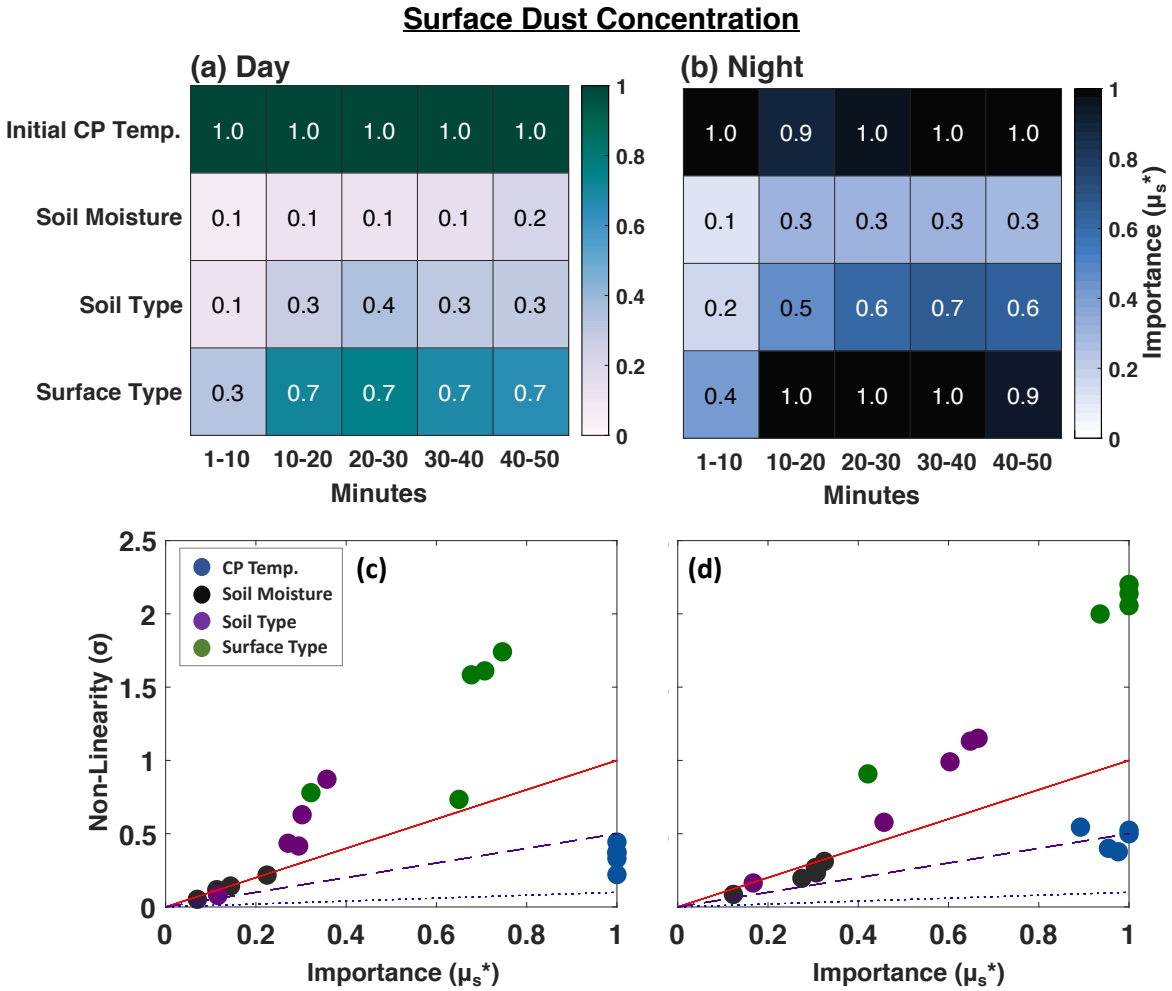

Figure 4.11) Same as Figure 4.7 but for surface dust concentration.

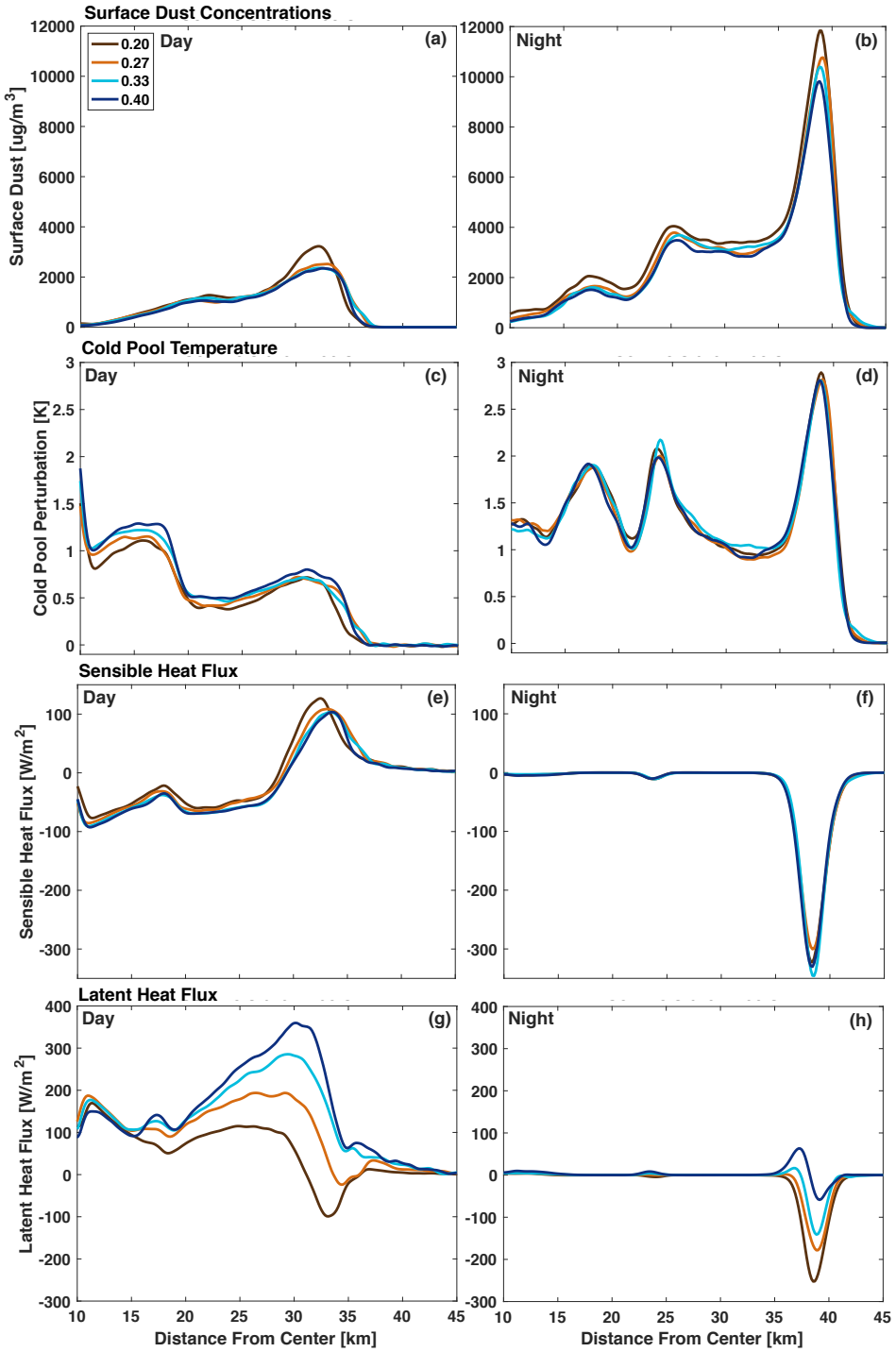

Figure 4.12) The effect of initial soil moisture on (a-b) surface dust concentrations, (c-d) cold pool temperature perturbation, (e-f) sensible heat flux, and (g-h) latent heat flux for day (left) and night (right) at t = 25 minutes. The lines represent 20 % soil saturation (dark brown), 27 % (light brown), 33 % (light blue), and 40 % (dark blue) initial soil moisture. The simulations were all initialized with a -16.66 K cold pool, silt loam soil, and a short grassland surface and are identical besides the initial soil moisture.

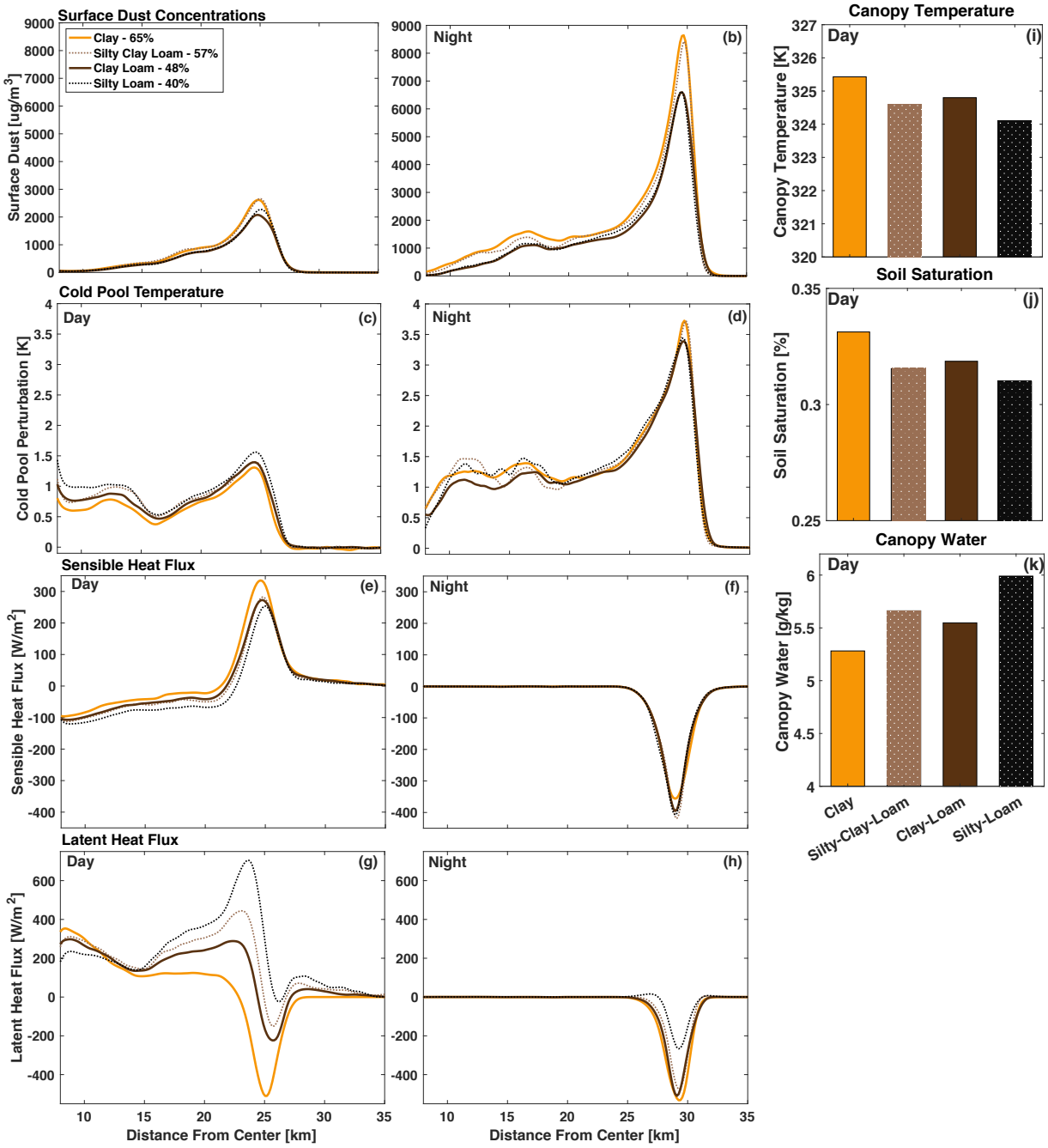

Figure 4.13) (a-h): Similar to Figure 4.12 but for soil type at t = 25 minutes. The lines represent clay (65 % - orange), silty-clay-loam (57 % - light brown), clay-loam (48 % - dark brown), and silty-loam (40 % - black) soils. Loamy soils are indicated by hatching. (i-k): Plots of canopy temperature, soil saturation, and canopy water for the daytime simulations. The colors and hatchings are the same as in plots (a-h). The simulations were all initialized with a -13.33 K cold pool, 33% soil moisture, and a cropland surface and are identical besides the initial soil type.

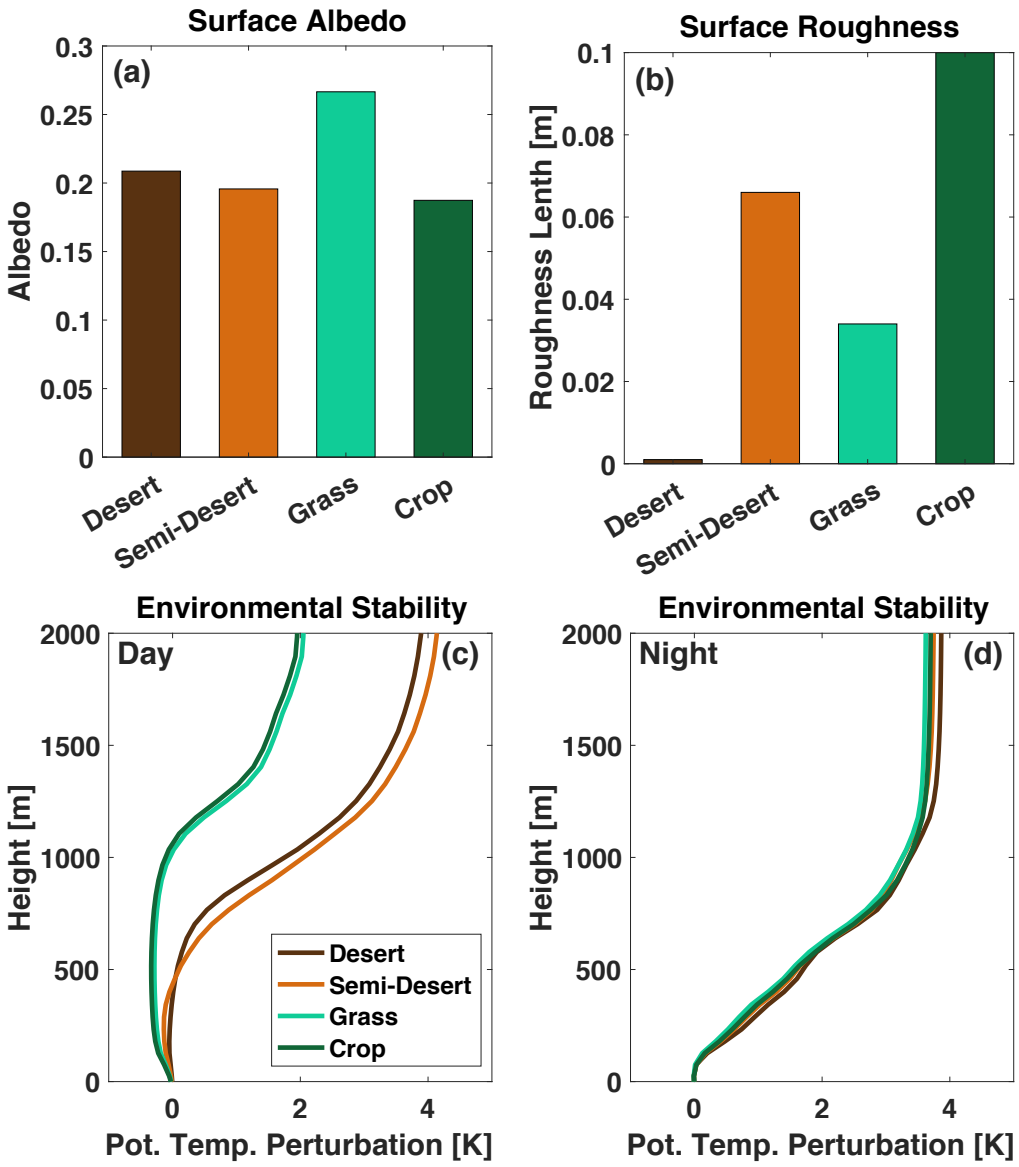

Figure 4.14) (a) surface albedo, (b) surface roughness, (c) daytime and (d) nighttime environmental stability for the four different surface types: desert (dark brown), semi-desert (orange), grassland (light green), and cropland (dark green). The simulations were all initialized with a -10 K cold pool, 40 % soil moisture, silty-clay-loam soil and are identical besides the surface type.

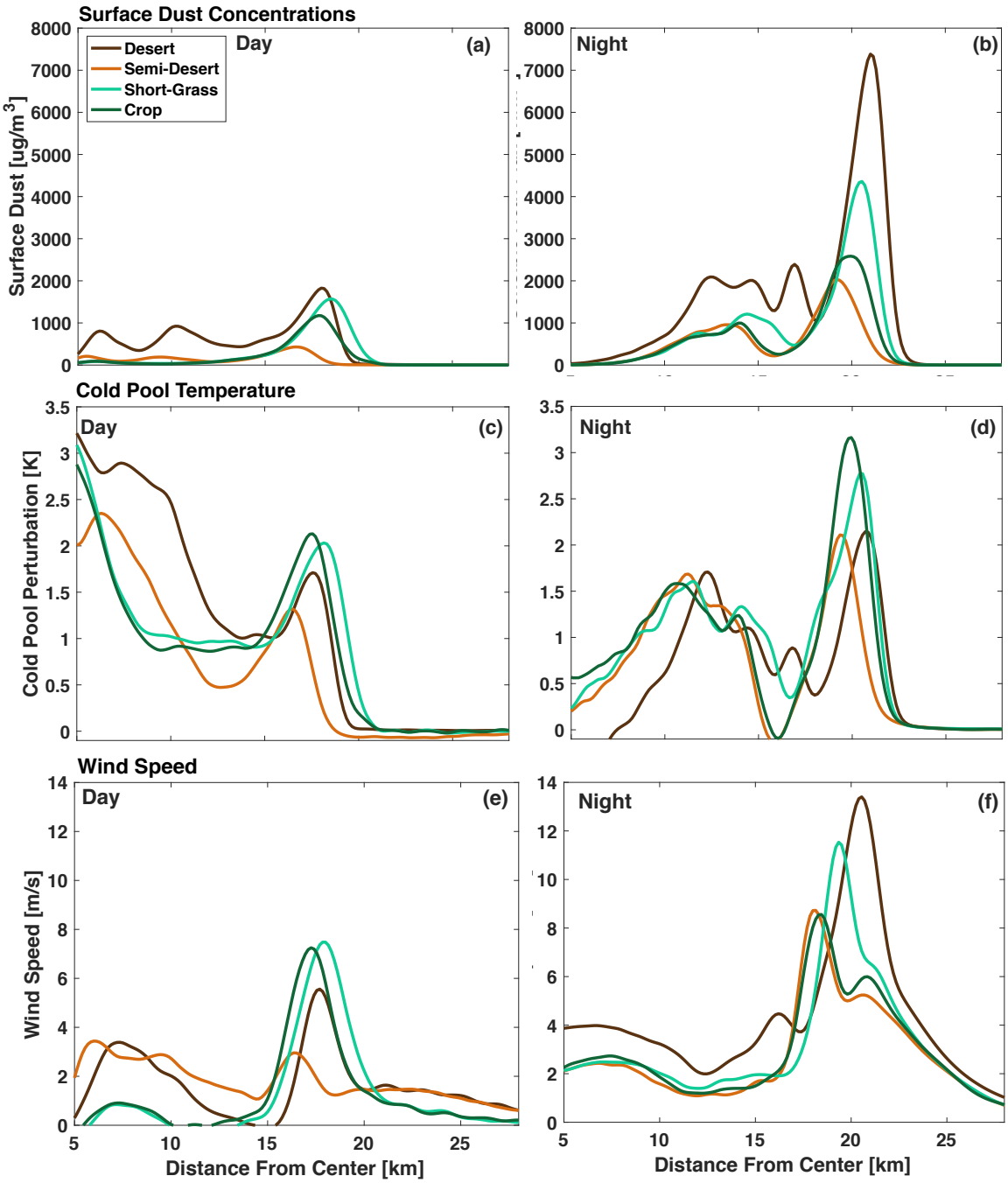

Figure 4.15) (a-f): Similar to Figure 4.12 but for surface type at t = 20 minutes. Colors and simulation details are the same as in Figure 4.14.

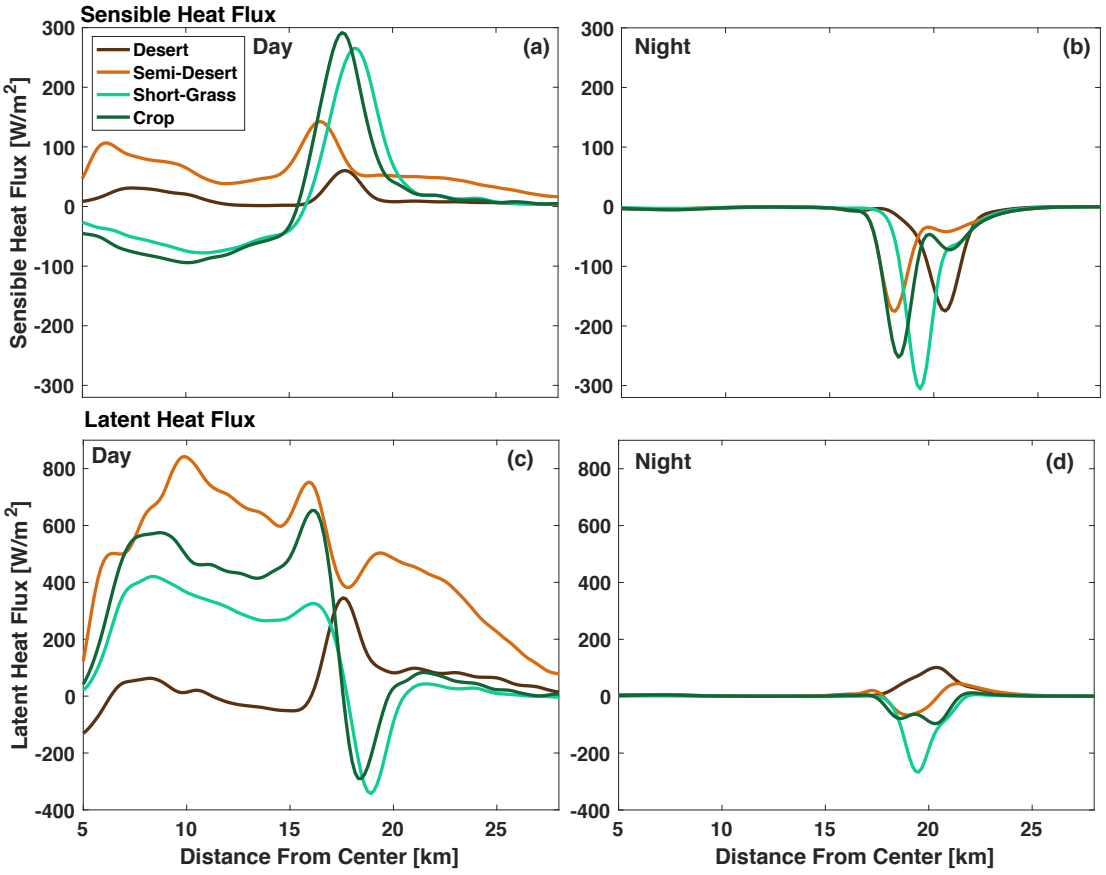

Figure 4.16) (a-d): Similar to Figure 4.12 but for surface type at t = 20 minutes. Colors and simulation details are the same as in Figure 4.14.

CHAPTER 5: CONCLUSIONS

5.1) Summary of Results

Atmospheric mineral dust has extensive effects on humans and our environment. From health and safety concerns to impacts on the climate and global ecosystems, dust has been the focus of a myriad of studies throughout the years in numerous fields of intersecting research. And yet, gaps in our knowledge of dust processes in the Earth system persist. The goal of this dissertation was to address some of these remaining uncertainties related to convective dust events and feedbacks between dust storms and the environment. Specifically, our aims were to: (1) identify the uncertainties related to modeling convective dust events at different scales, (2) investigate the effect of dust radiation interactions on haboobs, and (3) explore feedbacks between the land surface, cold pools, and dust mobilization.

In Chapter 2, we investigated the response of dust fields in the regional numerical model WRF-Chem to increasing horizontal resolution for a multiple day dust event in the Arabian Peninsula. Specifically, testing the difference between parameterized and convection-allowing resolutions was important because dust forecast models are run at grid spacings that parameterize convection. Some of the key findings of Chapter 2 were:

- Convection-permitting simulations exhibit higher surface wind speeds, more frequent and stronger convective activity, and drier soil, which combine to loft roughly twice as much dust mass into the atmosphere compared to those with parameterized convective processes.
- More frequent and stronger updrafts in convection-allowing simulations will transport dust further aloft and increase its atmospheric lifetime.

- The uncertainty in dust concentrations due to different cumulus parameterizations is much smaller than the difference between the parameterized and convection-permitting convection cases.
- Representation of the bimodal daily maximum in dust emissions is sensitive to model resolution. Coarse simulations overestimate the contribution from the nocturnal low level jet and underestimate the role of convection in dust emissions.
- The difference in dust mass across the simulations leads to a significant modification of the radiation budget, specifically the aerosol heating rate at low levels. In the lowest levels there is a change in the sign of the aerosol radiation response depending on whether convection is parameterized or not.

In Chapter 3, we expanded the investigation of dust-radiation interactions to haboobs by simulating a similar case study to Chapter 2, using WRF-Chem and the TOBAC tracking algorithm to quantify the effect that dust radiation has on cold pool properties, strength, dust emissions, and deposition. While dust radiation in convective environments has been previously studied, it had not been applied directly to haboobs. We found that:

- The radiative effect depends strongly on the amount of incoming shortwave radiation and nocturnal cooling, and hence on the diurnal cycle. Three separate regimes were identified for the day, the evening transition, and night.
- In the day, dust scattering cools the surface and increases the temperature gradient between the cold pool and its environment. This leads to stronger density currents with higher windspeeds, enhanced turbulence, and increased dust emissions and concentrations.

- In the evening transition between day and night, longwave absorption aloft and emission toward the surface leads to a warmer surface and warmer cold pools with a reduced temperature gradient between cold pool air and the environment. This results in weaker density currents with suppressed turbulence, windspeeds, dust lofting, and sensible heat fluxes.
- At night, longwave warming due to dust absorption leads to the cold pool being less stable than the rapidly cooling pristine environment surrounding it. Therefore, the outflow boundary is warmer, but not necessarily weaker because it contains stronger windspeeds, enhanced turbulence and sensible heat fluxes, and higher dust emissions. We hypothesize this is due to the less stable haboob air moving into the pristine and more statically stable nocturnal boundary layer.
- Dust-on-dust feedbacks are inconclusive and require more study for the evening and nighttime cases.

Lastly, in Chapter 4 we explored additional haboob feedbacks, only this time with the focus on the surface rather than on radiation. Using 120 idealized RAMS simulations of daytime and nighttime haboobs coupled to the Morris-one-at-a-Time sensitivity analysis, we isolated which surface parameters, specifically surface type, soil moisture, and soil type, are most significant in predicting haboob dust and propagation. We learned that:

- All else being equal, nighttime haboobs are stronger than those in the day due to negative sensible heat fluxes and a more stable environment.

- The most important input factors for predicting haboob dust concentrations and properties are ranked as follows: initial cold pool temperature, surface type, soil type, and finally soil moisture.
- Most of the surface parameters modify the cold pool via their impacts on surface fluxes, although the effect of surface type is dominated by the change in roughness length.
- Many of the factors have a non-linear relationship and feedback on each other. However, a quasi-linear relationship between dust concentrations in a haboob and cold pool temperature was identified. A relationship is derived to combine dust flux and cold pool intensity and relate haboob dust concentrations to the thermodynamic environment.

Overall, while many new conclusions were reached in these studies, we have only begun to address some of the major limitations in our knowledge of the complex and non-linear feedbacks between convective dust events and their environment. There are numerous avenues for future work, and we will conclude this dissertation by discussing what we have learned, what is still missing, and ways to expand upon what we have uncovered here.

5.2) Implications and Future Work

Through this dissertation, one of the central themes has been to establish which factors are important for understanding, modeling, and predicting convective dust events, and how removing particular effects impacts the results in offline interpretation. In Chapter 2, we discovered that even though coarse simulations could double the scaling factor in dust emissions

schemes (or the output can be doubled offline to match the integrated dust values of convection-permitting simulations), a surface tuning factor cannot accurately represent the vertical transport of dust without accurately representing convection. This implies that more work needs to be done to better represent the transport of dust to higher altitudes in parameterized convection simulations. While the increase in dust concentrations as resolution increases is robust across the scales we tested (45 km to 3 km), it is unclear how this relationship changes at even finer grid spacings. Although 3 km is considered "convection-allowing," there are still many processes unresolved at this resolution. It is also uncertain whether the improvements in dust forecasts at higher resolutions are worth the computational expense. However, the results from Chapter 2 can aid in model development, including regionally-refined models with variable grid-spacings that require scale-aware cumulus parametrizations. The high-resolution simulations provide a benchmark for the type of behavior to aim for when developing these parametrizations.

In Chapter 3, we unearthed a few relationships that can be applied to first-order haboob prediction when dust radiation interactions are not included. Namely, during the day haboobs will be stronger and propagate faster, while in the evening they will be warmer and slower. Nevertheless, because the radiative effects are dependent on the dust index of refraction, these results could change based on the ratio of scattering to absorption. This effect needs to be tested with different indices of refraction, as well as under different environmental conditions. Because the amount and wavelength of radiation matters, more temporal and seasonal conditions should also be investigated. It is possible that ensemble modeling tests could potentially result in identifying statistical relationships between dust type and concentration, and dynamics and thermodynamics and lead to parameterizations for use in coarse models and forecast models that do not predict online aerosol and aerosol feedbacks.

Chapter 4 indicated that the most important factors for predicting haboob dust concentrations were cold pool temperature and surface type. Interestingly, soil moisture was consistently ranked as the least essential factor and allows us to conclude that if it is dry enough to loft dust, soil moisture is relatively unimportant. However, the surface type was important because of roughness length, and the higher order effects of surface type, such as albedo and transpiration, are still unknown. Additional simulations would be necessary where the roughness length is held constant to better understand the partitioning of surface fluxes. More research is also needed to understand which surface types loft dust, what the roughness factor is for these surfaces, and which types of thermodynamic environments correlate to those surface types. However, identifying which factors are most important for dust uplift in haboobs is useful for model development and indicates which input fields must be the most accurate. Furthermore, from a data assimilation perspective, observations and assimilation of the most important surface parameters will provide the most value in prediction.

While we now know more concerning haboob physics, there is still much more work to be done. Maybe the most significant limitation of this dissertation is that these studies focused only on the Arabian Peninsula. In reality, there are several major dust regions on Earth, including the Sahara, the Gobi Desert, the Western Australian deserts, and the deserts and drylands of the western United States, which differ in many ways including at the surface (albedo, surface roughness, dust mineralogy), as well as storm frequency and intensity. In terms of albedo, the Sahara and Arabia are the most reflective, while the Gobi, American Southwest, and Western Australia are similar in albedo and less reflective (Rechid et al., 2009). Surface roughness is estimated from satellite retrievals to be quite low and similar across the Sahara, Arabia, the Gobi Desert, and Western Australia (0.15-0.30 cm), whereas the American Southwest has higher

roughness lengths (0.45 cm) (Chen et al., 2014). However, more localized in-situ observations report a broad range in values for surface roughness on the same order as Chen et al. (2014), or even an order of magnitude lower depending on the coverage of roughness elements (Marticorena et al., 2006 and references therein), which can vary substantially over small horizontal scales requires high-resolution databases and observations to accurately represent this parameter in models.

Recent research has highlighted the effect that dust mineralogy can have on radiation based on the concentration of active iron oxide minerals (hematite and goethite), which affect the SW single scattering albedo (Journet et al., 2014; Li et al. 2020; Di Biagio et al., 2019; 2020). Specifically, the ratio of these two minerals matters, with geothite strongly absorbing in the SW and reducing the SSA more than hematite. Dust in Arabia, the Gobi, Australia, and the Southwest all have a higher SSA and scatters more than dust in the Sahara (Journet et al., 2014). This implies that while the physical mechanisms from Chapters 2-3 hold across regions, the sign may differ based on location because of the underlying dust minerology. Efforts are currently underway to address these uncertainties by observing and characterizing dust minerals through projects such as the Earth Surface Mineral Dust Source Investigation (EMIT).

In terms of storm characteristics across dust source regions, it is more difficult to make sweeping characterizations because of meteorology-aerosol covariability. Haboobs necessitate a balance between favorable storm conditions and surface aridity, which is not necessarily captured in climatology studies. Furthermore, these environments will undoubtedly depend on the season (e.g. Southwest monsoon) and each region needs to be characterized separately for its potential to produce haboobs and their frequency. For instance, Pantillon et al. (2016) ran a year-long simulation of the Sahara to characterize haboob frequency and found a strong seasonal

component in terms of the meteorology-dust covariance. Similar characterizations of thunderstorm-dust correlations for other regions will need to be performed because each of these locations is unique.

The results of this dissertation could and need to be expanded to test different dust source environments. Moreover, as climate change and desertification alter ecosystems, so will it alter dust emissions via changes to the surface and background environment. As dryland environments shift towards more frequent and persistent droughts and desertification rates increase in a warmer climate, the need to study atmospheric mineral dust becomes more imperative. Here, we have taken first steps towards enhancing our knowledge of feedbacks between mineral dust and the environment and identifying the most important factors for haboob prediction in future studies.

REFERENCES

Abu-Hamdeh, N. (2003). Thermal properties of soils as affected by density and water content. *Biosystems Engineering*, 86, 97-102. https://doi.org/10.1016/S1537-5110(03)00112-0

Ackerman, A. S., Toon, O. B., Stevens, D. E., Heymsfield, A. J., Ramanathan, V., and Welton, E. J. (2000). Reduction of tropical cloudiness by soot. *Science*, 288, 1042-1047. https://doi.org/10.1126/science.288.5468.1042

Alamirew, N. K., Todd, M. C., Ryder, C. L., Marsham, J. H., and Wang, Y. (2018). The early summertime Saharan heat low: sensitivity of the radiation budget and atmospheric heating to water vapour and dust aerosol. *Atmos. Chem. Phys.*, 18, 1241–1262. https://doi.org/10.5194/acp-18-1241-2018

Alfaro, S. C. and Gomes, L. (2001). Modeling mineral aerosol production by wind erosion: emission intensities and aerosol size distributions in source areas. *J. Geophys. Res.*, 106, 18075–18084. https://doi.org/10.1029/2000JD900399

Alizadeh Choobari, O., Zawar-Reza, P., and Sturman, A. (2013). Low level jet intensification by mineral dust aerosols. *Ann. Geophys.,* 31, 625–632. https://doi.org/10.5194/angeo-31-625-2013

Almazroui, M. (2011). Calibration of TRMM rainfall climatology over Saudi Arabia during 1998–2009. *Atmos. Res.*, 99, 400–414. https://doi.org/10.1016/J.ATMOSRES.2010.11.006

Arakawa, A. and Schubert, W. H. (1974). Interaction of a cumulus cloud ensemble with the large-scale environment, Part I. *J. Atmos. Sci.,* 31, 674–701. https://doi.org/10.1175/1520-0469(1974)031<0674:IOACCE>2.0.CO;2

Babu, C. A., Jayakrishnan, P. R., and Varikoden, H. (2016). Characteristics of precipitation pattern in the Arabian Peninsula and its variability associated with ENSO. *Arab. J. Geosci.,* 9, 186. https://doi.org/10.1007/s12517-015-2265-x

Baddock, M. C., Strong, C. L., Leys, J. F., Heidenreich, S. K., Tews, E. K., and McTainsh, G. H. (2014). A visibility and total suspended dust relationship. *Atm. Env.*, 89, 329–336. https://doi.org/10.1016/J.ATMOSENV.2014.02.038

Baddock, M. C., Strong, C. L., Murray, P. S., and McTainsh, G. H. (2013). Aeolian dust as a transport hazard. *Atm. Env.,* 71, 7-14. https://doi.org/10.1016/j.atmosenv.2013.01.042

Bangert, M., Nenes, A., Vogel, B., Vogel, H., Barahona, D., Karydis, V. A., Kumar, P., Kottmeier, C., and Blahak, U. (2012). Saharan dust event impacts on cloud formation and radiation over Western Europe. *Atmos. Chem. Phys.*, 12, 4045–4063. https://doi.org/10.5194/acp-12-4045-2012

Banks, J. R., Brindley, H. E., Hobby, M., and Marsham, J. H. (2014). The daytime cycle in dust aerosol direct radiative effects observed in the central Sahara during the Fennec campaign in June 2011. *J. Geophys. Res. Atmos.*, 119, 13861–13876. https://doi.org/10.1002/2014JD022077

Barbaro, E., Vilà-Guerau de Arellano, J., Krol, M. C., and Holtslag, A. A. M. (2013). Impacts of aerosol shortwave radiation absorption on the dynamics of an idealized convective atmospheric boundary layer. *Boundary-Layer Meteorol*, 148, 31-49. https://doi.org/10.1007/s10546-013-9800-7

Barnard, J. C., Fast, J. D., Paredes-Miranda, G., Arnott, W. P., and Laskin, A. (2010). Technical Note: Evaluation of the WRF-Chem "Aerosol Chemical to Aerosol Optical Properties" Module using data from the MILAGRO campaign. *Atmos. Chem. Phys.,* 10, 7325–7340. https://doi.org/10.5194/acp-10-7325-2010

Beegum, S. N., Gherboudj, I., Chaouch, N., Temimi, M., and Ghedira, H. (2018). Simulation and analysis of synoptic scale dust storms over the Arabian Peninsula. *Atmos. Res.*, 199, 62–81. https://doi.org/10.1016/J.ATMOSRES.2017.09.003

Behzad, H., Mineta, K., and Gojobori, T. (2018). Global ramifications of dust and sandstorm microbiota. *Genome Biology and Evolution*, 10(8), 1970–1987. https://doi.org/10.1093/gbe/evy134

Bell, J. E., Brown, C. L., Conlon, K., Herring, S., Kunkel, K. E., Lawrimore, J., Luber, G., Schreck, C., Smith, A., and Uejio. C. (2018). Changes in extreme events and the potential impacts on human health. *Journal of the Air & Waste Management Association,* 68:4, 265-287. https://doi.org/_10.1080/10962247.2017.1401017

Belnap, J., Phillips, S. L., *and* Miller, M. E. *(*2004*)*. Response of desert biological soil crusts to alterations in precipitation frequency. *Oecologia,* 141, 306–316. https://doi.org/10.1007/s00442-003-1438-6

Benedetti, A., Baldasano, J. M., Basart, S., Benincasa, F., Boucher, O., Brooks, M. E., Chen, J.-P., Colarco, P. R., Gong, S., Huneeus, N., Jones, L., Lu, S., Menut, L., Morcrette, J.-J., Mulcahy, J., Nickovic, S., Pérez García-Pando, C., Reid, J. S., Sekiyama, T. T., Tanaka, T. Y., Terradellas, E., Westphal, D. L., Zhang, X.-Y., and Zhou, C.-H. (2014). Operational Dust Prediction. In: P. Knippertz, J.-B. W. Stuut (eds.), *Mineral Dust: A Key Player in the Earth System* (pp. 223–265). Dordrecht: Springer Netherlands.

Benedetti, A., Reid, J. S., Knippertz, P., Marsham, J. H., Di Giuseppe, F., Rémy, S., Basart, S., Boucher, O., Brooks, I. M., Menut, L., Mona, L., Laj, P., Pappalardo, G., Wiedensohler, A., Baklanov, A., Brooks, M., Colarco, P. R., Cuevas, E., da Silva, A., Escribano, J., Flemming, J., Huneeus, N., Jorba, O., Kazadzis, S., Kinne, S., Popp, T., Quinn, P. K., Sekiyama, T. T., Tanaka, T., and Terradellas, E. (2018). Status and future of numerical atmospheric aerosol prediction with a focus on data requirements. *Atmos. Chem. Phys.*, 18, 10615–10643. https://doi.org/10.5194/acp-18-10615-2018

Benjamin, T. B. (1968). Gravity currents and related phenomena. *J. Fluid Mech.,* 31, 209–248. https://doi.org/10.1017/S0022112068000133

Bergametti, G., Marticorena, B., Rajot, J. L., Chatenet, B., Féron, A., Gaimoz, C., and Zakou, A. (2017). Dust uplift potential in the central Sahel: An analysis based on 10 years of meteorological measurements at high temporal resolution. *J. Geophys. Res.*,122, 12433–12448. https://doi.org/10.1002/2017JD027471

Bishop, J. K. B., Davis, R. E., and Sherman, J. T. (2002). Robotic observations of dust storm enhancement of carbon biomass in the North Pacific. *Science*, 298(5594), 817-821. https://doi.org/10.1126/science.1074961

Boose, Y., Welti, A., Atkinson, J., Ramelli, F., Danielczok, A., Bingemer, H. G., Plötze, M., Sierau, B., Kanji, Z. A., and Lohmann, U. (2016). Heterogeneous ice nucleation on dust particles sourced from nine deserts worldwide -- Part 1: Immersion freezing. *Atmos. Chem. Phys.,* 16(23), 15075–15095. https://doi.org/10.5194/acp-16-15075-2016

Bou Karam, D., Flamant, C., Tulet, P., Chaboureau, J.-P., Dabas, A., and Todd, M. C. (2009). Estimate of Sahelian dust emissions in the intertropical discontinuity region of the West African monsoon. *J. Geophys. Res.*, 114, D13106. https://doi.org/doi:10.1029/2008JD011444

Bou Karam, D., Williams, E., Janiga, M., Flamant, C., McGraw-Herdeg, M., Cuesta, J., Auby, A., and Thorncroft, C. (2014). Synoptic-scale dust emissions over the Sahara Desert initiated by a moist convective cold pool in early August 2006. *Q.J.R. Meteorol. Soc.*, 140, 2591-2607. https://doi.org/10.1002/qj.2326

Bouet, C., Cautenet, G., Bergametti, G., Marticorena, B., Todd, M. C., and Washington, R. (2012). Sensitivity of desert dust emissions to model horizontal grid spacing during the Bodélé Dust Experiment 2005. *Atmos. Environ.*, 50, 377–380. https://doi.org/10.1016/J.ATMOSENV.2011.12.037

Brahney, J., Ballantyne, A. P., Sievers, C., and Neff, J. C. (2013). Increasing Ca2+ deposition in the western US: The role of mineral aerosols. *Aeolian Res.*,10, 77-87. https://doi.org/10.1016/j.aeolia.2013.04.003

Bryan, G. H. and Morrison, H. (2012). Sensitivity of a simulated squall line to horizontal resolution and parameterization of microphysics. *Mon. Weather Rev.,* 140, 202–225. https://doi.org/10.1175/MWR-D-11-00046.1

Bryan, G. H. and Rotunno, R. (2014). Gravity currents in confined channels with environmental shear. *J. Atmos. Sci.,* 71, 1121-1141. https://doi.org/10.1175/JAS-D-13-0157.1

Bukowski, J. and van den Heever, S. C. (2020). Convective distribution of dust over the Arabian Peninsula: the impact of model resolution. *Atmos. Chem. Phys.,* 20, 2967–2986. https://doi.org/10.5194/acp-20-2967-2020

Burrell, A. L., Evans, J. P., and De Kauwe, M. G. (2020). Anthropogenic climate change has driven over 5 million km^2 of drylands towards desertification. *Nat. Commun.* 11, 3853. https://doi.org/10.1038/s41467-020-17710-7

Camino, C., Cuevas, E., Basart, S., Alonso-Pérez, S., Baldasano, J. M., Terradellas, E., Marticorena, B., Rodríguez, S., and Berjón, A. (2015). An empirical equation to estimate mineral dust concentrations from visibility observations in Northern Africa. *Aeolian Res.*, 16, 55–68. https://doi.org/10.1016/J.AEOLIA.2014.11.002

Campolongo, F., Cariboni, J., and Saltelli, A. (2007). An effective screening design for sensitivity analysis of large models. *Environmental Modelling & Software*, 22, 1509-1518. https://doi.org/10.1016/j.envsoft.2006.10.004

Cantero, M. I., Balachandar, S., García, M. H., *and* Bock, D. *(*2008*)*. Turbulent structures in planar gravity currents and their influence on the flow dynamics. *J. Geophys. Res.,* 113*, C08018*. https://doi.org/10.1029/2007JC004645

Carlson, T. N. and Benjamin, S. G. (1980). Radiative heating rates for Saharan dust. *J. Atmos. Sci.*, 37(1), 193-213. https://doi.org/10.1175/1520-0469(1980)037<0193:RHRFSD>2.0.CO;2

Chen, D., Liu, Z., Davis, C., and Gu, Y. (2017). Dust radiative effects on atmospheric thermodynamics and tropical cyclogenesis over the Atlantic Ocean using WRF-Chem coupled with an AOD data assimilation system. *Atmos. Chem. Phys.,* 17, 7917-7939. https://doi.org/10.5194/acp-17-7917-2017

Chen, W. and Fryrear, D. W. (2002). Sedimentary characteristics of a haboob dust storm. *Atm. Research,* 61, 1, 75-85. https://doi.org/10.1016/S0169-8095(01)00092-8

Chen, X. Z., Li, Y., Su, Y. X., Han, L. S., Liao, J. S., and Yang, S. B. (2014). Mapping global surface roughness using AMSR-E passive microwave remote sensing. *Geoderma*, 235–236, 308-315. https://doi.org/10.1016/j.geoderma.2014.07.026

Chou, M.-D. and Suarez, M. J. (1999). Technical Report Series on Global Modeling and Data Assimilation A Thermal Infrared Radiation Parameterization for Atmospheric Studies Revised May 2003. *Nasa Tech. Memo. 15*, NASA, 40 pp.

Copernicus Climate Change Service (C3S). (2017). ERA5: Fifth generation of ECMWF atmospheric reanalyses of the global climate. Copernicus Climate Change Service Climate Data Store (CDS). https://cds.climate.copernicus.eu/cdsapp#!/home

Cotton, W. R., Pielke, R. A., Walko, R. L., Liston, G. E., Tremback, C. J., Jiang, H., and Co-Authors. (2003). RAMS 2001: Current status and future directions. *Meteorology and Atmospheric Physics*, 82(1–4), 5–29. https://doi.org/10.1007/s00703-001-0584-9

Cowie, S. M., Marsham, J. H., and Knippertz, P. (2015). The importance of rare, high-wind events for dust uplift in northern Africa. *Geophys. Res. Lett.,* 42, 8208–8215. https://doi.org/10.1002/2015GL065819

Cuesta, J., Marsham, J. H., Parker, D. J., and Flamant, C. (2009). Dynamical mechanisms controlling the vertical redistribution of dust and the thermodynamic structure of the West Saharan atmospheric boundary layer during summer. *Atmosph. Sci. Lett.,* 10, 34-42. https://doi.org/10.1002/asl.207

Darmenova, K., Sokolik, I. N., Shao, Y., Marticorena, B., and Bergametti, G. (2009). Development of a physically based dust emission module within the Weather Research and Forecasting (WRF) model: Assessment of dust emission parameterizations and input parameters for source regions in Central and East Asia. *J. Geophys. Res.*, 114, D14201. https://doi.org/10.1029/2008JD011236

Dayan, U., Ziv, B., Margalit, A., Morin, E., and Sharon, D. (2001). A severe autumn storm over the middle-east: synoptic and mesoscale convection analysis. *Theor. Appl. Climatol.*, 69, 103–122. https://doi.org/10.1007/s007040170038

DeMott, P. J., Sassen, K., Poellot, M. R., Baumgardner, D., Rogers, D. C., Brooks, S. D., Prenni, A. J., and Kreidenweis, S. M. (2003). African dust aerosols as atmospheric ice nuclei. *Geophys. Res. Lett.*, 30, 1732,. https://doi.org/10.1029/2003GL017410

Di Biagio, C., Balkanski, Y., Albani, S., Boucher, O., and Formenti, P. (2020). Direct radiative effect by mineral dust aerosols constrained by new microphysical and spectral optical data. *Geophys. Res. Lett.*, 47, e2019GL086186. https://doi.org/10.1029/2019GL086186

Di Biagio, C., and Coauthors. (2017). Global scale variability of the mineral dust long-wave refractive index: a new dataset of in situ measurements for climate modeling and remote sensing. *Atmos. Chem. Phys.*, 17, 1901-1929. https://doi.org/10.5194/acp-17-1901-2017

Di Biagio, C., and Coauthors. (2019). Complex refractive indices and single-scattering albedo of global dust aerosols in the shortwave spectrum and relationship to size and iron content. *Atmos. Chem. Phys.*, 19, 15503–15531. https://doi.org/10.5194/acp-19-15503-2019

Dipu, S., Prabha, T. V., Pandithurai, G., Dudhia, J., Pfister, G., Rajesh, K., and Goswami, B. N. (2013). Impact of elevated aerosol layer on the cloud macrophysical properties prior to monsoon onset. *Atm. Env.,* 70, 454–467. https://doi.org/10.1016/J.ATMOSENV.2012.12.036

Drager, A. J., Grant, L. D., and van den Heever, S. C. (2020). Cold pool responses to changes in soil moisture. *J. Adv. Model. Earth Syst.*, 12, e2019MS001922. https://doi.org/10.1029/2019MS001922

Drager, A. J. and van den Heever, S. C. (2017). Characterizing convective cold pools. *J. Adv. Model. Earth Syst.*, 9, 1091– 1115. https://doi.org/10.1002/2016MS000788

Dubovik, O., Sinyuk, A., Lapyonok, T., Holben, B. N., Mishchenko, M., Yang, P., Eck, T. F., Volten, H., Muñoz, O., Veihelmann, B., van der Zande, W. J., Leon, J.-F., Sorokin, M., and Slutsker, I. (2006). Application of spheroid models to account for aerosol particle nonsphericity in remote sensing of desert dust. *J. Geophys. Res.*, 111, D11208, https://doi.org/10.1029/2005JD006619

Emmel, C., Knippertz, P., and Schulz, O. (2010). Climatology of convective density currents in the southern foothills of the Atlas Mountains. *J. Geophys. Res.*, 115, D11115. https://doi.org/10.1029/2009JD012863

Fan, J., Zhang, R., Tao, W.-K., and Mohr, K. I. (2008). Effects of aerosol optical properties on deep convective clouds and radiative forcing. *J. Geophys. Res.*, 113, D08209. https://doi.org/10.1029/2007JD009257

Fast, J. D., Berg, L. K., Feng, Z., Mei, F., Newsom, R., Sakaguchi, K., and Xiao, H. (2019). The impact of variable land-atmosphere coupling on convective cloud populations observed during the 2016 HI-SCALE field campaign. *J. Adv. Model. Earth Syst.*, 11, 2629– 2654. https://doi.org/10.1029/2019MS001727

Fast, J. D., Gustafson Jr., W. I., Easter, R. C., Zaveri, R. A., Barnard, J. C., Chapman, E. G., Grell, G. A., and Peckham, S. E. (2006). Evolution of ozone, particulates, and aerosol direct radiative forcing in the vicinity of Houston using a fully coupled meteorology-chemistry-aerosol model. *J. Geophys. Res.-Atmos.,* 111, D21305. https://doi.org/10.1029/2005JD006721

Fecan, F., Marticorena, B., and Bergametti, G. (1999). Parameterization of the increase of the Aeolian erosion threshold wind friction velocity due to soil moisture for arid and semi-arid areas. *Ann. Geophys.*, 17, 149–157. https://doi.org/10.1007/s00585-999-0149-7

Fiedler, S., Schepanski, K., Heinold, B., Knippertz, P., and Tegen, I. (2013). Climatology of nocturnal low-level jets over North Africa and implications for modeling mineral dust emission. *J. Geophys. Res.-Atmos.,* 118, 6100–6121. https://doi.org/10.1002/jgrd.50394

Field, P. R., Möhler, O., Connolly, P., Krämer, M., Cotton, R., Heymsfield, A. J., Saathoff, H., and Schnaiter, M. (2006). Some ice nucleation characteristics of Asian and Saharan desert dust. *Atmos. Chem. Phys.*, 6(10), 2991–3006. https://doi.org/10.5194/acp-6-2991-2006

Flamant, C., Chaboureau, J.-P., Parker, D. J., Taylor, C. M., Cammas, J. P., Bock, O., Timouk, F., Pelon, J. (2007). Airborne observations of the impact of a convective system on the planetary boundary layer thermodynamics and aerosol distribution in the intertropical discontinuity region of the west African monsoon. *Q. J. Roy. Meteor. Soc.*, 133, 1175-1189. https://doi.org/10.1002/qj.97

Garcia Sanchez, D., Lacarrière, B., Musy, M., and Bourges, B. (2014). Application of sensitivity analysis in building energy simulations: Combining first- and second-order elementary effects methods. *Energy and Buildings*, 68, Part C, 741-750. https://doi.org/10.1016/j.enbuild.2012.08.048

Gentine, P., Garelli, A., Park, S.-B., Nie, J., Torri, G., and Kuang, Z. (2016). Role of surface heat fluxes underneath cold pools. *Geophys. Res. Lett.*, 43, 874– 883. https://doi.org/10.1002/2015GL067262

Giannakopoulou, E. M. and Toumi, R. (2012). The Persian Gulf summertime low-level jet over sloping terrain. *Q. J. Roy. Meteor. Soc.*, 138, 145–157. https://doi.org/10.1002/qj.901

Ginoux, P., Chin, M., Tegen, I., Prospero, J. M., Holben, B., Dubovik, O., and Lin, S.-J. (2001). Sources and distributions of dust aerosols simulated with the GOCART model. *J. Geophys. Res.-Atmos.*, 106, 20255–20273. https://doi.org/10.1029/2000JD000053

Ginoux, P., Prospero, J. M., Gill, T. E., Hsu, N. C., and Zhao, M. (2012). Global-scale attribution of anthropogenic and natural dust sources and their emission rates based on MODIS Deep Blue aerosol products. *Rev. Geophys.,* 50, *RG3005*. https://doi.org/*10.1029/2012RG000388*

Goudie, A. S. (2014). Desert dust and human health disorders. *Environment International,* 63, 101-113. https://doi.org/10.1016/j.envint.2013.10.011

Grant, L. D. and van den Heever, S. C. (2015). Cold pool and precipitation responses to aerosol loading: modulation by dry layers. *J. Atmos. Sci.*, 72, 1398-1408. https://doi.org/10.1175/JAS-D-14-0260.1

Grant, L. D. and van den Heever, S. C. (2016). Cold pool dissipation. *J. Geophys. Res. Atmos.*, 121, 1138–1155. https://doi.org/10.1002/2015JD023813

Grant, L. D. and van den Heever, S. C. (2018). Cold pool-land surface interactions in a dry continental environment. *J. Adv. Model. Earth Syst.,* 10, 1513–1526. https://doi.org/10.1029/2018MS001323

Grell, G. A. and Dévényi, D. (2002). A generalized approach to parameterizing convection combining ensemble and data assimilation techniques. *Geophys. Res. Lett.*, 29, https://doi.org/10.1029/2002GL015311

Grell, G. A., Peckham, S. E., Schmitz, R., McKeen, S. A., Frost, G., Skamarock, W. C., and Eder, B. (2005). Fully coupled "online" chemistry within the WRF model. *Atm. Env.*, 39, 6957–6975. https://doi.org/10.1016/J.ATMOSENV.2005.04.027

Griffin D. W. (2007). Atmospheric movement of microorganisms in clouds of desert dust and implications for human health. *Clinical Microbiology Reviews*, 20(3), 459–477. https://doi.org/10.1128/CMR.00039-06

Gyamfi, C., Ndambuki, M., and Salim, R.W. (2016). Spatial variability modeling of soil erodibility index in relation to some soil properties at field scale. *Environment and Natural Resources Research*, 6(2), 16-27. https://doi.org/10.5539/enrr.v6n2p16

Han, J. and Pan, H.–L. (2011). Revision of convection and vertical diffusion schemes in the NCEP Global Forecast System. *Weather Forecast.*, 26, 520–533. https://doi.org/10.1175/WAF-D-10-05038.1

Hansell, R. A., Tsay, S. C., Ji, Q., Hsu, N. C., Jeong, M. J., Wang, S. H., Reid, J. S., Liou, K. N., and Ou, S. C. (2010). An assessment of the surface longwave direct radiative effect of airborne Saharan dust during the NAMMA field campaign. *J. Atmos. Sci.,* 67, 1048–1065. https://doi.org/10.1175/2009JAS3257.1

Hansen, J., Sato, M., and Ruedy, R. (1997). Radiative forcing and climate response. *J. Geophys. Res.*, 102(D6), 6831–6864. https://doi.org/10.1029/96JD03436

Harrington, J. Y. (1997). *The effects of radiative and microphysical processes on simulated warm and transition season Arctic stratus*. (Doctoral dissertation). Colorado State Univ., Fort Collins.

Hasanean, H. and Almazroui, M. (2015). Rainfall: features and variations over Saudi Arabia, a review. *Climate*, 3, 578–626. https://doi.org/10.3390/cli3030578

Haywood, J. M., Allan, R. P., Culverwell, I., Slingo, T., Milton, S., Edwards, J., and Clerbaux, N. (2005). Can desert dust explain the outgoing longwave radiation anomaly over the Sahara during July 2003?. *J. Geophys. Res. Atmos.,* 110, D05105. https://doi.org/10.1029/2004JD005232

Haywood, J., Francis, P., Osborne, S., Glew, M., Loeb, N.,Highwood, E., Tanre, D., Myhre, G., Formenti, P., and Hirst, E. (2003). Radiative properties and direct radiative effect of Saharan dust measured by the C-130 aircraft during SHADE: 1. Solar Spectrum. *J. Geophys. Res.*, 108, 8577. https://doi.org/10.1029/2002JD002687

He, Y., Gu, Z., Shui, Q., Liu, B., Lu, W., Zhang, R., Zhang, S., Yu, C. W. (2020). RANS simulation of local strong sandstorms induced by a cold pool with vorticity. *Atmosphere,* 2020, 11(4), 321. https://doi.org/10.3390/atmos11040321

Heald, C. L., Ridley, D. A., Kroll, J. H., Barrett, S. R. H., Cady-Pereira, K. E., Alvarado, M. J., and Holmes, C. D. (2014). Contrasting the direct radiative effect and direct radiative forcing of aerosols. *Atmos. Chem. Phys.,* 14(11), 5513–5527. https://doi.org/10.5194/acp-14-5513-2014

Heikenfeld, M., Marinescu, P. J., Christensen, M., Watson-Parris, D., Senf, F., van den Heever, S. C., and Stier, P. (2019). Tobac 1.2: towards a flexible framework for tracking and analysis of clouds in diverse datasets. *Geosci. Model Dev.*, 12, 4551–4570. https://doi.org/10.5194/gmd-12-4551-2019

Heinold, B., Helmert, J., Hellmuth, O., Wolke, R., Ansmann, A., Marticorena, B., Laurent, B., and Tegen, I. (2007). Regional modeling of Saharan dust events using LM-MUSCAT: Model description and case studies. *J. Geophys. Res.*, 112, D11204. https://doi.org/10.1029/2006JD007443

Heinold, B., Knippertz, P., Marsham, J. H., Fiedler, S., Dixon, N. S., Schepanski, K., Laurent, B., and Tegen, I. (2013). The role of deep convection and nocturnal low-level jets for dust emission in summertime West Africa: Estimates from convection-permitting simulations. *J. Geophys. Res.-Atmos.,* 118, 4385–4400. https://doi.org/10.1002/jgrd.50402

Heinold, B., Tegen, I., Schepanski, K., and Hellmuth, O. (2008). Dust radiative feedback on Saharan boundary layer dynamics and dust mobilization. *Geophys. Res. Lett.*, 35, L20817. https://doi.org/10.1029/2008GL035319

Heintzenberg, J. (2009). The SAMUM-1 experiment over Southern Morocco: overview and introduction. *Tellus B*, 61, 2–11. https://doi.org/10.1111/j.1600-0889.2008.00403.x

Helmert, J., Heinold, B., Tegen, I., Hellmuth, O., and Wendisch, M. (2007). On the direct and semidirect effects of Saharan dust over Europe: A modeling study. *J. Geophys. Res.*, 112, D13208, https://doi.org/10.1029/2006JD007444

Hill, G. E. (1974). Factors controlling the size and spacing of cumulus clouds as revealed by numerical experiments. *J. Atmos. Sci.*, 31(3), 646–673. https://doi.org/10.1175/1520-0469(1974)031%3C0646:FCTSAS%3E2.0.CO;2

Huang, Q., Marsham, J. H., Tian, W., Parker, D. J., and Garcia-Carreras, L. (2018). Large-eddy simulation of dust-uplift by a haboob density current. *Atm. Env.*, 179, 31-39, https://doi.org/10.1016/j.atmosenv.2018.01.048

Huneeus, N., Schulz, M., Balkanski, Y., Griesfeller, J., Prospero, J., Kinne, S., Bauer, S., Boucher, O., Chin, M., Dentener, F., Diehl, T., Easter, R., Fillmore, D., Ghan, S., Ginoux, P., Grini, A., Horowitz, L., Koch, D., Krol, M. C., Landing, W., Liu, X., Mahowald, N., Miller, R., Morcrette, J.-J., Myhre, G., Penner, J., Perlwitz, J., Stier, P., Takemura, T., and Zender, C. S. (2011). Global dust model intercomparison in AeroCom phase I. *Atmos. Chem. Phys.,* 11, 7781–7816. https://doi.org/10.5194/acp-11-7781-2011

Iacono, M. J., Delamere, J. S., Mlawer, E. J., Shephard, M. W., Clough, S. A., and Collins, W. D. (2008). Radiative forcing by long–lived greenhouse gases: Calculations with the AER radiative transfer models. *J. Geophys. Res.*, 113, D13103. https://doi.org/10.1029/2008JD009944

Jacobson, M. Z. and Kaufman, Y. J. (2006). Wind reduction by aerosol particles. *Geophys. Res. Lett.*, 33, L24814. https://doi.org/10.1029/2006GL027838

Janjic, Z. I. (1994). The Step–Mountain Eta Coordinate Model: Further developments of the convection, viscous sublayer, and turbulence closure schemes. *Mon. Weather Rev.,* 122, 927–945. https://doi.org/10.1175/1520-0493(1994)122<0927:TSMECM>2.0.CO;2

Jiang, H. and Feingold, G. (2006). Effect of aerosol on warm convective clouds: Aerosol-cloud-surface flux feedbacks in a new coupled large eddy model. *J. Geophys. Res.*, 111, D01202. https://doi.org/10.1029/2005JD006138

Jickells, T. and Moore, C. M. (2015). The Importance of atmospheric deposition for ocean productivity. *Annu. Rev. Ecol. Evol. Syst.*, 46(1), 481–501. https://doi.org/10.1146/annurev-ecolsys-112414-054118

Jish Prakash, P., Stenchikov, G., Kalenderski, S., Osipov, S., and Bangalath, H. (2015). The impact of dust storms on the Arabian Peninsula and the Red Sea. *Atmos. Chem. Phys.,* 15, 199–222. https://doi.org/10.5194/acp-15-199-2015

Johnson, B. T., Shine, K.P., and Forster, P.M. (2004). The semi-direct aerosol effect: Impact of absorbing aerosols on marine stratocumulus. *Q. J. R. Meteorol. Soc.,* 130: 1407-1422. https://doi.org/10.1256/qj.03.61

Jung, E., Shao, Y., and Sakai, T. (2005). A study on the effects of convective transport on regional-scale Asian dust storms in 2002. *J. Geophys. Res.-Atmos.*, 110, D20201. https://doi.org/10.1029/2005JD005808

Journet, E., Balkanski, Y., and Harrison, S. P. (2014). A new data set of soil mineralogy for dust-cycle modeling. *Atmos. Chem. Phys.,* 14, 3801–3816. https://doi.org/10.5194/acp-14-3801-2014

Kain, J. S. (2004). The Kain–Fritsch convective parameterization: an update. *J. Appl. Meteorol.,* 43, 170–181. https://doi.org/10.1175/1520-0450(2004)043<0170:TKCPAU>2.0.CO;2

Kalenderski, S. and Stenchikov, G. (2016). High-resolution regional modeling of summertime transport and impact of African dust over the Red Sea and Arabian Peninsula. *J. Geophys. Res.-Atmos.*, 121, 6435–6458. https://doi.org/10.1002/2015JD024480

Kalenderski, S., Stenchikov, G., and Zhao, C. (2013). Modeling a typical winter-time dust event over the Arabian Peninsula and the Red Sea. *Atmos. Chem. Phys.*, 13, 1999–2014. https://doi.org/10.5194/acp-13-1999-2013

Karami, S., Ranjbar, A., Mohebalhojeh, A. R., and Moradi, M. (2017). A rare case of haboob in Tehran: Observational and numerical study. *Atm. Research*, 185, 169-185. https://doi.org/10.1016/j.atmosres.2016.10.010

Karydis, V. A., Kumar, P., Barahona, D., Sokolik, I. N., and Nenes, A. (2011). On the effect of dust particles on global cloud condensation nuclei and cloud droplet number. *J. Geophys. Res. Atmos.*, 116, D23204. https://doi.org/10.1029/2011JD016283

Kellogg, C. A. and Griffin, D. W. (2006). Aerobiology and the global transport of desert dust, *Trends in Ecology & Evolution*, 21(11), 638-644. https://doi.org/10.1016/j.tree.2006.07.004

Kinne, S., Lohmann, U., Feichter, J., Schulz, M., Timmreck, C., Ghan, S., Easter, R., Chin, M., Ginoux, P., Takemura, T., Tegen, I., Koch, D., Herzog, M., Penner, J., Pitari, G., Holben, B., Eck, T., Smirnov, A., Dubovik, O., Slutsker, I., Tanre, D., Torres, O., Mishchenko, M., Geogdzhayev, I., Chu, D. A., and Kaufman, Y. (2003). Monthly averages of aerosol properties: A global comparison among models, satellite data, and AERONET ground data. *J. Geophys. Res. Atmos.,* 108(D20), 4634. https://doi.org/10.1029/2001JD001253

Kishcha, P., Alpert, P., Barkan, J., Kirschner, I., and Machenhauer, B. (2011). Atmospheric response to Saharan dust deduced from ECMWF reanalysis (ERA) temperature increments. *Tellus B Chem. Phys. Meteorol.*, 55(4), 901–913. https://doi.org/10.3402/tellusb.v55i4.16380

Klich, C. A. and Fuelberg, H. E. (2014). The role of horizontal model resolution in assessing the transport of CO in a middle latitude cyclone using WRF-Chem. *Atmos. Chem. Phys.*, 14, 609–627. https://doi.org/10.5194/acp-14-609-2014

Klein, C. and Taylor, C. M. (2020). Dry soils can intensify mesoscale convective systems. *Proceedings of the National Academy of Sciences*, 117(35), 21132-21137. https://doi.org/10.1073/pnas.2007998117

Klose, M. and Shao, Y. (2012). Stochastic parameterization of dust emission and application to convective atmospheric conditions. *Atmos. Chem. Phys.,* 12, 7309–7320. https://doi.org/10.5194/acp-12-7309-2012

Knippertz, P., Deutscher, C., Kandler, K., Müller, T., Schulz, O., and Schütz, L. (2007). Dust mobilization due to density currents in the Atlas region: Observations from the Saharan Mineral Dust Experiment 2006 field campaign. *J. Geophys. Res.*, 112, D21109. https://doi.org/10.1029/2007JD008774

Knippertz, P. and Todd, M. C. (2012). Mineral dust aerosols over the Sahara: meteorological controls on emission and transport and implications for modeling. *Rev. Geophys.*, 50, 140-147. https://doi.org/10.1029/2011RG000362

Knippertz, P., Trentmann, J., and Seifert, A. (2009). High-resolution simulations of convective cold pools over the northwestern Sahara. *J. Geophys. Res.*, 114, D08110. https://doi.org/10.1029/2008JD011271.

Knopf, D. A. and Koop, T. (2006). Heterogeneous nucleation of ice on surrogates of mineral dust. *J. Geophys. Res. Atmos.,* 111, D12201. https://doi.org/10.1029/2005JD006894

Koch, D. and Del Genio, A. D. (2010). Black carbon semi-direct effects on cloud cover: review and synthesis. *Atmos. Chem. Phys.*, 10, 7685–7696. https://doi.org/10.5194/acp-10-7685-2010

Kok., J. F. (2011). A scaling theory for the size distribution of emitted dust aerosols suggests climate models underestimate the size of the global dust cycle. *Proceedings of the National Academy of Sciences*, 108(3), 1016-1021. https://doi.org/10.1073/pnas.1014798108

Kok, J. F., Mahowald, N. M., Fratini, G., Gillies, J. A., Ishizuka, M., Leys, J. F., Mikami, M., Park, M.-S., Park, S.-U., Van Pelt, R. S., and Zobeck, T. M. (2014). An improved dust emission model – Part 1: Model description and comparison against measurements. *Atmos. Chem. Phys.*, 14(23), 13023–13041. https://doi.org/10.5194/acp-14-13023-2014

Kok, J. F., Parteli, E. J. R., Michaels, T. I., and Bou Karam, D. (2012). The physics of wind-blown sand and dust. *Rep. Prog. Phys.,* 75(10), 106901. https://doi.org/10.1088/0034-4885/75/10/106901

Kok, J. F., Ward, D. S., Mahowald, N. M., and Evan, A. T. (2018). Global and regional importance of the direct dust-climate feedback, *Nat. Commun.*, 9(1), 241. https://doi.org/10.1038/s41467-017-02620-y

Kurowski, M. J., Suselj, K., Grabowski, W. W., and Teixeira, J. (2018). Shallow-to-Deep transition of continental moist convection: cold pools, surface fluxes, and mesoscale organization. *J. Atmos. Sci.,* 75, 12, 4071-4090. https://doi.org/10.1175/JAS-D-18-0031.1

Lemaître, C., Flamant, C., Cuesta, J., Raut, J.-C., Chazette, P., Formenti, P., and Pelon, J. (2010). Radiative heating rates profiles associated with a springtime case of Bodélé and Sudan dust transport over West Africa. *Atmos. Chem. Phys.,* 10, 8131–8150. https://doi.org/10.5194/acp-10-8131-2010

Lancaster, N. (2013). Climate change and aeolian processes. *Treatise on Geomorphology*, 132-151. https://doi.org/10.1016/B978-0-12-374739-6.00349-3

Largeron, Y., Guichard, F., Bouniol, D., Couvreux, F., Kergoat, L., and Marticorena, B. (2015). Can we use surface wind fields from meteorological reanalyses for Sahelian dust emission simulations?. *Geophys. Res. Lett.,* 42, 2490–2499. https://doi.org/10.1002/2014GL062938

Lawson, T. (1971). Haboob structure at Khartoum. *Weather,* 26, 105–112.

Lee, J. A., Baddock, M. C., Mbuh, M. J., and Gill, T. E. (2012). Geomorphic and land cover characteristics of aeolian dust sources in West Texas and eastern New Mexico, USA. *Aeolian Res.,* 3(*4*), 459–466. https://doi.org/*10.1016/j.aeolia.2011.08.001*

Lee, Y. H., Chen, K., and Adams, P. J. (2009). Development of a global model of mineral dust aerosol microphysics, *Atmos. Chem. Phys.*, 9(7), 2441–2458. https://doi.org/10.5194/acp-9-2441-2009

LeGrand, S. L., Polashenski, C., Letcher, T. W., Creighton, G. A., Peckham, S. E., and Cetola, J. D. (2019). The AFWA dust emission scheme for the GOCART aerosol model in WRF-Chem v3.8.1. *Geosci. Model Dev.*, 12, 131–166. https://doi.org/10.5194/gmd-12-131-2019

Lensky, I. M. and Rosenfeld, D. (2008). Clouds-Aerosols-Precipitation Satellite Analysis Tool (CAPSAT). *Atmos. Chem. Phys.*, 8, 6739–6753. https://doi.org/10.5194/acp-8-6739-2008

Leys, J. F., Heidenreich, S. K., Strong, C. L., McTainsh, G. H., and Quigley, S. (2011). PM10 concentrations and mass transport during "Red Dawn" – Sydney 23 September 2009. *Aeolian Research*, 3, 327-342. https://doi.org/10.1016/j.aeolia.2011.06.003

Li, L., Mahowald, N. M., Miller, R. L., Pérez García-Pando, C., Klose, M., Hamilton, D. S., Gonçalves Ageitos, M., Ginoux, P., Balkanski, Y., Green, R. O., Kalashnikova, O., Kok, J. F., Obiso, V., Paynter, D., and Thompson, D. R. (2020). Quantifying the range of the dust direct radiative effect due to source mineralogy uncertainty. *Atmos. Chem. Phys. Discuss.* [preprint], https://doi.org/10.5194/acp-2020-547, in review.

Lilly, D. K. (1962). On the numerical simulation of buoyant convection. *Tellus*, 14(2), 148–172. https://doi.org/10.1111/j.2153-3490.1962.tb00128.x

Liu, C., and Moncrieff, M. W. (2000). Simulated density currents in idealized stratified environments. *Mon. Weather Rev.*, 128, 1420–1437. https://doi.org/10.1175/1520-0493(2000)128<1420:SDCIIS>2.0.CO;2

Liu, L., Huang, X., Ding, A., and Fu, C. (2016). Dust-induced radiative feedbacks in north China: A dust storm episode modeling study using WRF-Chem. *Atm. Env.*, 129, 43-54. https://doi.org/10.1016/j.atmosenv.2016.01.019

Mahowald, N., Albani, S., Kok, J. F., Engelstaeder, S., Scanza, R., Ward, D. S., and Flanner, M. G. (2014). The size distribution of desert dust aerosols and its impact on the Earth system. *Aeolian Research*, 15, 53-71. https://doi.org/10.1016/j.aeolia.2013.09.002

Mahowald, N. M., Baker, A. R., Bergametti, G., Brooks, N., Duce, R. A., Jickells, T. D., Kubilay, N., Prospero, J. M., and Tegen, I. (2005). Atmospheric global dust cycle and iron inputs to the ocean. *Global Biogeochem. Cycles, 19, GB4025*. https://doi.org/10.1029/2004GB002402

Mahowald, N. M., Ballantine, J. A., Feddema, J., and Ramankutty, N. (2007). Global trends in visibility: implications for dust sources. *Atmos. Chem. Phys.*, 7(12), 3309–3339. https://doi.org/10.5194/acp-7-3309-2007

Mahowald, N. M., Kloster, S., Engelstaedter, S., Moore, J. K., Mukhopadhyay, S., McConnell, J. R., Albani, S., Doney, S. C., Bhattacharya, A., Curran, M. A. J., Flanner, M. G., Hoffman, F. M., Lawrence, D. M., Lindsay, K., Mayewski, P. A., Neff, J., Rothenberg, D., Thomas, E., Thornton, P. E., and Zender, C. S. (2010). Observed 20th century desert dust variability: impact on climate and biogeochemistry. *Atmos. Chem. Phys.,* 10, 10875–10893. https://doi.org/10.5194/acp-10-10875-2010

Mallet, M., Tulet, P., Serça, D., Solmon, F., Dubovik, O., Pelon, J., Pont, V., and Thouron, O. (2009). Impact of dust aerosols on the radiative budget, surface heat fluxes, heating rate profiles and convective activity over West Africa during March 2006. *Atmos. Chem. Phys.*, 9, 7143–7160. https://doi.org/10.5194/acp-9-7143-2009

Manktelow, P. T., Carslaw, K. S., Mann, G. W., and Spracklen, D. V. (2010). The impact of dust on sulfate aerosol, CN and CCN during an East Asian dust storm. *Atmos. Chem. Phys.*, 10(2), 365–382. https://doi.org/10.5194/acp-10-365-2010

Marsham, J. H., Knippertz, P., Dixon, N. S., Parker, D. J., and Lister, G. M. S. (2011). The importance of the representation of deep convection for modeled dust-generating winds over West Africa during summer. *Geophys. Res. Lett.,* 38, D21102. https://doi.org/10.1029/2011GL048368

Marsham, J. H., Parker, D. J., Grams, C. M., Taylor, C. M., and Haywood, J. M. (2008). Uplift of Saharan dust south of the intertropical discontinuity. *J. Geophys. Res.-Atmos.,* 113, D21102. https://doi.org/10.1029/2008JD009844

Marsham, J. H., Parker, D. J., Todd, M. C., Banks, J. R., Brindley, H. E., Garcia-Carreras, L., Roberts, A. J., and Ryder, C. L. (2016). The contrasting roles of water and dust in controlling daily variations in radiative heating of the summertime Saharan heat low. *Atmos. Chem. Phys.*, 16, 3563–3575. https://doi.org/10.5194/acp-16-3563-2016

Marsham, J. H. and Co-Authors. (2013). Meteorology and dust in the central Sahara: observations from Fennec supersite-1 during the June 2011 Intensive Observation Period. *J. Geophys. Res. Atmos.*, 118, 4069–4089. http://doi.org/10.1002/jgrd.50211

Marticorena, B. and Bergametti, G. (1995). Modeling the atmospheric dust cycle: 1. Design of a soil-derived dust emission scheme. *J. Geophys. Res.-Atmos.*, 100, 16415–16430. https://doi.org/10.1029/95JD00690

Marticorena, B., Kardous, M., Bergametti, G., Callot, Y., Chazette, P., Khatteli, H., Le Hégarat-Mascle, S., Maillé, M., Rajot, J.-L., Vidal-Madjar, D., and Zribi, M. (2006). Surface and aerodynamic roughness in arid and semiarid areas and their relation to radar backscatter coefficient. *J. Geophys. Res.*, 111, F03017. https://doi.org/10.1029/2006JF000462

Martin, J. H. (1991). Iron still comes from above. *Nature*, 353(6340), 123. https://doi.org/10.1038/353123b0

Meloni, D., Junkermann, W., di Sarra, A., Cacciani, M., De Silvestri, L., Di Iorio, T., Estellés, V., Gómez-Amo, J. L., Pace, G., and Sferlazzo, D. M. (2015). Altitude-resolved shortwave and longwave radiative effects of desert dust in the Mediterranean during the GAMARF campaign: Indications of a net daily cooling in the dust layer. *J. Geophys. Res. Atmos.*, 120, 3386– 3407. https://doi.org/ 10.1002/2014JD022312

Menut, L. (2008). Sensitivity of hourly Saharan dust emissions to NCEP and ECMWF modeled wind speed. *J. Geophys. Res.*, 113, D16201. https://doi.org/10.1029/2007JD009522

Membery, D. A. (1985). A gravity-wave haboob?. *Weather*, 40, 214-221. https://doi.org/10.1002/j.1477-8696.1985.tb06877.x

Mesinger, F., and Arakawa, A. (1976). Numerical methods used in atmospheric models. *GARP Publ*, Ser. 17, vol. 1, WMO, Geneva, Switzerland, 66 pp.

Middleton, N. J. (2017). Desert dust hazards: A global review. *Aeolian Research*, 24, 53-63. https://doi.org/10.1016/j.aeolia.2016.12.001

Middleton, N. and Kang, U. (2017). Sand and dust storms: impact mitigation. *Sustainability,* 9, 1053. https://doi.org/10.3390/su9061053

Miller, R. L., Perlwitz, J., and Tegen, I. (2004). Feedback upon dust emission by dust radiative forcing through the planetary boundary layer. *J. Geophys. Res.*, 109, D24209, https://doi.org/10.1029/10.1029/2004JD004912

Miller, S. D., Grasso, L. D., Bian, Q., Kreidenweis, S. M., Dostalek, J. F., Solbrig, J. E., Bukowski, J., van den Heever, S. C., Wang, Y., Xu, X., Wang, J., Walker, A. L., Wu, T.-C., Zupanski, M., Chiu, C., and Reid, J. S. (2019). A Tale of Two Dust Storms: analysis of a complex dust event in the Middle East, *Atmos. Meas. Tech.*, 12, 5101–5118. https://doi.org/10.5194/amt-12-5101-2019

Miller, S. D., Kuciauskas, A. P., Liu, M., Ji, Q., Reid, J. S., Breed, D. W., Walker, A. L., and Mandoos, A. A. (2008). Haboob dust storms of the southern Arabian Peninsula. *J. Geophys. Res.-Atmos.,* 113, D01202. https://doi.org/10.1029/2007JD008550

Milton, S. F., Greed, G., Brooks, M. E., Haywood, J., John-son, B., Allan, R. P., Slingo, A., and Grey, M. F. (2008). Modeledand observed atmospheric radiation balance during the West African dry season: role of mineral dust, biomass burning aerosol, and surface albedo, *J. Geophys. Res.*, 113, D00C02. https://doi.org/10.1029/2007JD009741

Mishra, A. K., Klingmueller, K., Fredj, E., Lelieveld, J., Rudich, Y., and Koren, I. (2014). Radiative signature of absorbing aerosol over the eastern Mediterranean basin. *Atmos. Chem. Phys.*, 14, 7213–7231. https://doi.org/10.5194/acp-14-7213-2014

Mokhtari, M., Gomes, L., Tulet, P., and Rezoug, T. (2012). Importance of the surface size distribution of erodible material: an improvement on the Dust Entrainment And Deposition (DEAD) Model. *Geosci. Model Dev.*, 5, 581–598. https://doi.org/10.5194/gmd-5-581-2012

Moncrieff, M. W. and Liu, C. (1999). Convection initiation by density currents: role of convergence, shear, and dynamical organization. *Mon. Weather Rev.*, 127, 2455-2464. https://doi.org/10.1175/1520-0493(1999)127<2455:CIBDCR>2.0.CO;2

Morris, M. D. (1991). Factorial sampling plans for preliminary computational experiments. *Technometrics*, 33:2, 161-174. https://doi.org/10.1080/00401706.1991.10484804

Morrison, H., Curry, J. A., and Khvorostyanov, V. I. (2005). A new double-moment microphysics parameterization for application in cloud and climate models. Part I: description. *J. Atmos. Sci.*, 62, 1665–1677. https://doi.org/10.1175/JAS3446.1

Morrison, H., Thompson, G., and Tatarskii, V. (2009). Impact of cloud microphysics on the development of trailing stratiform precipitation in a simulated squall line: comparison of one- and two-moment schemes. *Mon. Weather Rev.,* 137, 991–1007. https://doi.org/10.1175/2008MWR2556.1

Munson, S. M., Belnap, J., and Okin, G. S. (2011). Responses of wind erosion to climate-induced vegetation changes on the Colorado Plateau. *Proceedings of the National Academy of Sciences*, 108(10), 3854-3859. https://doi.org/10.1073/pnas.1014947108

Nabat, P., Somot, S., Mallet, M., Sevault, F., Chiacchio, M., and Wild, M. (2015). Direct and semi-direct aerosol radiative effect on the Mediterranean climate variability using a coupled regional climate system model. *Clim. Dyn.,* 44, 1127–1155. https://doi.org/10.1007/s00382-014-2205-6

Nakanishi, M. and Niino, H. (2006). An improved Mellor–Yamada Level-3 model: its numerical stability and application to a regional prediction of advection fog. *Bound.-Lay. Meteorol.*, 119, 397–407. https://doi.org/10.1007/s10546-005-9030-8

Nakanishi, M. and Niino, H. (2009). Development of an improved turbulence closure model for the atmospheric boundary layer. *J. Meteorol. Soc. Jpn. Ser. II*, 87, 895–912. https://doi.org/10.2151/jmsj.87.895

National Centers for Environmental Prediction/National Weather Service/NOAA/U.S Department of Commerce: NCEP FNL Operational Model Global Tropospheric Analyses, continuing from July 1999. (2000). Research Data Archive at the National Center for Atmospheric Research, Computational and Information Systems Laboratory, Boulder, CO. https://doi.org/10.5065/D6M043C6

National Centers for Environmental Prediction/National Weather Service/NOAA/U.S. Department of Commerce: NCEP GDAS/FNL 0.25 Degree Global Tropospheric Analyses and Forecast Grids. (2015). Research Data Archive at the National Center for Atmospheric Research, Computational and Information Systems Laboratory, Boulder, CO. https://doi.org/10.5065/D65Q4T4Z

Neff, J. C., Ballantyne, A., Farmer, G., Mahowald, N. M., Conroy, J. L., Landry, C. C., Overpeck, J. T., Painter, T. H., Lawrence, C. R., and Reynolds, R. L. (2008). Increasing eolian dust deposition in the western United States linked to human activity. *Nat. Geosci.,* 1, 189–195. https://doi.org/10.1038/ngeo133

Nickovic, S., Vukovic, A., Vujadinovic, M., Djurdjevic, V., and Pejanovic, G. (2012). Technical Note: High-resolution mineralogical database of dust-productive soils for atmospheric dust modeling. *Atmos. Chem. Phys.*, 12, 845–855. https://doi.org/10.5194/acp-12-845-2012

Niu, G.-Y., Yang, Z.-L., Mitchell, K. E., Chen, F., Ek, M. B., Barlage, M., Kumar, A., Manning, K., Niyogi, D., Rosero, E., Tewari, M., and Xia, Y. (2011). The community Noah land surface model with multiparameterization options (Noah-MP): 1. Model description and evaluation with local-scale measurements. *J. Geophys. Res.-Atmos.*, 116, D12109. https://doi.org/10.1029/2010JD015139

Pantillon, F., Knippertz, P., Marsham, J. H., and Birch, C. E. (2015). A parameterization of convective dust storms for models with mass-flux convection schemes. *J. Atmos. Sci.*, 72, 2545–2561. https://doi.org/10.1175/JAS-D-14-0341.1

Pantillon, F., Knippertz, P., Marsham, J. H., Panitz, H., and Bischoff-Gauss, I. (2016). Modelling haboob dust storms in large-scale weather and climate models. *J. Geophys. Res. Atmos.*, 121, 2090-2109. https://doi.org/10.1002/2015JD024349

Pérez, C., Nickovic, S., Pejanovic, G., Baldasano, J. M., and Özsoy, E. (2006). Interactive dust-radiation modeling: A step to improve weather forecasts. *J. Geophys. Res. Atmos.*, 111, D16206. https://doi.org/10.1029/2005JD006717

Peris-Ferrús, C., Gómez-Amo, J. L., Marcos, C., Freile-Aranda, M. D., Utrillas, M. P., and Martínez-Lozano, J. A. (2017). Heating rate profiles and radiative forcing due to a dust storm in the Western Mediterranean using satellite observations. *Atm. Env.*, 160, 142-153. https://doi.org/10.1016/j.atmosenv.2017.04.023

Perlwitz, J., Tegen, I., and Miller, R. L. (2001). Interactive soil dust aerosol model in the GISS GCM: 1. Sensitivity of the soil dust cycle to radiative properties of soil dust aerosols. *J. Geophys. Res.*, 106(D16), 18167– 18192. https://doi.org/10.1029/2000JD900668

Pianosi, F., Beven, K., Freer, J., Hall, J. W., Rougier, J., Stephenson, D. B., and Wagener, T. (2016). Sensitivity analysis of environmental models: a systematic review with practical workflow. *Environmental Modelling & Software*, 79, 214-232. https://doi.org/10.1016/j.envsoft.2016.02.008

Pianosi, F., Sarrazin, F., and Wagener, T. (2015). A Matlab toolbox for Global Sensitivity Analysis. *Environmental Modelling & Software*, 70, 80-85. https://doi.org/10.1016/j.envsoft.2015.04.009

Pielke, R. A., Cotton, W. R., Walko, R. L., Tremback, C. J., Lyons, W. A., Grasso, L. D., Nicholls, M. E., Moran, M. D., Wesley, D. A., Lee, T. J., and Copeland, J. H. (1992). A comprehensive meteorological modeling system – RAMS. *Meteorol. Atmos. Phys.*, 49, 69–91. https://doi.org/10.1007/BF01025401

Pierre, C., Bergametti, G., Marticorena, B., Mougin, E., Bouet, C., and Schmechtig, C. (2012). Impact of vegetation and soil moisture seasonal dynamics on dust emissions over the Sahel. *J. Geophys. Res.,* 117, D06114. https://doi.org/10.1029/2011JD016950

Pope, R. J., Marsham, J. H., Knippertz, P., Brooks, M. E., and Roberts, A. J. (2016). Identifying errors in dust models from data assimilation. *Geophys. Res. Lett.,* 43, 9270–9279. https://doi.org/10.1002/2016GL070621

Prospero, J. M. (1999). Long-term measurements of the transport of African mineral dust to the southeastern United States: Implications for regional air quality. *J. Geophys. Res. Atmos.*, 104(D13), 15917–15927. https://doi.org/10.1029/1999JD900072

Prospero, J. M., Ginoux, P., Torres, O., Nicholson, S. E., and Gill, T. E. (2002). Environmental characterization of global sources of atmospheric soil dust identified with the Nimbus 7 Total Ozone Mapping Spectrometer (TOMS) absorbing aerosol product. *Reviews of Geophysics*, 40, 1002. https://doi.org/10.1029/2000RG000095

Provod, M., Marsham, J. H., Parker, D. J., and Birch, C. E. (2016). A characterization of cold pools in the West African Sahel. *Mon. Weather Rev.*, 144, 1923–1934. https://doi.org/10.1175/MWR-D-15-0023.1

Purdom, J. F. W. (1982). Subjective interpretation of geostationary satellite data for nowcasting. In K. Browning (ed.), *Nowcasting* (pp. 149-156). New York: Academic Press.

Quijano, A. L., Sokolik, I. N., and Toon, O. B. (2000). Radiative heating rates and direct radiative forcing by mineral dust in cloudy atmospheric conditions. *J. Geophys. Res.*, 105(D10), 12207– 12219. https://doi.org/10.1029/2000JD900047

Rechid, D., Raddatz, T. J., and Jacob, D. (2009). Parameterization of snow-free land surface albedo as a function of vegetation phenology based on MODIS data and applied in climate modelling. *Theor. Appl. Climatol.*, 95**,** 245–255. https://doi.org/10.1007/s00704-008-0003-y

Reheis, M. C. and Urban, F. E. (2011). Regional and climatic controls on seasonal dust deposition in the southwestern U.S. *Aeolian Res.*, 3(1), 3-21. https://doi.org/10.1016/j.aeolia.2011.03.008

Reinfried, F., Tegen, I., Heinold, B., Hellmuth, O., Schepanski, K., Cubasch, U., Huebener, H., and Knippertz, P. (2019). Simulations of convectively-driven density currents in the Atlas region using a regional model: Impacts on dust emission and sensitivity to horizontal resolution and convection schemes. *J. Geophys. Res.-Atmos.,* 114, D08127. https://doi.org/10.1029/2008JD010844

Rempel, A. R. and Rempel, A. W. (2016). Intrinsic evaporative cooling by hygroscopic Earth materials. *Geosciences*, *6*(3), 38. https://doi.org/10.3390/geosciences6030038

Rémy, S., Benedetti, A., Bozzo, A., Haiden, T., Jones, L., Razinger, M., Flemming, J., Engelen, R. J., Peuch, V. H., and Thepaut, J. N. (2015). Feedbacks of dust and boundary layer meteorology during a dust storm in the eastern Mediterranean. *Atmos. Chem. Phys.*, 15, 12909–12933. https://doi.org/10.5194/acp-15-12909-2015

Ridley, D. A., Heald, C. L., Pierce, J. R., and Evans, M. J. (2013). Toward resolution-independent dust emissions in global models: Impacts on the seasonal and spatial distribution of dust. *Geophys. Res. Lett.,* 40, 2873–2877. https://doi.org/10.1002/grl.50409

Roberts, A. J. and Knippertz, P. (2012). Haboobs: convectively generated dust storms in West Africa. *Weather*, 67, 311-316. https://doi.org/10.1002/wea.1968

Roberts, A. J. and Knippertz, P. (2014). The formation of a large summertime Saharan dust plume: Convective and synoptic-scale analysis. *J. Geophys. Res. Atmos.*, 119, 1766–1785. https://doi.org/10.1002/2013JD020667

Roberts, A. J., Woodage, M. J., Marsham, J. H., Highwood, E. J., Ryder, C. L., McGinty, W., Wilson, S., and Crook, J. (2018). Can explicit convection improve modelled dust in summertime West Africa?. *Atmos. Chem. Phys.*, 18, 9025–9048. https://doi.org/10.5194/acp-18-9025-2018

Rotunno, R., Klemp, J. B., and Weisman, M. L. (1988). A theory for strong, long-lived squall lines. *J. Atmos. Sci.,* 45, 463-485.

Saleeby, S. M., and van den Heever, S. C. (2013). Developments in the CSU-RAMS aerosol model: Emissions, nucleation, regeneration, deposition, and radiation. *Journal of Applied Meteorology and Climatology*, 52(12), 2601–2622. https://doi.org/10.1175/JAMC-D-12-0312.1

Saleeby, S. M., van den Heever, S. C., Bukowski, J., Walker, A. L., Solbrig, J. E., Atwood, S. A., Bian, Q., Kreidenweis, S. M., Wang, Y., Wang, J., and Miller, S. D. (2019). The influence of simulated surface dust lofting and atmospheric loading on radiative forcing. *Atmos. Chem. Phys.*, 19, 10279–10301. https://doi.org/10.5194/acp-19-10279-2019

Saltelli, A., Ratto, M., Andres, T., Campolongo, F., Cariboni, J., Gatelli, D., Saisana, M., and Tarantola, S. (2008). Global sensitivity analysis: the primer. John Wiley & Sons, Ltd, West Sussex, England. https://doi.org/10.1002/9780470725184

Saltelli, A., Tarantola, S., Campolongo, F., and Ratto, M. (2004). Sensitivity analysis in practice: a guide to assessing scientific models. West Sussex, England, John Wiley & Sons Ltd. http://doi.org/10.1002/0470870958

Sarrazin, F., Pianosi, F., and Wagener, T., (2016). Global sensitivity analysis of environmental models: convergence and validation. *Environmental Modelling & Software*, 79, 135-152. https://doi.org/10.1016/j.envsoft.2016.02.005

Sayre, R., Karagulle, D., Frye, C., Boucher, T., Wolff, N. H., Breyer, S., Wright, D., Martin, M., Butler, K., Van Graafeiland, K., Touval, J., Sotomayor, L., McGowan, J., Game, E. T., and Possingham, H. (2020). An assessment of the representation of ecosystems in global protected areas using new maps of World Climate Regions and World Ecosystems. *Global Ecology and Conservation*, 21, e00860. https://doi.org/10.1016/j.gecco.2019.e00860

Schepanski, K., Knippertz, P., Fiedler, S., Timouk, F., and Demarty, J. (2015). The sensitivity of nocturnal low-level jets and near-surface winds over the Sahel to model resolution, initial conditions and boundary-layer set-up. *Q. J. R. Meteor. Soc.,* 141, 1442–1456. https://doi.org/10.1002/qj.2453

Schepanski, K., Tegen, I., Laurent, B., Heinold, B., and Macke, A. (2007). A new Saharan dust source activation frequency map derived from MSG-SEVIRI IR-channels. *Geophys. Res. Lett.,* 34, L18803. http://doi.org/10.1029/2007GL030168

Seigel, R. B. and van den Heever, S. C. (2012a): Simulated density currents beneath embedded stratified layers. *J. Atmos. Sci.*, 69, 2192–2200. https://doi.org/10.1175/JAS-D-11-0255.1

Seigel, R. B. and van den Heever, S. C. (2012b). Dust lofting and ingestion by supercell storms. *J. Atmos. Sci.*, 69, 1453–1473. https://doi.org/10.1175/JAS-D-11-0222.1

Seigel, R. B., van den Heever, S. C., and Saleeby, S. M. (2013). Mineral dust indirect effects and cloud radiative feedbacks of a simulated idealized nocturnal squall line. *Atmos. Chem. Phys.,* 13, 4467–4485. https://doi.org/10.5194/acp-13-4467-2013

Shao, Y. (2001). A model for mineral dust emission. *J. Geophys. Res.*, 106, 20239–20254. https://doi.org/10.1029/2001JD900171

Shwehdi, M. H. (2005). Thunderstorm distribution and frequency in Saudi Arabia. *J. Geophys. Eng.*, 2, 252–267. https://doi.org/10.1088/1742-2132/2/3/009

Skamarock, W. C., Klemp, J. B., Dudhia, J. O. G. D., and Barker, D. M. (2008). A description of the Advanced Research WRF version 3. *NCAR Tech*, Note NCAR/TN-4751STR, NCAR, https://doi.org/10.5065/D68S4MVH, Boulder, CO.

Slingo, A., Ackerman, T. P., Allan, R. P., Kassianov, E. I., McFarlane, S. A., Robinson, G. J., Barnard, J. C., Miller, M. A., Harries, J. E., Russell, J. E., and Dewitte, S. (2006). Observations of the impact of a major Saharan dust storm on the atmospheric radiation balance. *Geophys. Res. Lett.*, 33, L24817. https://doi.org/10.1029/2006GL027869

Smagorinsky, J. (1963). General circulation experiments with the primitive equations. I. The basic experiment. *Mon. Weather Rev.*, 91(3), 99–164. https://doi.org/10.1175/1520-0493(1963)091%3C0099:GCEWTP%3E2.3.CO;2

Sokolik, I. N. and Toon, O. B. (1996). Direct radiative forcing by anthropogenic airborne mineral aerosols. *Nature*, 381(6584), 681–683. https://doi.org/10.1038/381681a0

Solomos, S., Kallos, G., Mavromatidis, E., and Kushta, J. (2012). Density currents as a desert dust mobilization mechanism. *Atmos. Chem. Phys.*, 12, 11199–11211. https://doi.org/10.5194/acp-12-11199-2012

Sprigg, W. A. (2016). Dust storms, human health and a global early warning system. In: S. Steinberg, W. Sprigg (eds.), *Extreme Weather, Health, and Communities. Extreme Weather and Society, Springer, Cham.* (pp. 59-87). Switzerland: Springer International Publishing. https://doi.org/10.1007/978-3-319-30626-1_4

Stafoggia, M., Zauli-Sajani, S., Pey, J., Samoli, E., Alessandrini, E., Basagaña, X., and Co-Authors. (2016): Desert dust outbreaks in Southern Europe: contribution to daily PM_{10} concentrations and short-term associations with mortality and hospital admissions. *Environ. Health Perspect.*, 124(4), 413–419. https://doi.org/10.1289/ehp.1409164

Stephens, G. L., L'Ecuyer, T., Forbes, R., Gettelmen, A., Golaz, J.-C., Bodas-Salcedo, A., Suzuki, K., Gabriel, P., and Haynes, J. (2010). Dreary state of precipitation in global models. *J. Geophys. Res.*, 115, D24211. https://doi.org/10.1029/2010JD014532

Stokowski, D. (2005). *The addition of the direct radiative effect of atmospheric aerosols into the Regional Atmospheric Modeling System (RAMS)*. (M.S. thesis). Atmospheric Science Paper 637, 89, Dept. of Atmospheric Science, Colorado State Univ., Fort Collins.

Stout, J. E. and Lee, J. A. (2003). Indirect evidence of wind erosion trends on the Southern High Plains of North America. *J. Arid Environ.*, 55, 43–61. https://doi.org/10.1016/S0140-1963(02)00266-5

Strong, C. L., Parsons, K., McTainsh, G. H., and Sheehan, A. (2011). Dust transporting wind systems in the lower Lake Eyre Basin, Australia: A preliminary study. *Aeolian Res.*, 2, 205–214. https://doi.org/ 10.1016/j.aeolia.2010.11.001

Sun, Y., Solomon, S., Dai, A., and Portmann, R. W. (2006). How often does it rain?. *J. Climate*, 19, 916–934. https://doi.org/10.1175/JCLI3672.1

Takemi, T. (2005). Explicit simulations of convective-scale transport of mineral dust in severe convective weather. *J. of the Met. Society of Japan*, 83A, 187—203. https://doi.org/10.2151/jmsj.83A.187

Tanaka, T. Y. and Chiba, M. (2006). A numerical study of the contributions of dust source regions to the global dust budget. *Global Planet. Chang.*, 52, 88–104. https://doi.org/10.1016/J.GLOPLACHA.2006.02.002

Taylor, C., Belušić, D., Guichard, F., Parker, D. J., Vischel, T., Bock, O., Harris, P. P., Janicot, S., Klein, C., and Panthou, G. (2017). Frequency of extreme Sahelian storms tripled since 1982 in satellite observations. *Nature,* 544, 475–478. https://doi.org/10.1038/nature22069

Tegen, I. and Lacis, A. A. (1996). Modeling of particle size distribution and its influence on the radiative properties of mineral dust aerosol. *J. Geophys. Res. Atmos.,* 101(D14), 19237–19244. https://doi.org/10.1029/95JD03610

Teixeira, J. C., Carvalho, A. C., Tuccella, P., Curci, G., and Rocha, A. (2016). WRF-chem sensitivity to vertical resolution during a Saharan dust event. *Phys. Chem. Earth Pt. A/B/C*, 94, 188–195. https://doi.org/10.1016/J.PCE.2015.04.002

Tiedtke, M. (1989). A comprehensive mass flux scheme for cumulus parameterization in large–scale models. *Mon. Weather Rev.*, 117, 1779–1800.

Thorpe, A. J., Miller, M. J., and Moncrieff, M. W. (1982). Two-dimensional convection in non-constant shear: a model of mid-latitude squall lines. *Q. J. R. Meteor. Soc.*, 108, 739–826762. https://doi.org/10.1002/qj.49710845802

Todd, M. C., Bou Karam, D., Cavazos, C., Bouet, C., Heinold, B., Baldasano, J. M., Cautenet, G., Koren, I., Perez, C., Solmon, F., Tegen, I., Tulet, P., Washington, R., and Zakey, A. (2008). Quantifying uncertainty in estimates of mineral dust flux: An intercomparison of model performance over the Bodélé Depression, northern Chad. *J. Geophys. Res.-Atmos.,* 113, D24107. https://doi.org/10.1029/2008JD010476

Tompkins, A. M. (2001). Organization of tropical convection in low vertical wind shears: the role of cold pools. *J. Atmos. Sci.*, 58, 1650–1672. https://doi.org/10.1175/1520-0469(2001)058<1650:OOTCIL>2.0.CO;2

Torri, G., Kuang, Z., and Tian, Y. (2015). Mechanisms for convection triggering by cold pools. *Geophys. Res. Lett.*, 42, 1943– 1950. https://doi.org/10.1002/2015GL063227

Trzeciak, T. M., Garcia-Carreras, L., and Marsham, J. H. (2017). Cross-Saharan transport of water vapor via recycled cold pool outflows from moist convection. *Geophys. Res. Lett.*, 44, 1554– 1563. https://doi.org/10.1002/2016GL072108

Tsikerdekis, A., Zanis, P., Georgoulias, A. K., Alexandri, G., Katragkou, E., Karacostas, T., and Solmon, F. (2019). Direct and semi-direct radiative effect of North African dust in present and future regional climate simulations. *Clim. Dyn.,* 53, 4311–4336. https://doi.org/10.1007/s00382-019-04788-z

Tulet, P., Crahan-Kaku, K., Leriche, M., Aouizerats, B., and Crumeyrolle, S. (2010). Mixing of dust aerosols into a mesoscale convective system: generation, filtering and possible feedbacks on ice anvils. *Atm. Research,* 96, 302-314. https://doi.org/10.1016/j.atmosres.2009.09.011

Twohy, C. H., Kreidenweis, S. M., Eidhammer, T., Browell, E. V, Heymsfield, A. J., Bansemer, A. R., Anderson, B. E., Chen, G., Ismail, S., DeMott, P. J., and van den Heever, S. C. (2009). Saharan dust particles nucleate droplets in eastern Atlantic clouds. *Geophys. Res. Lett.,* 36, L01807. https://doi.org/10.1029/2008GL035846

Twomey, S. (1974). Pollution and the planetary albedo. *Atm. Env.*, 8, 1251-1256, https://doi.org/10.1016/0004-6981(74)90004-3

Ukhov, A., Ahmadov, R., Grell, G., and Stenchikov, G. (2021). Improving dust simulations in WRF-Chem v4.1.3 coupled with the GOCART aerosol module. *Geosci. Model Dev.*, 14, 473–493. https://doi.org/10.5194/gmd-14-473-2021

Uno, I., Wang, Z., Chiba, M., Chun, Y. S., Gong, S. L., Hara, Y., Jung, E., Lee, S.-S., Liu, M., Mikami, M., Music, S., Nickovic, S., Satake, S., Shao, Y., Song, Z., Sugimoto, N., Tanaka, T., and Westphal, D. L. (2006). Dust model intercomparison (DMIP) study over Asia: Overview. *J. Geophys. Res.-Atmos.,* 111, D12213. https://doi.org/10.1029/2005JD006575

United States Department of Agriculture (USDA), Natural Re-sources Conservation Service (NRCS), Soil Taxonomy: A Basic system of Soil Classification for Making and Interpreting Soil Surveys Agr. Handb. 436. U.S. Govt. Print. Office, Washington DC, 20402, 870 pp., second edn., 1999.

Vaezi, A. R., Hasanzadeh, H., Cerdà, A. (2016). Developing an erodibility triangle for soil textures in semi-arid regions, NW Iran, *CATENA,* 142, 221-232. https://doi.org/10.1016/j.catena.2016.03.015

van den Heever, S. C., Carrio, G. G., Cotton, W. R., DeMott, P. J., and Prenni, A. J. (2006). Impacts of nucleating aerosol on Florida storms. Part I: Mesoscale simulations. *J. Atmos. Sci*., 63, 1752-1775. https://doi.org/10.1175/JAS3713.1

van Donkelaar, A., Martin, R. V., Brauer, M., Kahn, R., Levy, R., Verduzco, C., and Villeneuve, P. J. (2010). Global estimates of ambient fine particulate matter concentrations from satellite-based aerosol optical depth: development and application. *Environ. Health Perspect*., 118(6), 847–855. https://doi.org/10.1289/ehp.0901623

Vescio, M. D. and Johnson, R. H. (1992). The wind response to transient mesoscale pressure fields associated with squall lines. *Mon. Weather Rev*., 120, 1837-1850.

Vukovic, A., Vujadinovic, M., Pejanovic, G., Andric, J., Kumjian, M. R., Djurdjevic, V., Dacic, M., Prasad, A. K., El-Askary, H. M., Paris, B. C., Petkovic, S., Nickovic, S., and Sprigg, W. A. (2014). Numerical simulation of "an American haboob." *Atmos. Chem. Phys*., 14, 3211–3230. https://doi.org/10.5194/acp-14-3211-2014

Walker, A. L., Liu, M., Miller, S. D., Richardson, K. A., and Westphal, D. L. (2009). Development of a dust source database for mesoscale forecasting in southwest Asia. *J. Geophys. Res*., 114, D18207. doi:10.1029/2008JD011541

Walko, R. L., Band, L. E., Baron, J., Kittel, T. G. F., Lammers, R., Lee, T. J., and Co-Authors. (2000). Coupled atmosphere–biophysics–hydrology models for environmental modeling. *Journal of Applied Meteorology*, 39(6), 931–944. https://doi.org/10.1175/1520-0450(2000)039%3C0931:CABHMF%3E2.0.CO;2

Weaver, J. F. and Nelson, S. P. (1982). Multiscale aspects of thunderstorm gust fronts and their effects on subsequent storm development. *Mon. Weather Rev.,* 110, 707–718. https://doi.org/10.1175/1520-0493(1982)110<0707:MAOTGF>2.0.CO;2

Weisman, M. L. and Rotunno, R. (2004). "A theory for strong, long-lived squall lines'' revisited, *J. Atmos. Sci.*, 61(4), 361–382. https://doi.org/10.1175/1520-0469(2004)061<0361:ATFSLS>2.0.CO;2

Wilson, J. W. and Schreiber, W. E. (1986). Initiation of convective storms at radar-observed boundary-layer convergence lines. *Mon. Weather Rev.*, 114, 2516–2536. https://doi.org/10.1175/1520-0493(1986)114<2516:IOCSAR>2.0.CO;2

Woodage, M. J. and Woodward, S. (2014). U.K. HiGEM: Impacts of desert dust radiative forcing in a high-resolution atmospheric GCM. *J. Clim.*, 27(15), 5907–5928. https://doi.org/10.1175/JCLI-D-13-00556.1

Yang, Q., Easter, R. C., Campuzano-Jost, P., Jimenez, J. L., Fast, J. D., Ghan, S. J., Wang, H., Berg, L. K., Barth, M. C., Liu, Y., Shrivastava, M. B., Singh, B., Morrison, H., Fan, J., Ziegler, C. L., Bela, M., Apel, E., Diskin, G. S., Mikoviny, T., and Wisthaler, A. (2015). Aerosol transport and wet scavenging in deep convective clouds: A case study and model evaluation using a multiple passive tracer analysis approach. *J. Geophys. Res.-Atmos.*, 120, 8448–8468. https://doi.org/10.1002/2015JD023647

Yang, Z.-L., Niu, G.-Y., Mitchell, K. E., Chen, F., Ek, M. B., Barlage, M., Longuevergne, L., Manning, K., Niyogi, D., Tewari, M., and Xia, Y. (2011). The community Noah land surface model with multiparameterization options (Noah-MP): 2. Evaluation over global river basins. *J. Geophys. Res.-Atmos.*, 116, D12110. https://doi.org/10.1029/2010JD015140

Yu, H., Chin, M., Yuan, T., Bian, H., Remer, L. A., Prospero, J. M., Omar, A., Winker, D., Yang, Y., Zhang, Y., Zhang, Z., and Zhao, C. (2015). The fertilizing role of African dust in the Amazon rainforest: A first multiyear assessment based on data from Cloud-Aerosol Lidar and Infrared Pathfinder Satellite Observations. *Geophys. Res. Lett.,* 42, 1984–1991. https://doi.org/10.1002/2015GL063040

Yu, Y., Notaro, M., Kalashnikova, O. V., and Garay, M. J. (2016). Climatology of summer Shamal wind in the Middle East. *J. Geophys. Res.-Atmos.*, 121, 289–305. https://doi.org/10.1002/2015JD024063

Yuter, S. E. and Houze, R. A. (1995). Three-Dimensional kinematic and microphysical evolution of Florida cumulonimbus. Part II: Frequency distributions of vertical velocity, reflectivity, and differential reflectivity. *Mon. Weather Rev.*, 123, 1941–1963. https://doi.org/10.1175/1520-0493(1995)123<1941:TDKAME>2.0.CO;2

Zender, C. S., Miller, R. L. L., and Tegen, I. (2004). Quantifying mineral dust mass budgets: terminology, constraints, and current estimates. *Eos Trans. AGU*, 85(48), 509–512. https://doi.org/10.1029/2004EO480002

Zhang, C., Wang, Y., and Hamilton, K. (2011). Improved representation of boundary layer clouds over the southeast pacific in ARW–WRF using a modified Tiedtke cumulus parameterization scheme. *Mon. Weather Rev.,* 139, 3489–3513. https://doi.org/10.1175/MWR-D-10-05091.1

Zhang, K. and Wang, X. (1997). Investigation report and some thinking on strong sand storm in Northwest China, May 5, 1993. *Journal of Beijing Forestry University*, 19, 1.

Zhao, C., Liu, X., Leung, L. R., Johnson, B., McFarlane, S. A., Gustafson Jr., W. I., Fast, J. D., and Easter, R. (2010). The spatial distribution of mineral dust and its shortwave radiative forcing over North Africa: modeling sensitivities to dust emissions and aerosol size treatments. *Atmos. Chem. Phys.*, 10, 8821–8838. https://doi.org/10.5194/acp-10-8821-2010